

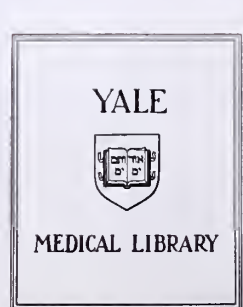
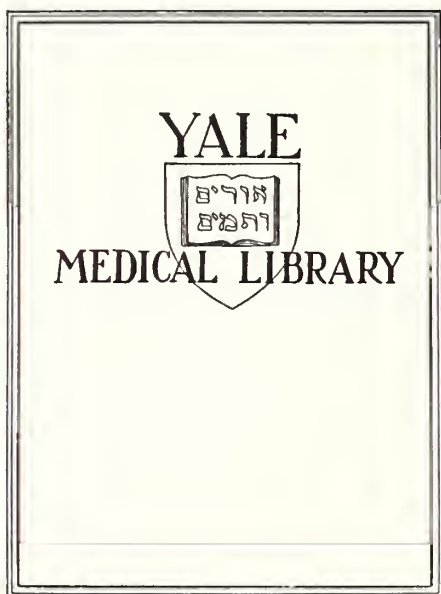


3 9002 08676 2136

QUASIELASTIC LIGHT SCATTERING FROM MACROMOLECULES

STUART BRIAN DUBIN

1970





Digitized by the Internet Archive
in 2017 with funding from
Arcadia Fund

<https://archive.org/details/quasielasticligh00dubi>

QUASIELASTIC LIGHT SCATTERING FROM MACROMOLECULES

by

Stuart Brian Dubin

B.A., Yale College

(1965)

SUBMITTED IN PARTIAL FULFILLMENT OF THE

REQUIREMENTS FOR THE DEGREE OF

DOCTOR OF PHILOSOPHY

at the

MASSACHUSETTS INSTITUTE OF TECHNOLOGY

January, 1970

to the memory of my mother
to my father

to the accept
and the reason for the motion

QUASIELASTIC LIGHT SCATTERING

FROM MACROMOLECULES

by

STUART BRIAN DUBIN

Submitted to the Department of Physics on January 12, 1970 in partial fulfillment of the requirements for the degree of Doctor of Philosophy.

ABSTRACT

We present the results of ultrahigh resolution spectral determinations on the light quasielastically scattered by various solutions of macromolecules. These results demonstrate the range of application and utility of light-mixing spectroscopy to the study of large molecules.

By combining the values of diffusion constants determined by light scattering with those of the sedimentation constants measured conventionally in the ultracentrifuge, we have used the method of sedimentation-diffusion to determine the molecular weights of the bacteriophages T4, T5, T7, and λ . We find these to be (in millions) 192.5 ± 6.6 , 109.2 ± 4.0 , 50.4 ± 1.8 , and 45.2 ± 2.0 respectively. From the percentage of each phage which is DNA we determine the phage-DNA molecular weights to be (in millions) 105.7 ± 3.8 , 67.3 ± 3.1 , 25.8 ± 1.0 , and 24.2 ± 1.0 respectively. Because most conventional means of determining molecular weights become marginal above about 10 million, these values are among the most precise determinations yet made for phage-DNA molecular weights.

This thesis also demonstrates that self-beating spectroscopy may be successfully applied to systems with very small scattering cross sections. We have studied the chemical denaturation of lysozyme (at 1% protein concentration) by guanidine hydrochloride (GuCl) for thirty values of $[GuCl]$ between 0M and 6M. We find that D decreases from $(10.6 \pm 0.1) \times 10^{-7} \text{ cm}^2/\text{sec}$ to $(7.3 \pm 0.1) \times 10^{-7} \text{ cm}^2/\text{sec}^{20,w}$ over this range. This change is shown to be insufficient to demonstrate whether more than one type of lysozyme molecule was present for any value of $[GuCl]$. The denaturation curve (diffusion constant versus $[GuCl]$) resembles that of the changes in other physical parameters such as optical rotation.

Self-beating spectroscopy has been applied to the study of the anisotropy scattering from tobacco mosaic virus. We have determined the rotary diffusion constant of this molecule to be $(276 \pm 10)/\text{sec}$ (corrected to 20°C and water), in good agreement with the appropriate hydrodynamic calculation.

We present a detailed study of the expected intensity and spectral width of the light scattered by fluctuations in concentration and optical isotropy in macromolecular solutions. These results are combined with an analysis of the self-beating spectrometer to calculate the signal-to-noise ratio obtainable in such experiments and hence their feasibility. We also include a discussion of the difficulty of resolving non-Lorentzian spectral profiles and hence of detecting polydispersity in macromolecular solutions.

Thesis supervisor: George B. Benedek Title: Professor of Physics



TABLE OF CONTENTS

<u>Chapter No.</u>	<u>Title</u>	<u>Page No.</u>
I	INTRODUCTION	9
	A. Historical Background	9
	B. Motivation	14
	Bibliography	22
II	THEORY OF THE SCATTERING AND ITS APPLICATIONS	25
	A. Introduction	25
	B. Intensity of the Scattered Light	26
	1. Isotropic Molecules	26
	2. Anisotropic Molecules	45
	a. Theory of Anisotropy Scattering	45
	b. Critique of Literature on Depolarization Measurements	56
	C. Spatial Coherence of the Scattered Light	61
	D. Temporal Coherence of the Scattered Light	68
	E. Applications of the Information in the Spectrum of the Scattered Light	77
	1. Determination of Bacteriophage Molecular Weights	77
	2. The Chemical Denaturation of Lysozyme	80
	Bibliography	82
III	EXPERIMENTAL APPARATUS, METHODS, AND MATERIALS	85
	A. Introduction	85
	B. The Square-Law Spectrometer	85
	1. Theory of Operation	85
	2. Experimental configuration and Evaluation of Signal-to-Noise Ratio	98
	3. Optical Alignment and Detection	112
	4. Electronic Detection	119
	5. The Lasers	124
	C. Experimental Samples and Sample Preparation	127
	1. The Bacteriophages (T4, T5, T7, and λ)	127
	2. Lysozyme	131
	3. Tobacco Mosaic Virus	136
	Bibliography	138



<u>Chapter No.</u>	<u>Title</u>	<u>Page No.</u>
IV	DATA REDUCTION	141
	A. Introduction	141
	B. Determination of Spectral Shape and Linewidth	141
	1. The Bacteriophages and Tobacco Mosaic Virus	141
	2. Lysozyme	142
	C. Reduction to Standard Conditions (Temperature, Viscosity, and Density)	156
	1. Diffusion Constants	156
	2. Sedimentation Constants	158
	Bibliography	160
V	RESULTS AND DISCUSSION	161
	A. Introduction	161
	B. Experimental Results	161
	1. Bacteriophage Molecular Weights	161
	2. The Denaturation of Lysozyme	178
	3. The Rotational Diffusion Constant of Tobacco Mosaic Virus	186
	4. Concluding Remarks	192
	Bibliography	193
Appendix	THE EFFECT OF POLYDISPERSITY ON THE SPECTRUM OF THE LIGHT SCATTERED BY MACROMOLECULES	195
BIOGRAPHICAL NOTE		204
ACKNOWLEDGMENTS		205

LIST OF ILLUSTRATIONS

<u>Figure Number</u>	<u>Title</u>	<u>Page Number</u>
2.1	The Scattering Geometry	27
2.2	Geometric Representation of the Scattering Process	30
2.3	Multiple Scattering Process	43
2.4	Geometry for the Observation of Light Scattered by Anisotropic Molecules	48
2.5	Geometry for Determination of the Coherence Area in the Far Field of the Scattered Light	62
2.6	Spread in Wave Vector of Incident Light due to Finite Beam Dimensions	65
2.7	Forces Acting on a Particle Accelerated to its Terminal Velocity in a Viscous Medium	79
3.1	The Power Spectrum of the Photocurrent	93
3.2	Block Diagram of Self-Beating Spectrometer	99
3.3	The Correlation Function of the Photocurrent	110
3.4	Block Diagram of Optical Setup Employed in Concentration Fluctuation Scattering	113
3.5	Block Diagram of Optical Setup Employed in Anisotropy Scattering	116
3.6	Electronic Detection System	120
3.7	Block Diagram of the Laser Servo	125
3.8	Length Distribution in Sample of Tobacco Mosaic Virus	137

<u>Figure Number</u>	<u>Title</u>	<u>Page Number</u>
4.1	Self-Beat Spectrum of the Light Scattered by a Two-Component Mixture	153
4.2	Width and RMS Deviation of Best Single Lorentzian Fit to the Self-Beat Spectrum of the Light Scattered by Various Two-Component Mixtures	155
4.3	Temperature Dependence of the Viscosity of Buffered Guanidine Hydrochloride Solutions	159
5.1	Outlines of Several Bacteriophages	162
5.2	Self-Beat Spectrum of the Light Scattered at $\theta = 33.9^\circ$ by T4 Bacteriophage	164
5.3	Self-Beat Spectrum of the Light Scattered at $\theta = 160^\circ$ by T4 Bacteriophage	165
5.4	$(\Gamma_D/2\pi)$ versus K^2 for T4 Bacteriophage	166
5.5	Concentration Dependence of the Diffusion Constants of Bacteriophages T5 and T7	167
5.6	Self-Beat Spectrum of the Light Scattered by Bacteriophage T7	169
5.7	Concentration Dependence of the Sedimentation Constants of Bacteriophages T4, T5, T7, and λ	170
5.8	Self-Beat Spectrum of the Light Scattered by a 1% Lysozyme Solution	179
5.9	Self-Beat Spectrum of the Light Scattered by a 1% Lysozyme-4.37M GuCl Solution	180
5.10	Effect of Chemical Denaturation on the Diffusion Constant of Lysozyme	183
5.11	$D_{20,w}$ versus Concentration for Guanidine Hydrochloride	187
5.12	Self-Beat Spectrum of the Anisotropy Scattering at $\theta = 1.61^\circ$ from Tobacco Mosaic Virus	189



<u>Figure Number</u>	<u>Title</u>	<u>Page Number</u>
A.1	Width and RMS Deviation of Best Single Lorentzian Fit to the Heterodyne-Beat Spectrum of the Light Scattered by Various Two-Component Mixtures	196
A.2	Width and RMS Deviation of Best Single Lorentzian Fit to the Heterodyne-Beat Spectrum of the Light Scattered by Various Uniform Distributions of Molecules Differing only in Diffusion Constant	198
A.3	Width and RMS Deviation of Best Single Lorentzian Fit to the Heterodyne-Beat Spectrum of the Light Scattered by Various Uniform Distributions of Spheres	201
A.4	Width and RMS Deviation of Best Single Lorentzian Fit to the Heterodyne-Beat Spectrum of the Light Scattered by Various Uniform Distributions of Rods	202



LIST OF TABLES

<u>Table Number</u>	<u>Title</u>	<u>Page Number</u>
1.1	Phage and Phage-DNA Molecular Weights for Several Bacteriophages	15
2.1	Refractive Index Increment $\partial n / \partial C$ for Various Biological Macromolecules	40
2.2	Rayleigh Ratios of Representative Liquids	41
3.1	Physical Parameters to Evaluate $\left(\frac{\text{SIG}}{\text{NOISE}} \right)_{\text{PRE}}$	103
3.2	Solvents Employed in the Determination of Bacteriophage Diffusion Coefficients	128
5.1	$S_{20,w}^0$, $D_{20,w}$, and \bar{v} for Phages T4, T5, T7, and λ	172
5.2	Molecular Weights and % DNA of T4, T5, T7, and λ Bacteriophages	173
5.3	Comparison of Derived Phage Partial Specific Volumes (Assuming v Additivity) and Actual Partial Specific Volumes	175
5.4	Effect of Chemical Denaturation on the Diffusion Constant of Lysozyme	182



Chapter I

INTRODUCTION

"Men may say of something, 'Ah, this is new.' But it existed long ago, before our time. The men of that old time are now forgotten, as men to come shall be forgotten by the folk who follow them."

Ecclesiastes

A. Historical Background

When light traverses any material medium, some of the incident light will be scattered. Lord Rayleigh⁽¹⁾ was the first (1871) to consider the information contained in the scattered light, and obtained expressions appropriate for a dilute gas. For a sufficiently dilute solution of macromolecules, Rayleigh's results should be valid to calculate the excess intensity of light scattered by the macromolecules over that scattered by the solvent. There was nevertheless a good deal of confusion in the experimental literature on this matter, until Putzeys and Brosteaux,⁽²⁾ in a very elegant but little-known paper, used Rayleigh's formula in the first determination of macromolecular weights using light scattering. Although their results were accurate, and demonstrated the utility of this method, their 1935 paper apparently had little impact.

As the density of the material increases, Rayleigh's results gradually break down until the apparent paradox is reached that very dense materials (liquids and solids) scatter much less light than predicted by the Rayleigh formula. This occurs because neighboring atoms exhibit cooperative behavior as their separation becomes small, so that Rayleigh's assumption of incoherent scattering (the phase of the light scattered by

one atom is randomly related to that scattered by any other atom) must be replaced by a description of coherent scattering. This description was not obtained until Einstein,⁽³⁾ stimulated by the work of von Smoluchowski⁽⁴⁾ on critical opalescence, introduced an interpretation of the scattering process which is readily applied to any system. He considered the scattering to be due to fluctuations in the local dielectric constant of the medium, ϵ . He demonstrated that scattering will occur if the wave vector of the fluctuation conserves wave vector between the incident and scattered light. Further, he provided methods for the calculation of the magnitude of such fluctuations.

Debye^(5,6) extended Einstein's fluctuation approach to the study of macromolecular solutions (1944). He interpreted the scattering to arise chiefly from fluctuations in the concentration of the macromolecules. It was this work that firmly established light scattering as a tool for the determination of molecular weights, and it was to be used extensively for this purpose, particularly in the succeeding decade.

The intensity of the light scattered by macromolecules contains much information beyond simply the molecular weight of the scattering bodies. As early as 1908, Mie⁽⁷⁾ had shown that the angular distribution of the scattered light can yield information on the size of molecules whose dimensions are comparable to the wavelength of light. This result obtains because, for such scatterers, interference can occur between light scattered from different portions of the same molecule. Although the resulting angular dependence is generally a function of both the size and shape of the molecule, Guinier⁽⁸⁾ obtained the significant result that, for small scattering angles, the angular dependence becomes a measure solely of the



radius of gyration of the scatterer. This technique has been formalized into a so-called "Zimm Plot"⁽⁹⁾ in which a set of measurements at various angles and concentrations yields both the radius of gyration and molecular weight of the macromolecule under investigation. The complete angular dependence of the intensity of the scattered light gives, in addition, the shape of the molecule, and such distributions have been tabulated for a variety of shapes.⁽¹⁰⁾

The polarization of the scattered light can, in principle, also yield information on the size and shape of macromolecules.⁽¹¹⁾ In general, however, the depolarization scattering is so slight that the technique has not been fruitful.⁽¹²⁾ On the other hand, the allied fields of electric⁽¹³⁾ and flow⁽¹⁴⁾ birefringence, in which partial alignment of the molecules occurs, have utilized the slight optical anisotropy of the scatterers to obtain information on size and conformation.

This brief review describes the situation at the time when laser light sources became available around 1964. Up to that point, the time-dependence of the fluctuations which give rise to the scattering had not been considered experimentally, but rather only the time-average quantity $\langle(\Delta\epsilon)^2\rangle$, through the measurement of the intensity of the scattered light. Although significant, the information contained in the intensity measurements is limited, as described above. The laser, with its high monochromaticity and high power-per-spatial-mode output, introduced the possibility of observing the spectrum of the light scattered by macromolecules. This was to be achieved by the new methods of optical mixing spectroscopy.

In 1947, Forrester, Parkins, and Gerjuoy⁽¹⁵⁾ in the United States, and Gorelik⁽¹⁶⁾ in Russia proposed that, using a nonlinear device, the beat

note between light waves of different frequencies might be observable. Because of the very low power-per-spatial-mode of conventional light sources, such an experiment was extremely difficult at that time.^(17,18) Nevertheless, in an experimental tour de force, Forrester, Gudmundsen and Johnson^(19,20) were able, in 1955, to detect the beat note between the Zeemann split lines in mercury light. The method, however, had no practical application due to the extremely low signal-to-noise ratio which could be expected with any conventional light source.

By 1961, lasers had been developed, although they were not yet commercially available. Forrester⁽²¹⁾ observed that optical mixing spectroscopy could be used to detect the beat notes between different laser modes and showed that such an experiment could find practical application in space navigation. Townes⁽²²⁾ suggested that heterodyne beat spectroscopy be employed to study Rayleigh, Raman, and Brillouin scattering. Benedek⁽²³⁾ independently proposed optical mixing spectroscopy for the experimental detection of Brillouin scattering. In each case above, it is the vastly superior monochromaticity and power-per-spatial-mode of the laser relative to conventional light sources which made the suggested experiments feasible.

Cummins, Knable, and Yeh⁽²⁴⁾ made the first observation of the spectrum of light scattered by a suspension of independently diffusing particles, namely, polystyrene latex spheres. The spectral profile of this light is so narrow that it cannot be resolved by any conventional means such as the grating spectrograph or Fabry-Perot interferometer, even with an arbitrarily monochromatic light source. Cummins, Knable and Yeh⁽²⁴⁾ showed that the spectrum of the scattered light, which would have had a Doppler profile in

the absence of solvent, was sharply narrowed due to collisions of the spheres with water molecules. They used the method of optical heterodyne detection⁽²¹⁾ and obtained a resolving power of about 10^{13} , far beyond that of any conventional form of optical spectroscopy. They did not present, however, a quantitative determination of their observed spectral profile, and convection currents in their scattering cell prevented a precise determination of the width and angular dependence of the spectrum of the scattered light.

Simultaneously, Pecora⁽²⁵⁾ calculated the spectrum to be expected in an experiment like that of Cummins, Knable and Yeh. He employed a molecular point of view, in which he considered an assemblage of particles executing Brownian motion. Debye⁽²⁶⁾ explained the experimental results of Alpert, Yeh, and Lipworth in a binary mixture system⁽²⁷⁾ utilizing the fluctuation approach. He assumed that the fluctuations in concentration which produce the scattering obey the diffusion equation. Both Pecora and Debye predicted that, for a monodisperse suspension of spheres, the spectral profile of the scattered light should be Lorentzian and the width of the spectrum should vary as the square of the scattering fluctuation wave vector, and should be proportional to the diffusion coefficient of the spheres. In 1967, Dubin, Lunacek, and Benedek^(28,29) in the United States, and Arecchi, Giglio, and Tartari⁽³⁰⁾ in Italy showed quantitatively that these predictions described accurately the spectrum of light scattered by a suspension of latex spheres. They employed the method of "low level"⁽²¹⁾ or "self-beating"⁽³¹⁾ optical mixing spectroscopy suggested and described by Forrester,⁽²¹⁾ and independently developed by Ford and Benedek⁽³¹⁾ in a study of a pure fluid near its critical point.

Dubin, Lunacek, and Benedek^(28,29) also extended this method to the



study of diffusion coefficients of various proteins, deoxyribonucleic acid (DNA) and tobacco mosaic virus (TMV). They pointed out that the present method gave results in good agreement with the classical determinations of diffusion constants, but in much less time and with higher accuracy. This work initiated a series of investigations of light scattered quasielastically from macromolecular solutions, comprehensive reviews of which have been presented by Angus, Morrow, Dunning, and French,⁽³²⁾ and by French, Angus, and Walton.⁽³³⁾ These new investigations included scattering from binary mixtures,^(33,34) long rods (TMV),⁽³⁵⁾ a study of the spectrum of the depolarized light scattered by TMV,⁽³⁶⁾ the thermal denaturation of the protein ribonuclease,⁽³⁷⁾ observation of sperm cell motility,⁽³⁸⁾ and the present studies of protein denaturation⁽³⁹⁾ and bacteriophage molecular weight determination.⁽⁴⁰⁾ At this point, the field is growing very rapidly with several groups in the United States and Europe.

The advent of the laser and development of the methods of optical mixing spectroscopy have indeed led to a revival of interest in the information to be obtained by light scattering in macromolecular systems.

B. Motivation

We shall show in section II.E.1 that the diffusion constant of a macromolecule can be combined with other parameters to yield the molecular weight of the particle. This technique, called the method of "sedimentation-diffusion", has been used to great advantage for many years. However, for very large molecules (molecular weight greater than approximately ten million), very long times are required to determine the diffusion constant accurately using classical techniques. In fact, several weeks is not an uncommon figure in the case of viruses.⁽⁴¹⁾ It is obviously extremely difficult to maintain appropriate experimental conditions over such a period.

In addition, most of the alternative methods for determining molecular weight such as light scattering, osmotic pressure, and sedimentation-equilibrium also tend to be extremely difficult in this molecular weight range. It was therefore immediately apparent to virologists⁽⁴²⁾ that the spectral method for determining the diffusion coefficient of large molecules had great potential to alleviate the confused state of affairs in viral molecular weights. With this in mind, Professor David Freifelder of Brandeis University and Dr. Carter Bancroft of Harvard University suggested that we undertake a collaboration on this problem. This fruitful project has led to the determination of the molecular weights of the bacteriophages T4, T5, T7, and λ . By chemical analysis, we have been able to determine the percentage by weight of deoxyribonucleic acid (DNA) contained in each phage, and hence, the DNA molecular weight. The primary source of error in these experiments is the determination of the phage partial specific volume (v) and the percentage of DNA. The determination of the diffusion coefficients is accurate to better than 1%. The molecular weight results, obtained with an accuracy which is unprecedented in this area of investigation, are presented in Table 1.1 below:

Table 1.1

Phage and Phage-DNA Molecular
Weights for Several Bacteriophages

Phage	Phage Molecular Weight (in millions)	DNA Molecular Weight (in millions)
T4	192.5 \pm 6.6	105.7 \pm 3.8
T5	109.2 \pm 4.0	67.3 \pm 3.1
T7	50.4 \pm 1.8	25.8 \pm 1.0
λ	45.2 \pm 2.0	24.2 \pm 1.0

The significance and implications of these results, which are systematically and substantially lower than values usually reported in the literature, will be discussed extensively in Chapter V.

Although bacteriophages have presented various problems to the experimenter due to their large size and consequent very small diffusion constant, equally grave problems arise at the other end of the macromolecular weight scale. These molecules, such as the small proteins (molecular weight range of about ten to fifty thousand) diffuse so rapidly that any experimentally created concentration gradient is quickly "smeared out". This effect renders the analytical ultra-centrifuge far less useful than it is for the larger proteins, nucleic acids, and viruses. The centrifuge allows the experimenter to determine the terminal velocity of a macromolecule falling in a high gravitational field through a viscous medium - e.g., water. This velocity, which is proportional to the frictional coefficient and hence to the effective size of the molecule⁽⁴³⁾ is measured essentially by determining the time required for a boundary between two different concentrations of the molecules to traverse a given distance. For the very small molecules, this boundary is rendered rather broad due to the diffusion of the molecules. This boundary spreading problem occurs for such molecules even at the highest fields available in commercial centrifuges (approximately several hundred thousand g). Since the average velocity due to diffusion is zero, the boundary spreads symmetrically for a monodisperse system and is not a great difficulty. However, the spreading renders very difficult the detection of the simultaneous presence of two similar species of small molecules, to be contrasted with the fact that the centrifuge is an extremely sensitive tool for such detection in the case of larger molecules (molecular weight greater than approximately several hundred thou-



sand).⁽⁴³⁾ In addition, the centrifuge experimental runs take many hours or even days for these small molecules, instead of the several minutes required in the case of bacteriophages, for example.

In view of these limitations on the utility of the centrifuge in the study of small molecules, Professor George Feher of the University of California at San Diego suggested that light mixing spectroscopy might be a useful tool in the study of the very small protein, lysozyme (molecular weight approximately fourteen thousand). This protein is known to undergo a reversible denaturation under the action of guanidine hydrochloride (GuCl).^(44,45) It was not known, however, to what extent the conformation of the molecule changed during this transition. In addition, it was unknown whether the denaturation process was a continuous change from the native state to the denatured state through a continuum of intermediate states, or whether only two states existed (native and denatured), and the condition of partial denaturation consisted of a mixture of these states. This latter question could, in principle, be resolved by the fact that a mixture of two different conformations would not yield a Lorentzian profile for the spectrum of the scattered light. Finally, by studying the spectrum of the light as a function of concentration of the denaturant, the evolution of the conformational change upon denaturation could be mapped out.

This investigation has been carried out under the restriction of severe signal-to-noise ratio difficulties created by the small size (implying low scattering cross-section as well as wide spectral profile) of the molecule and the low concentration employed to avoid any complications due to molecular interactions. In addition, at high denaturant concentrations, the light scattered by the guanidine chloride (GuCl) itself had to be considered



carefully in the analysis of the results. The technical difficulties in this particular regime constitute a measure of exactly how far this technique can be extended in the study of macromolecules. The spectrum of the lysozyme-GuCl system was studied at one percent protein concentration for thirty values of the concentration of GuCl, between 0M and 6M. The value of the diffusion constant of lysozyme remained essentially constant at about $10.6 \times 10^{-7} \text{ cm}^2/\text{sec}$ between 0M and 2M GuCl concentration, then decreased smoothly to about $7.3 \times 10^{-7} \text{ cm}^2/\text{sec}$ at 5M GuCl, where it plateaued. However, as we shall discuss in Chapters IV and V, it was not possible to determine from an analysis of the spectral profile of the scattered light whether or not two species were present simultaneously at any GuCl concentration. Nevertheless, the values of the diffusion constant obtained for the completely native and completely denatured forms of lysozyme indicate that the molecule experiences an increase in effective volume of over a factor of three upon denaturation. This value is in excellent agreement with the observed change in intrinsic viscosity,⁽⁴⁴⁾ which quantity is a measure of the volume of solvent the molecule displaces.⁽⁴⁶⁾

The transition region we observe in this denaturation study has approximately the same width, and occurs over about the same range in GuCl concentration, as that for other physical parameters such as ultraviolet absorption,⁽⁴⁴⁾ optical rotation,^(44,45) and intrinsic viscosity.⁽⁴⁴⁾ This confirms that these parameters are indeed probes of molecular conformation. Finally, using the recent results of Glickson, McDonald, and Phillips⁽⁴⁷⁾ in a high resolution NMR study of lysozyme which indicate that lysozyme exists only in the native or denatured states, or a mixture of these states, we can calculate from the measured spectral profile of the scattered light

the relative concentrations of the two species as a function of GuCl concentration.

In each of the two experiments described above, we correctly assume that the principal source of the scattering is the fluctuations in dielectric constant which arise from concentration fluctuations. As we discuss in section II.B.2., this is always the greatest contribution by far to the scattered light. However, fluctuations in the optical isotropy can also scatter a small amount of light in macromolecular solutions. This "anisotropy scattering" is intimately related to the orientation of the molecules which produce the scattering. In fact, by employing heterodyne mixing spectroscopy⁽²¹⁾ to study the spectrum of the depolarized light scattered by tobacco mosaic virus (TMV), Wada, Suda, Tsuda and Soda⁽³⁶⁾ were able to determine a value for the rotational diffusion constant (D_R) of TMV:

$$D_R = (350 \pm 20)/\text{sec.}^*$$

It is difficult to rationalize most experimentally determined values of D_R for TMV (including the above-quoted value) with the values predicted on the basis of hydrodynamic models. Much of this difficulty arises because the models generally assume that TMV, which is essentially a cylinder, can be hydrodynamically represented by an ellipsoid of revolution of the same length and diameter. Haltner and Zimm⁽⁴⁸⁾ and Broersma⁽⁴⁹⁾ have presented experimental results on large (order of centimeters) cylinders which indicate that this assumption is inadequate. In addition, Broersma⁽⁴⁹⁾ has calculated D_R for cylinders to an accuracy which includes terms to first

* The authors do not indicate to what conditions (temperature and viscosity) this value is corrected.



order in the ratio of the width-to-length. Since this ratio is approximately 1/20 for TMV,⁽⁵⁰⁾ we would expect Broersma's results to be excellent in this case. Using the calculations of Broersma for a cylinder of width 180 \AA as given by x-ray diffraction⁽⁵¹⁾ and length of 3000 \AA as determined in the electron microscope,⁽⁵²⁾ we find a value of $D_R = 269/\text{sec}$ for TMV suspended in water at 20°C. Despite the appropriateness of Broersma's calculation to this particular system, the agreement of this value with the experimental literature is generally poor, although O'Konski and Haltner⁽⁵³⁾ report a reasonably close value of $D_R = (295 \pm 12)/\text{sec}$, corrected to 20°C and water.

We have therefore employed the method of self-beating⁽³¹⁾ spectroscopy to study the depolarized light scattered by TMV. We find a value of $D_R = (276 \pm 10)/\text{sec}$ (20°C, water), independent of scattering angle between 1.5 and 3 degrees. This appears to be the lowest value reported in the literature to this time, but is in excellent agreement with the results of Broersma.⁽⁴⁹⁾ This result confirms the appropriateness of a hydrodynamic treatment of cylinders, even on a molecular scale of only several thousand \AA . The validity of such a treatment for very small spheres has already been confirmed by Dubin, Lunacek, and Benedek,^(28,29) and by Arecchi, Giglio and Tartari⁽³⁰⁾ by light scattering experiments on polystyrene latex spheres.

This thesis demonstrates that the technique of high resolution self-beating spectroscopy can be applied to macromolecular systems such as lysozyme, whose scattering is as weak as that of pure fluids, as well as to the more intense scatterers such as bacteriophages. It extends the measurement of diffusion constants to values much smaller than those accurately obtainable with classical systems, and has thereby allowed the most accurate

determination of phage and phage-DNA molecular weights yet obtained. It has made possible the study of change in conformation of macromolecules of such a small size that the equivalent study in the ultracentrifuge is marginal. The rotational diffusion constant of tobacco mosaic virus has been determined with sufficient accuracy to confirm a hydrodynamic calculation for the diffusion coefficient of cylinders. Finally, we include a description of the feasibility of further experiments from the standpoint of signal-to-noise considerations and the ability to discern non-Lorentzian spectral profiles.

Chapter I References

1. Strutt, J. W. (Lord Rayleigh), Phil. Mag., 41, 107, 274, 447(1871).
2. Putzeys, P., and Brosteaux, J., Trans. Faraday Soc., 31, 1314 (1935).
3. Einstein, A., Ann. Physik, 33, 1275 (1910).
4. von Smoluchowski, M., Ann. Physik, 25, 205 (1908).
5. Debye, P., J. App. Phys., 15, 338 (1944).
6. Debye, P., J. Phys. and Colloid Chem., 51, 18 (1947).
7. Mie, G., Ann. Physik, 25, 377 (1908).
8. Guinier, A., Ann. Phys., 12, 161 (1939).
9. Zimm, B., J. Chem. Phys., 16, 1099 (1948).
10. An excellent summary of these distributions is found in Geiduschek, E.P., and Holtzer, A., Advances in Biol. and Med. Phys., 6, 431 (1958).
11. Lord Rayleigh, Phil. Mag., 35, 373 (1918).
12. Geiduschek, E. P., J. Polymer Sci., 13, 408 (1954).
13. Benoit, H., Ann. Phys., 6, 561 (1951).
14. Edsall, J. T., Advances in Colloid Sci., 1, 269 (1942).
15. Forrester, A. T., Parkins, W. E., and Gerjuoy, E., Phys. Rev., 72, 728 (1947).
16. Gorelik, G., Dokl. Akad. Nauk, 58, 45 (1947).
17. Griffin, L. R., Phys. Rev., 73, 922 (1948).
18. Gerjuoy, E., Forrester, A. T., and Parkins, W. E., Phys. Rev., 73, 922 (1948).
19. Forrester, A. T., Gudmundsen, R. A., and Johnson, P. O., Phys. Rev., 99, 1691 (1955).
20. Forrester, A. T., Am. J. Phys., 24, 192 (1956).
21. Forrester, A. T., J. Opt. Soc. Am., 51, 253 (1961).
22. Townes, C. H., in Singer, J. R. (ed.), "Advances in Quantum Electronics", Columbia University Press, New York, 1961, pp. 3-11.

23. Benedek, G. B., "Research in Materials Science and Engineering", MIT CMSE Annual Report, 1962-1963, p. 55.
24. Cummins, H. Z., Knable, N., and Yeh, Y., Phys. Rev. Letters, 12, 150 (1964).
25. Pecora, R., J. Chem. Phys., 40, 1604 (1964).
26. Debye, P., Phys. Rev. Letters, 14, 783 (1965).
27. Alpert, S. S., Yeh, Y., and Lipworth, E., Phys. Rev. Letters, 14, 486 (1965).
28. Dubin, S. B., Lunacek, J. H., and Benedek, G. B., Proc. Nat. Acad. Sci., 57, 1164 (1967).
29. Lunacek, J. H., Dubin, S. B., and Benedek, G. B., Bull. Am. Phys. Soc., 12, 544 (1967).
30. Arecchi, F. T., Giglio, M., and Tartari, U., Phys. Rev., 163, 186 (1967)
31. Ford, N. C., Jr., and Benedek, G. B., Phys. Rev. Letters, 15, 649 (1965).
32. Angus, J. C., Morrow, D. L., Dunning, J. W., Jr., and French, M. J., Ind. and Eng. Chem., 61, 8 (1969).
33. French, M. J., Angus, J. C., and Walton, A. G., Science, 163, 345 (1969).
34. Chu, B., Phys. Rev. Letters, 18, 200 (1967).
35. Cummins, H. Z., Carlson, F. D., Herbert, T. J., and Woods, G., Biophys. J., 9, 518 (1969).
36. Wada, A., Suda, N., Tsuda, T., and Soda, K., J. Chem. Phys., 50, 31 (1969).
37. Rimai, L., Hickmott, J. T., Cole, T., and Carew, E. B., to be published in the Biophys. J.
38. Berge, P., Volochine, B., Billard, R., and Hamelin, A., Compt. Rend., 265, 889 (1967).
39. Dubin, S. B., Feher, G., and Benedek, G. B., Biophys. J., 9, A213 (1969).
40. Dubin, S. B., and Benedek, G. B., Biophys. J., 9, A212 (1969).
41. Markham, R., in Maramorosch, K., and Koprowski, H., (ed.), "Methods in Virology", vol. 2, Academic Press, New York, 1967, p. 280.
42. ref. 41, p. 302.

43. Tanford, C., "Physical Chemistry of Macromolecules", John Wiley and Sons, Inc., New York, 1961, p. 364.
44. Hamaguchi, K., and Kurono, A., J. Biochem., 54, 111 (1963).
45. Tanford, C., Pain, R. H., and Otchin, N. S., J. Mol. Biol., 15, 489 (1966).
46. ref. 43, p. 334.
47. Glickson, J. D., McDonald, C. C., and Phillips, W. D., Contribution No. 1553, Central Research Department, E. I. du Pont Co., Wilmington, Del.
48. Haltner, A. J., and Zimm, B. H., Nature, 184, 265 (1959).
49. Broersma, S., J. Chem. Phys., 32, 1626 (1960).
50. Setlow, R. B., and Pollard, E. C., "Molecular Biophysics", Addison-Wesley Publishing Co., Inc., Reading, Mass., 1962, p. 151.
51. ref. 50, p. 152.
52. Hall, C. E., J. Am. Chem. Soc., 80, 2556 (1958).
53. O'Konski, C. T., and Haltner, A. J., J. Am. Chem. Soc., 78, 3604 (1956).

Chapter II

THEORY OF THE SCATTERING AND ITS APPLICATIONS

"I have always accounted as extraordinary foolish those who would make human comprehension the measure of what Nature has a power or knowledge to effect, whereas on the contrary, there is not any least effect in Nature which can be fully understood by the most speculative minds in the world. Their vain presumption of knowing all can take beginning solely from their never having known anything."

Sagredus, in Dialogue on the Great World Systems,
Galileo Galilei

A. Introduction

The two principal sources of quasi-elastic scattering in a macromolecular solution are fluctuations in concentration and optical isotropy. Expressions are obtained in section B. of this chapter, which indicate the relative contributions which can be expected from each type of scattering. In the case of concentration fluctuations, the intensity of the scattered light can be predicted readily on the basis of an easily-measured quantity, the refractive index increment $\frac{\partial n}{\partial C}$. There is no such convenient parameter in the case of molecular anisotropy. We therefore review critically the available literature in anisotropy scattering to obtain an idea of the expected intensity, and discuss this in terms of intrinsic and form anisotropy origins.

After considering the spatial coherence properties of the scattered light in section II.C., we examine the spectrum of this light in section II.D. It is shown that the spectrum of the light mirrors the spectrum of the fluctuations in concentration and isotropy which produced the scattering, and yields information on the translational and rotational diffusion constants of the molecule.

We conclude the chapter in section II.E. by outlining the principles of two experiments in which measurement of the translational diffusion coef-

ficient by light scattering techniques provides information not readily obtained by other techniques: the determination of the molecular weights of very large molecules (the bacteriophages), and the study of the chemical denaturation of the protein lysozyme. These experiments, combined with the determination of the rotational diffusion constant of tobacco mosaic virus, constitute the experimental basis of this thesis.

B. Intensity of the Scattered Light

(1) Isotropic Molecules

If light is incident upon a perfectly uniform transparent medium, it is a familiar result of electromagnetic theory⁽¹⁾ that the incident light is simply refracted upon entry into this medium. Consider a plane wave propagating in vacuum with electric field \vec{E}_o , wave vector \vec{k}_o , and frequency ω_o :

$$\vec{E}_v(\vec{r}, t) = \vec{E}_o e^{i(\vec{k}_o \cdot \vec{r} - \omega_o t)} . \quad (2.1)$$

If this wave is normally incident upon a perfectly uniform transparent medium of index of refraction n , the macroscopic field in the medium is given by⁽¹⁾

$$\vec{E}_M = \vec{E} e^{i(\vec{k} \cdot \vec{r} - \omega_o t)} , \quad (2.2)$$

$$\text{where } \vec{k} = n \vec{k}_o$$

$$\text{and } E = \left(\frac{2}{n+1} \right) E_o \text{ in the case of normal incidence.}$$

Any real medium, on the other hand, is not absolutely uniform, but has thermally excited fluctuations in the local polarizability per unit volume $\alpha(\vec{r}, t)$. In fact, we can write $\alpha(\vec{r}, t)$ as the sum of an average part

$\langle \alpha \rangle$, and a fluctuating part, $\delta\alpha(\vec{r}, t)$:

$$\alpha(\vec{r}, t) = \langle \alpha \rangle + \delta\alpha(\vec{r}, t). \quad (2.3)$$

It is $\langle \alpha \rangle$ which gives rise to the refraction of the incident light, with

$$n^2 = 1 + 4\pi \langle \alpha \rangle, \quad (2.4)$$

and, as we shall see, it is $\delta\alpha(\vec{r}, t)$ which produces the scattering.

If the fluctuations in $\alpha(\vec{r}, t)$ are small compared with $\langle \alpha \rangle$, we may conveniently use a perturbation approach to the problem.* The solution to the unperturbed system [$\delta\alpha(\vec{r}, t) = 0$] is, as we have seen, the refracted beam, $\vec{E}_M = \vec{E} e^{i(\vec{k} \cdot \vec{r} - \omega_0 t)}$. We then consider the perturbation $\delta\alpha(\vec{r}, t)$ on this solution. It will be convenient to refer to figure 2.1 below:

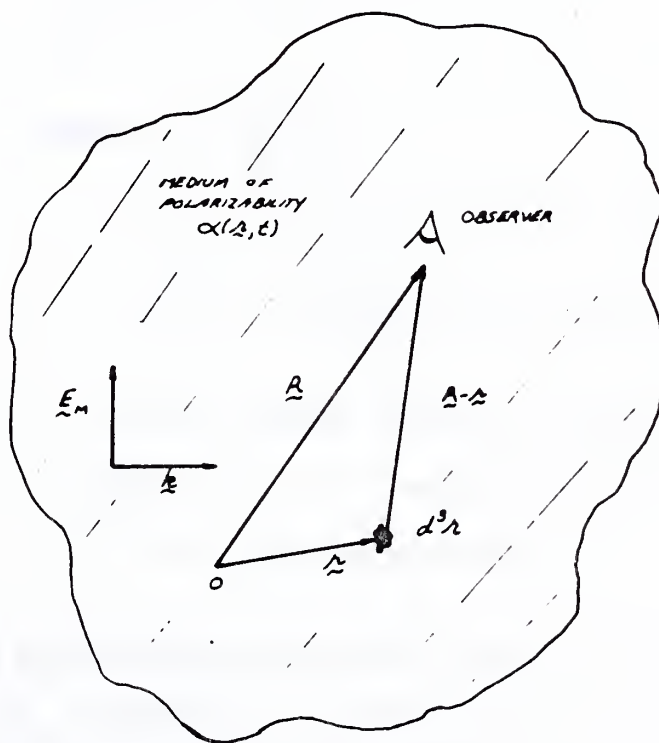


Fig. 2.1 The Scattering Geometry

* The same approach is called the "first Born approximation" when used in quantum mechanics.

For convenience, the observer is placed in the scattering medium. (Geometric optics can always remedy this later.) The macroscopic field in the medium $\vec{E}_M(\vec{r}, t)$ will induce a polarization in the (macroscopic) volume element, $d^3 r$

$$\delta \vec{P}(\vec{r}, t) = \delta\alpha(\vec{r}, t) \vec{E} e^{i(\vec{k} \cdot \vec{r} - \omega_0 t)} d^3 r , \quad (2.5)$$

where we have assumed at this point that $\delta\alpha$ is a scalar. This oscillating polarization will, in turn, radiate. We may then express the total amplitude of the electric field of the scattered light at the observing point \vec{R} in the far field as⁽²⁾

$$\vec{E}_s(\vec{R}, t) = \int_V \frac{1}{|\vec{R} - \vec{r}|} \frac{1}{<\epsilon>c_m^2} \hat{k}_s \times [\hat{k}_s \times \vec{P}(\vec{r}, t_r)] d^3 r , \quad (2.6)$$

$$\text{where } \hat{k}_s = \frac{(\vec{R} - \vec{r})}{|\vec{R} - \vec{r}|}$$

c_m = velocity of light in the medium

$$t_r = t - \frac{|\vec{R} - \vec{r}|}{c_m} \text{ (the retarded time)}$$

$<\epsilon>$ = average dielectric constant of the medium

$$<\epsilon>c_m^2 = c^2 \quad (c = \text{velocity of light in vacuum})$$

V = illuminated volume .

The dipole approximation we have used here is valid only in the far field, $R >> r$. If, in addition, we observe that the time variation in $\delta\alpha(\vec{r}, t)$ is very slow compared with that of $e^{i\omega_0 t}$, we may combine Eqs. (2.5 - 2.6) as

$$\begin{aligned} \vec{E}_s(\vec{R}, t) &= \frac{1}{<\epsilon>} \hat{k}_s \times (\hat{k}_s \times \vec{E}) \frac{e^{i(\vec{k}_s \cdot \vec{R} - \omega_0 t)}}{R} \\ &\quad \cdot \int_V \delta\alpha(\vec{r}, t) e^{i(\vec{k} - \vec{k}_s) \cdot \vec{r}} d^3 r , \end{aligned} \quad (2.7)$$

where \vec{k}_s is the wave vector of the scattered light, with magnitude $n k_0$, and where we have observed that $c_m = (c/n)$.

Equation (2.7) can be placed in a much more revealing form if the fluctuations in polarizability are decomposed into their Fourier components:

$$\delta\alpha(\vec{r}, t) = \frac{1}{(2\pi)^{3/2}} \int \delta\alpha(\vec{q}, t) e^{i\vec{q} \cdot \vec{r}} d^3 q . \quad (2.8)$$

Recalling that α is related to the dielectric constant (for a non-magnetic medium) through

$$\epsilon = 1 + 4\pi\alpha, \quad (2.9)$$

we may then express Eqs. (2.7-2.8) as

$$\begin{aligned} \vec{E}_s(\vec{R}, t) &= -\frac{1}{\langle \epsilon \rangle} \vec{k}_s \times (\vec{k}_s \times \vec{E}) \frac{e^{i(\vec{k}_s \cdot \vec{R} - \omega_0 t)}}{4\pi R} \\ &\cdot \frac{1}{(2\pi)^{3/2}} \int \delta\epsilon(\vec{q}, t) \left[\int_V e^{i(\vec{k}-\vec{k}_s + \vec{q}) \cdot \vec{r}} d^3 r \right] d^3 q . \end{aligned} \quad (2.10)$$

We recognize the bracketed portion of Eq. (2.10) as the three-dimensional delta function:

$$\int e^{i(\vec{k}-\vec{k}_s + \vec{q}) \cdot \vec{r}} d^3 r = (2\pi)^3 \delta^3(\vec{k} - \vec{k}_s + \vec{q}) . \quad (2.11)$$

Equations (2.10 - 2.11) contain the key to the understanding of the origin of the scattered light. For they indicate that of all the Fourier components of the fluctuation in dielectric constant, only that particular component whose wave vector is the difference between the wave vectors of the scattered and incident light is responsible for scattering in the direction

of observation. This particular component is appropriately called the "scattering fluctuation", with wave vector

$$\vec{k} = \vec{k}_s - \vec{k}. \quad (2.12)$$

A geometric representation of Eq. (2.12) gives additional insight into the scattering process:

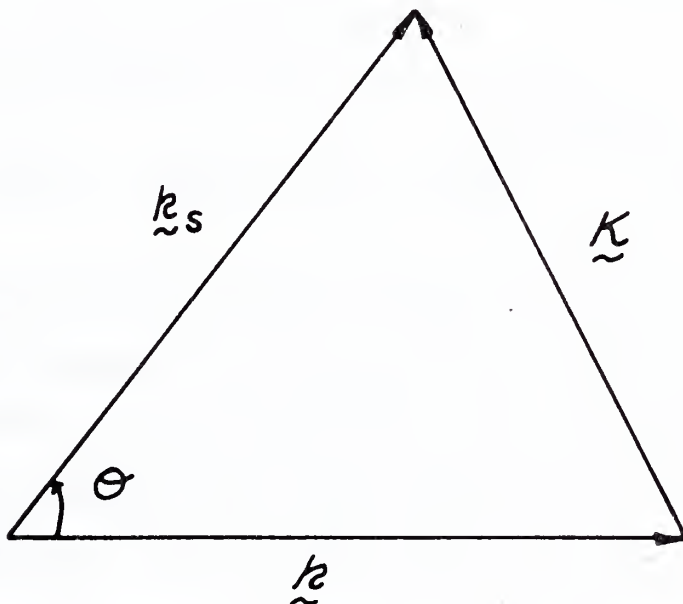


Fig. 2.2 Geometric Representation of the Scattering Process

From fig. 2.2, we may immediately write

$$K = 2k \sin\left(\frac{\theta}{2}\right) \quad (2.13a)$$

$$\text{or } \lambda = 2\lambda_f \sin\left(\frac{\theta}{2}\right) \quad (2.13b)$$

where θ is the scattering angle

λ_f is the wavelength of the scattering fluctuation, $\lambda_f = \frac{2\pi}{K}$

and λ is the wavelength of the incident and scattered light in the medium, $\lambda = \frac{2\pi}{k} = \frac{2\pi}{k_s} = \frac{2\pi}{nk_0}$.

The representation of the scattering process given in Eq. (2.13b) is a statement of the Bragg condition for the reflection of the incident beam by a "grating" of spacing, λ_f . This then connects the scattering of light with x-ray scattering from crystals and displays the underlying identity of these scattering processes.

We may now summarize Eqs. (2.10 - 2.12) as

$$\vec{E}_s(\vec{R}, t) = -\frac{1}{\langle \epsilon \rangle} \vec{k}_s \times (\vec{k}_s \times \vec{E}) \frac{e}{4\pi R} i(\vec{k}_s \cdot \vec{R} - \omega_0 t) (2\pi)^{3/2} \delta\epsilon(\vec{K}, t). \quad (2.14)$$

We thus see that the scattering process is a mapping of the fluctuation in dielectric constant of wave vector \vec{K} onto the amplitude of the electric field of the scattered light observed at a point \vec{R} . The time dependence of the scattered light exactly mirrors that of the fluctuation which produced it. To this point, however, we have had to say nothing specific about the nature or origin of this fluctuation. The beauty of the Einstein fluctuation approach to light scattering is that, once the general expression [Eq. (2.14)] for the electric field of the scattered light is obtained, one need only express $\delta\epsilon(\vec{K}, t)$ in a set of physically measurable variables appropriate to the particular system under investigation. For a solution, such a set consists of the solute concentration $C(\vec{R}, t)$, measured in grams of solute per cc of solution, the solution density $\rho(\vec{R}, t)$, in units of g/cc, and the solution temperature $T(\vec{R}, t)$ in °K. We may then express $\delta\epsilon(\vec{R}, t)$ as

$$\delta\epsilon(\vec{R}, t) = \left(\frac{\partial\epsilon}{\partial C}\right)_{\rho, T} \delta C(\vec{R}, t) + \left(\frac{\partial\epsilon}{\partial\rho}\right)_{C, T} \delta\rho(\vec{R}, t) + \left(\frac{\partial\epsilon}{\partial T}\right)_{C, \rho} \delta T(\vec{R}, t). \quad (2.15)$$

The last two terms in Eq. (2.15) are in general dominated by the contributions of the solvent alone, and these in turn are generally negligible compared with the first term*. We then express the fluctuation in dielectric constant as

$$\delta\epsilon(\vec{R}, t) = \left(\frac{\partial\epsilon}{\partial C}\right) \delta C(\vec{R}, t), \quad (2.16a)$$

which, upon Fourier transformation, becomes

$$\delta\epsilon(\vec{K}, t) = \left(\frac{\partial\epsilon}{\partial C}\right) \delta C(\vec{K}, t). \quad (2.16b)$$

The usually measured quantity is the index of refraction, n , instead of the dielectric constant, ϵ . For non-magnetic materials, $\epsilon = n^2$, so that we may write the fluctuation in dielectric constant as

$$\delta\epsilon(\vec{K}, t) = 2n \left(\frac{\partial n}{\partial C}\right) \delta C(\vec{K}, t). \quad (2.16c)$$

We may now proceed to calculate the intensity of the scattered light. Since the intensity, I , of light whose electric field is E may be expressed as $I = \frac{c}{8\pi} \langle |E|^2 \rangle_t$ where the symbol $\langle \rangle_t$ indicates a time average, we may combine Eqs. (2.2), (2.14) and (2.16c) to obtain the ratio of the intensity of the scattered light observed at \vec{R} to that of the incident light:

* This qualification will be made more explicit on page 42.

$$\frac{I_s(\vec{R})}{I_{\text{Inc}}} = \left(\frac{k_s}{n} \right)^4 \frac{\sin^2 \phi}{(4\pi R)^2} \left(2n \frac{\partial n}{\partial C} \right)^2 (2\pi)^3 \langle |\delta C(\vec{K}, t)|^2 \rangle_t , \quad (2.17)$$

where ϕ is the angle between \vec{k}_s and \vec{E} . This, of course, is the familiar dipole radiation pattern if $\langle |\delta C(\vec{K}, t)|^2 \rangle_t$ is angle-independent. The usual experimental condition is that $\phi = 90^\circ$, that is, \vec{E} is normal to the scattering plane. In this case, we see from Eq. (2.7) that the polarization of the scattered light is parallel to that of the incident light. For any other value of ϕ , Eq. (2.7) indicates that the polarization of the scattered light is no longer along \vec{E} , but the scattered light is still completely polarized. This will no longer be the case if the macromolecules are optically anisotropic, as will be discussed in section II.B.2.

It now remains to calculate $\langle |\delta C(\vec{K}, t)|^2 \rangle_t$. By the ergodic hypothesis, this is equal to the ensemble average of the quantity $|\delta C(\vec{K}, t)|^2$, which we indicate by $\langle |\delta C(\vec{r}, t)|^2 \rangle$. We then have, by definition, that

$$\langle |\delta C(\vec{K}, t)|^2 \rangle = \frac{1}{(2\pi)^3} \iint_{VV} \langle \delta C(\vec{r}, t) \delta C^*(\vec{r}', t) \rangle e^{-i\vec{K} \cdot (\vec{r} - \vec{r}')} d^3 r d^3 r'. \quad (2.18)$$

It is reasonable to assume that $\delta C(\vec{r}, t)$ is a stationary random process, and that $\langle \delta C(\vec{r}, t) \delta C^*(\vec{r}', t) \rangle$ is translationally invariant. Equation (2.18) then becomes simply

$$\langle |\delta C(\vec{K}, t)|^2 \rangle = \frac{V}{(2\pi)^3} \int_V \langle \delta C(\vec{r}, 0) \delta C^*(0, 0) \rangle e^{i\vec{K} \cdot \vec{r}} d^3 r . \quad (2.19)$$

The result presented in Eq. (2.19) is completely general and allows $\langle |\delta C(\vec{K}, t)|^2 \rangle$ to be calculated without any specializing assumptions. For example, $\langle \delta C(\vec{r}, 0) \delta C^*(0, 0) \rangle$, which is called the "spatial correlation function", can include a description of short and long-range molecular interactions if these effects are understood; or, conversely, measurement

of $\langle |\delta C(\vec{k}, t)|^2 \rangle$ can give this information, if the exact form of $\langle \delta C(\vec{r}, 0) \delta C^*(0, 0) \rangle$ is unknown. Similarly, the factor $e^{i\vec{k} \cdot \vec{r}}$ in Eq. (2.19) represents interference effects due to scattering from different portions of the same (large) molecule, or from different small molecules in a (large) region which are correlated due to molecular interactions. By "large", we mean of course regions sufficiently large that $\vec{k} \cdot \vec{r}$ is not negligibly close to zero over the entire region in which $\langle \delta C(\vec{r}, 0) \delta C^*(0, 0) \rangle$ is non-zero.

We can immediately write a closed-form expression for Eq. (2.19), if we make two assumptions which in reality are not restrictive. Let us assume that the solutions studied are of sufficient dilution that the spatial correlation function for the concentration fluctuations is zero beyond a molecular radius and a constant value within this radius. This simply means that the molecules are absolutely uncorrelated, except within their own dimensions. If we further assume that this molecular radius is sufficiently small so that $e^{i\vec{k} \cdot \vec{r}} \approx 1$ over the region in which the spatial correlation is non-zero, we have, from Eq. (2.19)

$$\langle |\delta C(\vec{k}, t)|^2 \rangle = \frac{V}{(2\pi)^3} \langle |\delta C_v(0, 0)|^2 \rangle v \quad (2.20)$$

where v is the volume of the macromolecule,

and C_v is the concentration in this volume.

It is important to repeat that the assumptions which yielded Eq. (2.20) from Eq. (2.19) are not restrictive, for we can always do a series of experiments at various concentrations and extrapolate the results to zero concentration. Furthermore, since $K = 2k \sin(\frac{\theta}{2})$ [Eq. (2.13a)], we can circumvent the restriction that $\vec{k} \cdot \vec{r}$ be small by also extrapolating the experimental results to zero angle. This double extrapolation is the

procedure followed in making a "Zimm Plot".⁽³⁾

We now proceed to calculate $\langle |\delta C_v(0,0)|^2 \rangle$. By definition, C_v is the microscopic concentration in g/cc. Hence,

$$C_v = \frac{n}{N_o} \frac{M}{V} \quad (2.21)$$

where n = number of molecules in a molecular volume v

N_o = Avogadro's number

M = molecular weight of the molecule

Thus we obtain

$$\langle |\delta C_v(0,0)|^2 \rangle = \frac{\langle (\delta n)^2 \rangle M^2}{N_o^2 v^2} . \quad (2.22)$$

Let there be N molecules in the illuminated volume, V . Then, since we assume no correlation among the molecules, we have the average number of molecules in a molecular volume as

$$\langle n \rangle = N\left(\frac{v}{V}\right) . \quad (2.23)$$

We may now proceed to calculate $\langle (\delta n)^2 \rangle$ as given by

$$\langle (\delta n)^2 \rangle = \langle (n - \langle n \rangle)^2 \rangle = \sum_{n=0}^1 P(n)(n - \langle n \rangle)^2 , \quad (2.24)$$

where $P(n)$ is the probability that there are n molecules in a molecular volume. Since the probability that there be one molecule in v is simply $N\left(\frac{v}{V}\right)$, and that there be none is therefore $1 - N\left(\frac{v}{V}\right)$, we have, from Eqs.

(2.23) and (2.24), that

$$\begin{aligned} \langle (\delta n)^2 \rangle &= \left[1 - N\left(\frac{v}{V}\right) \right] \left[- N\left(\frac{v}{V}\right) \right]^2 + \left[N\left(\frac{v}{V}\right) \right] \left[1 - N\left(\frac{v}{V}\right) \right]^2 \\ &= N\left(\frac{v}{V}\right) \left[1 - N\left(\frac{v}{V}\right) \right] \\ &\approx N\left(\frac{v}{V}\right) . \end{aligned} \quad (2.25)$$

Since the solution of macromolecules is assumed very dilute, $N(\frac{V}{V}) \ll 1$ and the approximation made in Eq. (2.25) is quite good.

We have thus obtained an expression for $\langle |\delta C_v(0,0)|^2 \rangle$ which is given solely in terms of measurable quantities. Combining Eqs. (2.22) and (2.25), we see that

$$\langle |\delta C_v(0,0)|^2 \rangle = NM^2 \cdot \frac{1}{vVN_o^2} \quad (2.26a)$$

or

$$\langle |\delta C_v(0,0)|^2 \rangle = C \frac{M}{N_o} \frac{1}{v} \quad (2.26b)$$

where $C = \frac{NM}{N_o V}$ is the average solute concentration in the illuminated volume expressed in g/cc. Combining Eqs. (2.26a) and (2.26b) with the expressions of Eqs. (2.17) and (2.20) we may write the ratio of the scattered to incident light intensities as

$$\frac{I_s(\vec{R})}{I_{Inc}} = \left(\frac{k_s}{n} \right)^4 \frac{\sin^2 \phi}{(4\pi R)^2} \left(2n \frac{\partial n}{\partial C} \right)^2 \frac{CMV}{N_o} \quad (2.27a)$$

or

$$\frac{I_s(\vec{R})}{I_{Inc}} = \left(\frac{k_s}{n} \right)^4 \frac{\sin^2 \phi}{(4\pi R)^2} \left(2n \frac{\partial n}{\partial C} \right)^2 \frac{NM^2}{N_o^2 V} \quad (2.27b)$$

simp.

Since the index of refraction, n , the refractive index increment, $\frac{\partial n}{\partial C}$ (cc/g), and the solute concentration, $C(g/cc)$, are all readily measured in the laboratory, we see that Eq. (2.27a) allows the determination of molecular weights of macromolecules. This expression has been of great utility in macromolecular physical chemistry and remains today as one of the chief methods of determining molecular weights.

Although Eqs. (2.27a) and (2.27b) are identical, by writing them in these two different ways, we gain insight on the scattering process. Equation (2.27b) indicates that the intensity of the scattered light is proportional to the number of macromolecules in the illuminated volume and to the square of their molecular weight. This expression then connects the Einstein fluctuation approach to the scattering problem with that of Rayleigh. It is appropriate to outline briefly the Rayleigh method and display this connection precisely. Instead of considering α , the polarizability per unit volume of the solution, we treat of the molecular polarizability, α_m . The incident electric field induces a radiating polarizability in each molecule,

$$\vec{p} = \alpha_m \vec{E}_{\text{Inc}} . \quad (2.28)$$

Proceeding as we did in the continuum case, we see that

$$\vec{E}_s \propto \sum_{i=1}^N (\alpha_m)_i \vec{E}_{\text{Inc}} \quad (2.29)$$

and that

$$I_s \propto \left\langle \sum_{i=1}^N \sum_{j=1}^N (\alpha_m)_i \vec{E}_{\text{Inc}} \cdot (\alpha_m)_j \vec{E}_{\text{Inc}}^* \right\rangle . \quad (2.30)$$

Since all the molecules are assumed strictly non-interacting, the scattering is completely incoherent, and the average value of all cross-terms in Eq. (2.30) vanishes. Hence, we have

$$\frac{I_s}{I_{\text{Inc}}} \propto N \alpha_m^2 . \quad (2.31)$$

Since α_m is itself proportional to the amount of polarizable material per molecule, that is, the molecular weight, we then obtain

$$\frac{I_s}{I_{Inc}} \propto NM^2. \quad (2.32)$$

This is, of course, in agreement with Eq. (2.27b), as it must be, since the Rayleigh approach is completely valid in the case of small, non-interacting molecules, which we have assumed to be the experimental regime. We shall treat the Rayleigh method in somewhat greater detail in section II.B.2 when we consider optically anisotropic molecules.

In either approach to the scattering problem, we perform averages which of necessity lose information. Indeed, by obtaining the ensemble average of $|\delta C(\vec{k}, t)|^2$, we lose all information on the spectrum of the scattered light. We shall regain this information when we consider the temporal history of the fluctuations and obtain the spectrum in section II.D.

Equation (2.27a) may be rewritten in a form which allows us to compare directly the intensity of the light scattered by various macromolecular solutions and also by other materials such as pure fluids. To do this, it is convenient to define the "Rayleigh ratio" \mathbf{R} for a system whose scattered light has uniform intensity* independent of the scattering angle θ as follows:

$$\mathbf{R} = \frac{I_s}{I_{Inc}} \frac{R^2}{2V \sin^2 \phi}. \quad (2.33)$$

By inspection of Eq. (2.33), we see that the Rayleigh ratio has units of reciprocal length, usually written in cm^{-1} . Hence, \mathbf{R} is seen to be an attenuation coefficient, and we will discuss this aspect of the Rayleigh ratio in greater detail when we consider the problem of multiple

* Such scattering is usually called "isotropic", which is not to be confused with isotropic polarizability. If the scattering is not isotropic, then the Rayleigh ratio must be qualified; e.g., $\mathbf{R}_{\theta=0^\circ}$ or $\mathbf{R}_{\theta=90^\circ}$ etc.

scattering.

For macromolecular solutions, we obtain from Eqs. (2.27b) and (2.33) that

$$\mathbf{R} = \frac{(k_s^4 / n)^4}{(4\pi)^2} \left[\sqrt{2} n \left(\frac{\partial n}{\partial C} \right) \right]^2 \frac{CM}{N_o} , \quad (2.34a)$$

or

$$\mathbf{R} = \frac{k_o^4}{(4\pi)^2} \left[\sqrt{2} n \left(\frac{\partial n}{\partial C} \right) \right]^2 \frac{CM}{N_o} . \quad (2.34b)$$

For such solutions, \mathbf{R} is often expressed as

$$\mathbf{R} = \mathbf{K} CM \quad (2.35)$$

where \mathbf{K} is given by

$$\mathbf{K} = \frac{k_o^4}{(4\pi)^2} \left(\sqrt{2} n \frac{\partial n}{\partial C} \right)^2 \frac{1}{N_o} . \quad (2.36)$$

We see that \mathbf{K} has units of $(\text{cm/g})^2$.

The work of this thesis and that of much of the current research in this field treats of dilute aqueous solutions of biological macromolecules (e.g., enzymes, nucleic acids, viruses, etc.). For such molecules the value of $(\frac{\partial n}{\partial C})$ is remarkably independent of the particular species as we can see in Table 2.1 below:

Table 2.1
 Refractive Index Increment $\frac{\partial n}{\partial C}$
 For Various Biological Macromolecules

Macromolecule	M	$\frac{\partial n}{\partial C}$ (cc/g)	Measured @ λ_0 $^{\circ}$ (Å)
Lysozyme ^a	14,000	0.1888	5460
DNA ^b	6×10^6	0.188	4350
TMV ^c	40×10^6	0.194	4360

- (a) Bruzzesi, M. R., Chiancone, E., and Antonini, E., Biochemistry, 4, 1796 (1965).
- (b) Reichmann, M. E., Rice, S. A., Thomas, C. A., and Doty, P., J. Am. Chem. Soc., 76, 3047 (1954).
- (c) Boedeker, H., and Simmons, N. S., J. Am. Chem. Soc., 80, 2550 (1958).

The results in this table cover the complete gamut of biological macromolecules from the small protein lysozyme to the large nucleic acid DNA to the very large plant virus TMV, and are quite representative of the values obtained for all such molecules. We thus have the somewhat surprising but very convenient result that **K** is roughly constant for all dilute aqueous solutions of biological macromolecules. We may then calculate the value of **K** for the 6328 $^{\circ}$ Å laser line, using $n \approx 1.33$ and $\frac{\partial n}{\partial C} \approx 1.90$:

$$\mathbf{K} \approx 1.3 \times 10^{-7} (\text{cm/g})^2 , \quad (2.37)$$

The fact that **K** is such a universal constant means that the Rayleigh ratios of all dilute solutions of biological molecules are related, to a reasonable approximation, to their respective products of $M \times C^*$. It will be helpful to determine **R** for one such molecule and then values for **R** for all other molecules are obtained immediately through $M \times C$. One of the systems studied in this thesis is a 1% (.01 g/cc) solution of the enzyme lysozyme, $M \approx 14,000$. For these values of M and C , together with our expression for **K** in Eq. (2.37), we then have

$$\mathbf{R}_{LYS,1\%} = 20 \times 10^{-6} \text{ cm}^{-1} . \quad (2.38)$$

We wish to compare this value with the Rayleigh ratios of various common liquids which have been used as "standards" in light scattering. Although there is some variation in the measured values of these Rayleigh ratios, the values presented in Table 2.2 below are representative and will allow us to compare the value of **R** for lysozyme with reasonable accuracy.

The values are taken from the review of light scattering by Fabelinskii,⁽⁴⁾ and all are corrected to 6328A:

Table 2.2
Rayleigh Ratios of Representative Liquids

Material	$10^6 \mathbf{R} (\text{cm}^{-1})$
Water	0.6
Ether	2.6
Carbon Tetrachloride	3.6
Benzene	6.2
Toluene	9.0
Carbon Disulfide	30

* For very large or interacting molecules, **R** must be measured by extrapolation to zero scattering angle and zero concentration as described previously.

It is clear from Table 2.2 that even a 1% solution of lysozyme scatters about the same amount of light as the most intense scatterers among the pure liquids. It is also obvious that, when making absolute intensity measurements of a solution that scatters about as much as a 1% lysozyme solution, the contribution to the scattered light due to the solvent alone must be subtracted. Hence, the expression for the scattered light's intensity [Eqs. (2.27a) and (2.27b)] refers actually to the "excess intensity" -- that of the solution less that of the solvent.

A significant result we have used thus far is that the light observed at a point \vec{R} arises due to a Bragg reflection of the incident light from a fluctuation in dielectric constant with the specific wave vector \vec{k} . This, of course, is true as shown in Eq. (2.10), but only if the scattered light has suffered just a single Bragg reflection when it has left the scattering cell. The following geometry (Fig. 2.3) also is consistent with Eq. (2.10) and is called "multiple scattering".

A fluctuation in dielectric constant of wave vector \vec{k} causes scattering at an angle θ in a direction \hat{k}_s as described in Eq. (2.10). However, light which is scattered at angle θ' due to the fluctuation \vec{k}' can be rescattered by the fluctuation \vec{k}'' to produce scattering in the direction \hat{k}_s . We have, of course, no means of distinguishing between these two processes in an actual experiment, except that some of the multiply scattered light may be depolarized. We can, however, calculate the probability of such a two-process event. To do this we rewrite Eq. (2.33) as

$$\frac{I_s(\vec{R})}{I_{\text{Inc}}} = \frac{2V \sin^2 \phi}{R^2} \mathbf{R} . \quad (2.39)$$

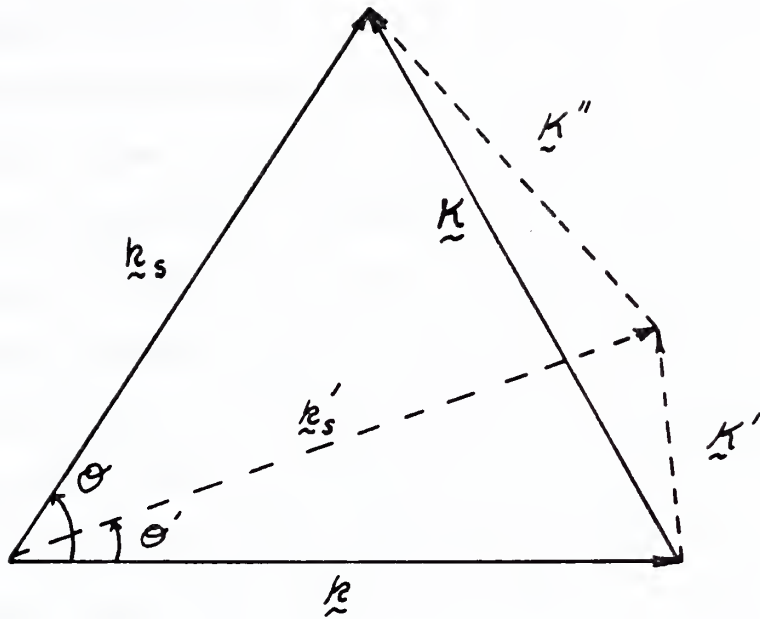


Fig. 2.3 Multiple Scattering Process

The power \mathbf{P}_{Inc} in the incident beam is its intensity times the beam area, \mathbf{A} . Similarly, the power scattered to a point \vec{R} due to the scattered light is $\mathbf{P}_s(\vec{R}) = I_s(\vec{R})R^2 d\Omega$, where $d\Omega$ is the observer's solid angle of acceptance. Hence, we have from Eq. (2.39) that

$$\frac{\mathbf{P}_s(\vec{R}, d\Omega)}{\mathbf{P}_{\text{Inc}}} = 2L \mathbf{R} \sin^2 \phi d\Omega, \quad (2.40)$$

where L is the length of the incident beam, $L = \frac{V}{A}$

The integral over $d\Omega$ is straightforward, and we thus obtain the following for the ratio of the total scattered power to the incident power:

$$\frac{\left(\mathbf{P}_s \right)_{\text{TOT}}}{\mathbf{P}_{\text{Inc}}} = \frac{16\pi}{3} \mathbf{R} L. \quad (2.41)$$

This displays the Rayleigh ratio in a more physically meaningful way, namely, as an attenuation coefficient. For example, $R_{1\%, \text{LYS}} = 20 \times 10^{-6} \text{ cm}^{-1}$. Hence, the incident power is reduced only about 3/100 of a percent in traversing a centimeter of a 1% lysozyme solution. Thus, multiply scattered light will be suppressed below singly scattered light by about this same ratio for the same path length. In general, the scattering geometry can be so arranged that the scattered light has only a very small distance to travel before exiting the cell. Hence, multiple scattering in systems with Rayleigh ratios of a 1% lysozyme, or even two or three orders of magnitude greater, can easily be made negligible and Eq. (2.17) is valid. We shall see, in addition, when we consider the effects of multi-component scattering in Chapter IV, that the effect of multiple scattering on the observed spectrum of the scattered light is far less than on the intensity. Hence, in light of the above comments on the intensity, we see that multiple scattering processes have negligible effect on the spectrum of the scattered light for any reasonable experimental situation.

We have thus obtained an expression for the expected intensity of the light scattered by macromolecular solutions. While this intensity was shown to be comparable to or greater than that from pure fluids (and much greater than that from solids, whose Rayleigh ratios are of the order of $1 \times 10^{-8} \text{ cm}^{-1}$), a spectrometer of ultra-high resolving power will be required to resolve the spectrum of this light, as it will be shown to be extremely narrow. This problem will be discussed in section II.D and III. B.

In the present section, we have shown that fluctuations in the local dielectric constant which arise due to concentration fluctuations will

scatter light. We have treated the medium's polarizability as a scalar in this development. We now proceed to show, in section II.B.2, that there is another mechanism for scattering light which arises if the molecules which make up this medium have an anisotropic polarizability.

(2) Anisotropic Molecules

a) Theory of Anisotropy Scattering

In the development of the preceding section, we assumed that a solution of macromolecules is optically isotropic. This assumption is always correct, but only in the sense that the index of refraction of such a solution is independent of the polarization or direction of propagation of the light used to measure the index, even if the macromolecules suspended in the solution are themselves highly anisotropic.⁽⁵⁾ This result follows immediately from the fact that we may write the index of refraction of a solution of macromolecules as

$$n = \left[1 + 4\pi \frac{N_s}{V} \langle \overset{\rightarrow}{\alpha}_s \rangle + 4\pi \frac{N}{V} \langle \overset{\rightarrow}{\alpha}_m \rangle \right]^{1/2}, \quad (2.42)$$

where $\overset{\rightarrow}{\alpha}_s$ is the polarizability tensor of a single solvent molecule;

$\frac{N_s}{V}$ is the number density of solvent molecules;

$\overset{\rightarrow}{\alpha}_m$ is the polarizability tensor of a single macromolecule;

$\frac{N}{V}$ is the number density of the macromolecules

Now, if the principal polarizabilities of the solvent molecule and the macromolecule are α'_1 , α'_2 , α'_3 and α_1 , α_2 , α_3 respectively, then we have the trivial result that

$$\langle \overset{\rightarrow}{\alpha}_s \rangle = \frac{1}{3} (\alpha'_1 + \alpha'_2 + \alpha'_3) \quad (2.43a)$$

$$\langle \overset{\rightarrow}{\alpha}_m \rangle = \frac{1}{3} (\alpha_1 + \alpha_2 + \alpha_3). \quad (2.43b)$$

That is, $\langle \overset{\leftrightarrow}{\alpha}_s \rangle$ and $\langle \overset{\leftrightarrow}{\alpha}_m \rangle$ are scalars, all off-diagonal elements averaging out. Hence, to repeat, from the point of view of index of refraction, a macromolecular solution is isotropic.*

As we will discuss in what follows, the intensity of the light scattered by macromolecular solutions is proportional to $\langle \overset{\leftrightarrow}{\alpha}_m^2 \rangle$, not $\langle \overset{\leftrightarrow}{\alpha}_m \rangle^2$. Hence, we will see that if the molecular polarizability is anisotropic (i.e., α_1, α_2 , and α_3 are not all equal), the light scattered by these molecules will not be completely polarized. This is due to the fact, as will be described below, that the "anisotropy scattering" (i.e., that portion of the light which is scattered due to the fact that the scattering molecules are optically anisotropic) is nearly completely unpolarized even if the incident light source is polarized. Hence, the light scattered by a solution of anisotropic macromolecules will contain a component with the same polarization as the incident light, which component comprises a contribution from concentration fluctuations and scattering due to optical anisotropy. The scattered light will also contain a component with polarization different from the incident light. This depolarized component is due solely to scattering which arises from the molecular anisotropy. The two components which arise due to the optical anisotropy of the molecules are called, collectively, the "anisotropy scattering".

It is desirable at this point to discuss the origins of the molecular anisotropy which necessitates these additional calculations. There

* When we performed the ensemble averages which yielded Eq. (2.43), we naturally assumed the molecules to be randomly oriented; if they are partially aligned by an external mechanism, the off-diagonal elements do not vanish. This is the principle behind the technique of electric and flow birefringence.

are two distinct sources*. First the molecules may have different indices of refraction along their different axes; this would arise from varying densities of polarizable electrons, and is therefore an intrinsic property of the molecule in question. It is therefore natural to call this the intrinsic anisotropy of the molecule, although this is not a universal terminology. Second, even a molecule with a uniform index of refraction m will have different polarizabilities along different directions, if it is immersed in a medium which has a different index of refraction, n . This anisotropy can be regarded as arising from surface charges which, except for the trivial case of a sphere, are so arranged as to incline the induced polarization slightly away from the external field. For example, it is a straightforward result of electrostatics⁽⁶⁾ that, if a dielectric ellipsoid of index m and principal axes a, b, c is immersed in a medium of index n , then the polarizabilities of the ellipsoid are

$$\alpha_{a,b,c} = \frac{V}{4\pi} \frac{1}{L_{a,b,c} + \frac{1}{(\frac{m}{n})^2 - 1}} \quad (2.44)$$

$$\text{where } L_a = \int_0^\infty \frac{abc}{2(s+a^2)^{3/2} (s+b^2)^{1/2} (s+c^2)^{1/2}} ds$$

with cyclic permutations for L_b, L_c , and

where V = volume of ellipsoid.

Since $L_a \neq L_b \neq L_c$ in general, the resulting polarizability of such an ellipsoid is not a scalar; that is, the particle is optically anisotropic.

Anisotropy of this type, resulting solely from geometric properties of

* We neglect here molecules so large that the incident beam is actually refracted by them and thus travels in a different direction inside the molecule than outside.

the molecule, is usually called form anisotropy.

We may now proceed to obtain an expression for the effect of such optical anisotropy on the intensity of the scattered light. We use the index m on $\hat{\alpha}_m$ to distinguish this molecular polarizability from that of the solution, $\hat{\alpha}$, employed in section II.B.1.

If we express the molecular polarizability in the coordinate system defined by its principal axes $x'y'z'$, it will of course be diagonal. We place the origin of this coordinate system at the origin of the laboratory coordinate system. Let the polarized plane wave $\left[\hat{x}E_x e^{i(kz - \omega_0 t)} + \hat{y}E_y e^{i(kz - \omega_0 t)} \right]$ be incident upon the molecule. This is summarized in fig. 2.4, below:

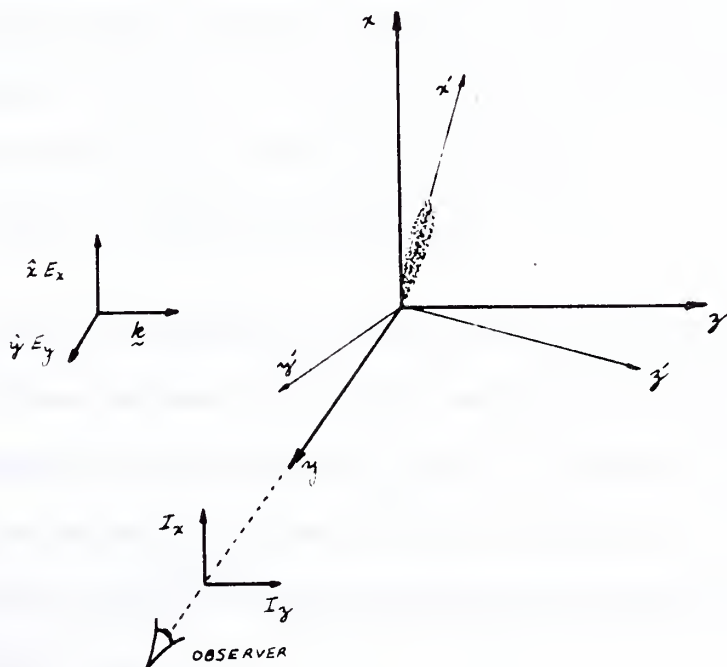


Fig. 2.4 Geometry for the Observation of Light Scattered by Anisotropic Molecules

We orient the polarized incident light with components of the electric field along the x and y axes so that we may obtain results appropriate to unpolarized light as well as polarized light. This is required to interpret the experimental literature, nearly all of which is obtained with unpolarized incident light.

The depolarization ratio ρ is defined as the ratio of the intensity of light scattered with polarization \hat{z} , called I_z , to that with polarization \hat{x} , called I_x , as seen by an observer looking along the y axis. The subscript u, v, or h is attached to ρ to indicate whether the incident light is unpolarized, has polarization along \hat{x} , or has polarization along \hat{y} .

We obtain the depolarization ratio most conveniently by considering scattering by individual molecules, since it is the molecular anisotropy which causes the depolarization. Let there be N molecules in the illuminated volume. The electric field of the incident light induces a dipole moment $\vec{p}(\vec{r}, t)$ in each macromolecule:

$$\vec{p}(\vec{r}, t) = \vec{\alpha}(\vec{r}, t) \cdot \vec{E} e^{i(kz - \omega_0 t)}. \quad (2.45)$$

Here, \vec{E} is the microscopic electric field in the vicinity of the molecule. Since we wish to form only the depolarization ratio, an exact expression for E in terms of E_0 is of no concern to us. Now, from Eq. (2.6), we may write the ratio of the z component to the x component of the electric field of the scattered light, as seen by an observer on the y axis, as

$$\frac{E_z}{E_x} = \frac{\sum_{i=1}^N [\ddot{p}_z(\vec{r}, t)]_i}{\sum_{l=1}^N [\ddot{p}_x(\vec{r}, t)]_l}. \quad (2.46)$$

If we observe that molecular reorientation times are quite long compared with the period of the incident light, we may rewrite Eq. (2.46) using Eq. (2.45) as:

$$\frac{E_z}{E_x} = \frac{\sum_{i=1}^N (-\omega_0^2) [p_z(\vec{r}, t)]_i}{\sum_{l=1}^N (-\omega_0^2) [p_x(\vec{r}, t)]_l},$$

and therefore

$$\frac{E_z}{E_x} = \frac{\sum_{i=1}^N [p_z(\vec{r}, t)]_i}{\sum_{l=1}^N [p_x(\vec{r}, t)]_l}. \quad (2.47)$$

We then immediately obtain the ratio of the intensity of light scattered with electric field polarization z to that with electric field polarization x as seen by an observer on the y axis, as:

$$\frac{I_z}{I_x} = \frac{\left\langle \sum_{i=1}^N \sum_{j=1}^N [p_z(\vec{r}, t)]_i [p_z^*(\vec{r}, t)]_j \right\rangle}{\left\langle \sum_{l=1}^N \sum_{m=1}^N [p_x(\vec{r}, t)]_l [p_x^*(\vec{r}, t)]_m \right\rangle}. \quad (2.48)$$

Since we assume the molecules are completely independent, the scattering is incoherent, the average value of all cross-terms is zero, and Eq. (2.48) becomes simply

$$\frac{I_z}{I_x} = \frac{N \langle |p_z(\vec{r}, t)|^2 \rangle}{N \langle |p_x(\vec{r}, t)|^2 \rangle}.$$

Hence, we have

$$\frac{I_z}{I_x} = \frac{\langle |p_z(\vec{r}, t)|^2 \rangle}{\langle |p_x(\vec{r}, t)|^2 \rangle}. \quad (2.49)$$

To evaluate Eq. (2.49) in terms of the principal polarizabilities of the molecule, we observe that in the principal axes (molecular) coordinate system, indicated by primes, we have:

$$\vec{p}'(\vec{r}', t) = \vec{\alpha}'_m(\vec{r}', t) \cdot \vec{E}'(\vec{r}', t) \quad (2.50)$$

where of course, $\vec{\alpha}'_m$ is diagonal. Let \vec{T} be the transformation matrix which links a vector in the molecular coordinate system to the laboratory system, i.e.,

$$\begin{aligned} \vec{p}(\vec{r}, t) &= \vec{T} \cdot \vec{p}'(\vec{r}', t) \\ \vec{E}(\vec{r}, t) &= \vec{T} \cdot \vec{E}'(\vec{r}', t). \end{aligned} \quad (2.51)$$

then,

$$\vec{p}(\vec{r}, t) = [\vec{T} \cdot \vec{\alpha}'(\vec{r}', t) \cdot \vec{T}^{-1}] \cdot \vec{E}(\vec{r}, t). \quad (2.52)$$

We then may rewrite Eq. (2.49) using Eq. (2.52) to obtain:

$$\frac{I_z}{I_x} = \frac{\langle |[\vec{T} \cdot \vec{\alpha}'(\vec{r}', t) \cdot \vec{T}^{-1}] \cdot \vec{E}(\vec{r}, t)|^2 \rangle_z}{\langle |[\vec{T} \cdot \vec{\alpha}'(\vec{r}', t) \cdot \vec{T}^{-1}] \cdot \vec{E}(\vec{r}, t)|^2 \rangle_x}. \quad (2.53)$$

The ensemble averages indicated in Eq. (2.53) are equivalent to averaging the quantities enclosed in the average signs over all molecular orientations. This is most conveniently done by expressing the relationship between the molecular and laboratory coordinates in terms of the Eulerian angles.⁽⁷⁾ The tedious integration over all orientations then yields⁽⁸⁾

$$\frac{I_z}{I_x} = \frac{(E_x^2 + E_y^2) [(\frac{1}{15})(\Delta - \beta)]}{E_x^2 [\frac{1}{5}\Delta + \frac{2}{15}\beta] + E_y^2 [\frac{1}{15}(\Delta - \beta)]} \quad (2.54)$$

$$\text{where } \Delta = \alpha_1^2 + \alpha_2^2 + \alpha_3^2$$

$$\beta = \alpha_1 \alpha_2 + \alpha_1 \alpha_3 + \alpha_2 \alpha_3$$

We now define expressions for the depolarization ratio for three particle cases:

$$\frac{I_z}{I_x} = \rho_u \quad E_x = E_y \quad (2.55a)$$

$$\frac{I_z}{I_x} = \rho_v \quad E_x \neq 0, E_y = 0 \quad (2.55b)$$

$$\frac{I_z}{I_x} = \rho_h \quad E_x = 0, E_y \neq 0 \quad (2.55c)$$

From the value of (I_z/I_x) given in Eq. (2.54) and the definitions in Eq. (2.55), we have

$$\rho_u = \frac{2(\Delta - \beta)}{4\Delta + \beta} \quad (2.56a)$$

$$\rho_v = \frac{(\Delta - \beta)}{3\Delta + 2\beta} \quad (2.56b)$$

$$\rho_h = 1 \quad (2.56c)$$

The most frequently quoted values in the literature are those of ρ_u .

However, combining Eqs. (2.56a) and (2.56b), we obtain

$$\rho_v = \frac{\rho_u}{2} / \left(1 - \frac{1}{2} \rho_u\right) \quad (2.57)$$

Since ρ_u is usually quite small ($\sim .01$), Eq. (2.57) indicates that

$$\rho_v = \frac{\rho_u}{2} \quad (2.58)$$

is an adequate approximation (error $\lesssim 1\%$) for all practical cases.

Equations (2.56a) and (2.56b) display the ratio of the intensity of light scattered with electric field polarized along \hat{z} to that with electric field polarized along \hat{x} . In each case, the ratio goes to zero if $\Delta = \beta$, that is, if all components of the polarizability tensor are the same. Even if the incident light is unpolarized, the scattered light is completely polarized if the molecules are optically isotropic.

However, as displayed in Eqs. (2.56a) and (2.56b), the depolarization ratios do not indicate the origins of the contributions to I_x and I_z . We would like to re-express our results in such a way as to show that, when the molecule is anisotropically polarizable, light scattered with electric field polarized in the same direction as that of the incident light contains contributions both from the diagonal and off-diagonal components of the polarizability tensor, and how this affects molecular weight determinations via light scattering.

We begin by observing that the expression given for the index of refraction of a macromolecular solution in Eq. (2.42), combined with Eq. (2.27), indicates that the intensity of the light scattered due to concentration fluctuations alone, here called I_C , is proportional to $\langle \vec{\alpha}_m^2 \rangle^2$. Thus, Eq. (2.38) then yields

$$I_C \propto \langle \vec{\alpha}_m^2 \rangle^2 = \frac{1}{3}[(\alpha_1 + \alpha_2 + \alpha_3)]^2 . \quad (2.59)$$

This expression is valid so long as the concentration fluctuations can be considered not to disturb the optical isotropy of the solution. This assumption is quite reasonable, since the concentration fluctuations are described by temporal and spatial variations in number density, and make no reference to the orientation of the molecules. For interacting molecules, this assumption breaks down, but we have assumed a system of

sufficient dilution to obviate this difficulty.

We now rewrite Eqs. (2.56a) and (2.56b) in terms of $\langle \vec{\alpha}_m \rangle^2$ and obtain, by algebraic manipulation, that

$$\rho_u = \frac{\frac{6}{45}(\Delta - \beta)}{\langle \vec{\alpha}_m \rangle^2 + \frac{7}{45}(\Delta - \beta)} \quad (2.60a)$$

$$\rho_v = \frac{\frac{3}{45}(\Delta - \beta)}{\langle \vec{\alpha}_m \rangle^2 + \frac{4}{45}(\Delta - \beta)} \quad (2.60b)$$

By definition of the depolarization ratios, the denominators of Eqs.

(2.60a) and (2.60b) are proportional to I_x . In the absence of anisotropy (i.e., when $\Delta = \beta$), we see that I_x is proportional to $\langle \vec{\alpha}_m \rangle^2$ and hence, from Eq. (2.59), all the scattered light is due to concentration fluctuations. However, if $\Delta \neq \beta$, I_x is no longer proportional to $\langle \vec{\alpha}_m \rangle^2$, but rather another term is present, either $\frac{4}{45}(\Delta - \beta)$ or $\frac{7}{45}(\Delta - \beta)$, depending on whether the incident light is polarized along \hat{x} or unpolarized. We define as anisotropy scattering the sum of the intensity of all the scattered light not due to concentration fluctuations.

Then, calling the anisotropy scattering I_A , we have

$$I_A \propto \frac{13}{45}(\Delta - \beta) \quad (2.61a)$$

(incident light unpolarized)

$$I_A \propto \frac{7}{45}(\Delta - \beta) \quad (2.61b)$$

(incident light polarized along x)

Hence, Eqs. (2.60a) and (2.60b) become

$$\rho_u = \frac{\frac{6}{13} I_A}{I_C + \frac{7}{13} I_A} \quad (2.62a)$$

$$\rho_v = \frac{\frac{3}{7} I_A}{I_C + \frac{4}{7} I_A} \quad (2.62b)$$

We see, then, that the effect of optical anisotropy is to add a contribution to the polarized part of the scattered light, as well as to bring about depolarization. In fact, if the anisotropy scattering were very large compared with that due to concentration fluctuation scattering, Eqs. (2.62a) and (2.62b) indicate that ρ_u and ρ_v would approach $\frac{6}{7}$ and $\frac{3}{4}$, respectively. In the case of pure liquids, the anisotropy scattering is often sufficiently large that the depolarization ratio for the anisotropy scattering alone has been measured verifying that $\rho_u = \frac{6}{7}$ for pure anisotropy scattering in various liquids.⁽⁹⁾ This is facilitated in the case of liquids by the fact that the anisotropy scattering has an extremely broad spectrum (molecular reorientation times are very short) which can be readily separated from other sources of scattering (Brillouin scattering and scattering from entropy fluctuations) using a spectrograph or Fabry-Perot interferometer. In the nematic liquid crystal methoxy benzyladine N-butyl aniline (MBBA), anisotropy scattering is vastly larger than any other source of scattering, and ρ_v was shown to be accurately $\frac{3}{4}$ by Litster and Stinson.⁽¹⁰⁾ Unfortunately, measurement of the depolarization ratio for pure anisotropy scattering in a macromolecular solution has not yet been reported. The measurement is extremely difficult for such solutions, both because $I_A \ll I_C$, and because the spectrum of each contribution is centered at the frequency of the incident light.

If one is to use intensity measurement to determine molecular weight, via Eq. (2.27), it is clear that all of the anisotropy scattering must be subtracted, not just the depolarized part, as was first pointed out by Cabannes.⁽¹¹⁾ However, in solutions of macromolecules, the anisotropy scattering is generally so slight as to make the so-called "Cabannes factor" unity. This is not at all the case in pure liquids, in which the anisotropy scattering may be several times larger than all other sources of scattering combined.⁽¹²⁾ In the case of asymmetric gases, e.g., air, the anisotropy scattering is sufficiently large (several percent) that Eq. (2.27) gives an erroneous value of Avogadro's number when the molecular weight of the gas is treated as the known parameter. It was this very fact that led Lord Rayleigh to make the first explanation of anisotropy scattering⁽¹³⁾ in 1918.

b) Critique of Literature on Depolarization Measurements

We now turn to a consideration of the experimentally determined values of the depolarization ratios. During an investigation of the protein serum albumin⁽¹⁴⁾ in this laboratory, the depolarization ratio ρ_v was measured⁽¹⁵⁾ and found to be $\lesssim 10^{-4}$. This was quite surprising because the prevailing value^(16,17) in the literature* for serum albumin is $\rho_v \gtrsim 0.01$. However, in a significant letter⁽¹⁸⁾ in 1954, Geiduschek reported the depolarization ratio, ρ_v , for serum albumin to be $\lesssim 10^{-4}$. He described in detail the considerations which make accurate depolarization measurements difficult, and brought much doubt upon the validity of all such measurements in the literature. He pointed out that fluorescence, optical activity, imperfect polarizers and analyzers,

* Literature values of ρ_u are corrected to ρ_v via Eq. (2.58).

detector anisotropy, finite acceptance solid angle, and multiple scattering can all contribute to improper measurement of the depolarization ratios. In our laboratory, it has become quite clear that strains in cell glass can make the glass itself somewhat birefringent. In general, it is reasonable to say that measurement of the very small depolarization ratios which arise in macromolecular solutions is difficult, especially when one considers the fact that the solvents, especially organic solvents, may themselves have very substantial anisotropy scattering.

The importance of sample purity cannot be overemphasized, particularly in regard to the presence of large size contamination such as dust. Doty and Stein⁽¹⁹⁾ reported that "only negligible amounts of suspended material could be detected by low-angle examination of the solutions irradiated with a parallel beam of light in a dark room". It is extremely difficult to define "negligible" quantitatively when one is discussing depolarization ratios of the order of 10^{-2} or less. The problem of large particulate contamination is particularly troublesome at the high salt concentrations required for some macromolecular solutions.^(20,21)

In light of the above discussion, one is forced to sort through the depolarization literature very carefully in order to get an idea of what reasonable depolarization ratios are. We are helped in this matter by the fact that we may use Eq. (2.44) to get some idea of the contribution of form effects to the optical anisotropy. Consider, for example, the case of tobacco mosaic virus (TMV). In an elegant and clear-cut experiment, Lauffer⁽²²⁾ showed in 1938 that TMV exhibits decreasing flow birefringence if placed in a solvent with index of

refraction increasing from that of water. At $n = 1.57$, the birefringence disappears completely. This means unambiguously that TMV is intrinsically optically isotropic, and that any depolarization of the scattered light in water solution must be due solely to form anisotropy.

Unfortunately, TMV's length of $\sim 3000\text{\AA}$ renders Eq. (2.44) not completely valid, since this expression assumes the molecule is immersed in a uniform electric field. However, since TMV is still less than one half the wavelength of red light, Eq. (2.44) can be considered to give a reasonable approximation. Treating TMV as an ellipsoid of revolution with axial ratio of 20 ($a/b = 20$, where a is semi-major axis and b is semi-minor axis), and index of refraction⁽²²⁾ of 1.57, we find from Eq. (2.44) that

$$\vec{\alpha}_m = \frac{V}{4\pi}(0.387, 0.324, 0.324).$$

We thus obtain, from Eqs. (2.56a) and (2.56b), that

$$\rho_v = .0023$$

$$\rho_u = .0045 .$$

Considering that the length of TMV is about half the wavelength of light, contrary to the assumption used to derive Eq. (2.44), this result is in reasonable agreement with literature values^(19,23) which are about 50% larger.

It is noteworthy that form anisotropy implies a depolarization ratio about the same as calculated above, even if a/b is only about 4/1 or larger. Hence, since most proteins have a refractive index⁽²⁴⁾ of around 1.6, and even the "globular" proteins are known to be asymmetric from hydrodynamic studies,⁽²⁵⁾ values of the axial ratio from 3/1 to

4/1 being typical,⁽²⁵⁾ we may conclude that form anisotropy alone would dictate a depolarization ratio ρ_u for nearly all large biological molecules of approximately 4×10^{-3} . Despite this, serum albumin, with an axial ratio⁽²⁶⁾ of around 5/1, has an accurately measured depolarization ratio⁽¹⁸⁾ of $\leq 1 \times 10^{-4}$. We can conclude only that the intrinsic anisotropy of serum albumin is such that the intrinsic polarizability of the molecule is less along the major axis than along the minor axis, and that intrinsic and form anisotropies tend to cancel one another. This conclusion has been reached in the case of various proteins by interpreting flow birefringence data.⁽²⁷⁾ We therefore cannot claim that depolarization ratios predicted on the basis of form anisotropy are a lower limit for the depolarization ratios. We can only use such values as a guideline in evaluating literature values.

It is unreasonable to assume, however, that form and intrinsic anisotropy will always be opposed to one another, and that even in those cases when they are, that they will so effectively cancel as they do in the case of serum albumin. Indeed, serum albumin seems to have one of the lowest anisotropies of the common proteins.⁽²⁷⁾ We thus conclude that values of ρ_v and ρ_u of 1 or 2×10^{-3} are not at all unreasonable for biological macromolecules, and they may well be higher in many cases. The evident reliability of the available experimental literature, however, is not adequate to render precise values, although the experimentally determined values are generally no larger than 1×10^{-2} .

In general, ρ_u for most proteins⁽²⁸⁾ is found, experimentally, to be around 5×10^{-3} . In those cases in which ρ_u is sometimes found to be substantially larger, there is usually a wide discrepancy among

various measurements in the literature. For example, Hawler, Nutting and Brice⁽¹⁶⁾ find ρ_u for ovalbumin (m.w. = 45,000) to be 0.024, which seems encouragingly large, yet Putzeys and Brosteaux⁽²⁹⁾ measure ρ_u for ovalbumin to be only 0.004. In view of the similar discrepancy in the case of serum albumin, which has already been discussed, it appears that the latter result is probably correct. In general, then, a value of $\rho_u \sim 0.005$ seems reasonable for protein solutions and for most other biological macromolecular solutions as well. The value for ρ_v is then about half as large.

If we take ρ_v as about 3×10^{-3} , then we see that the depolarized scattered light has very low intensity indeed. For, if the Rayleigh ratio of the material studied is R then the Rayleigh ratio for the depolarized light is only about $\rho_v \times R$. In the case of lysozyme, for example, R for a 1% solution was shown in section II.B.1 to be about $20 \times 10^{-6} \text{ cm}^{-1}$. Hence, even if ρ_v is as large as 3×10^{-3} for this substance, then the Rayleigh ratio for the depolarized light is only $0.06 \times 10^{-6} \text{ cm}^{-1}$, which means that the depolarized light scattered by a 1% lysozyme solution is only about 10% as intense as light scattered by water, the Rayleigh ratio of which is about $0.6 \times 10^{-6} \text{ cm}^{-1}$. Since water is not considered a strong scatterer from an experimental viewpoint, it is obvious that measuring depolarization ratios of dilute aqueous protein solutions is an elaborate and very difficult experiment, and the confusion in the literature is not hard to understand. This problem is obviously reduced for higher protein concentrations or larger proteins, or both, but then problems of multiple scattering become apparent. The work of Putzeys and Brosteaux,⁽²⁹⁾ for example, shows

a very strong dependence of ρ_u on protein concentration, which can only be due to multiple scattering effects.

Although the measurement of depolarization ratios, as discussed here, is obviously difficult and the literature must be viewed somewhat cautiously, it may indeed be quite possible to obtain useful information from the spectrum of the depolarized light, as we shall discuss in section II.D. This possibility hinges on the fact that, although the depolarized intensity cannot be distinguished easily from stray light and other complications which apparently plague depolarization intensity measurements, such a distinction may well be achieved in regard to the spectrum of the depolarized light and the spectrum of the spurious light. This possibility exists because the spectral widths of the light scattered by each mechanism will, in general, be markedly different.

C. Spatial Coherence of the Scattered Light

When Forrester, Parkins and Gerjuoy suggested⁽³⁰⁾ in 1947 that beat notes between light of different frequencies might be experimentally detectable, they were immediately challenged by Griffin⁽³¹⁾ who pointed out the limitations on the experiment imposed by a lack of spatial coherence of the light. We shall discuss this limitation in section III.B in the calculation of the signal-to-noise ratio expected in such mixing experiments. We will proceed here to determine the spatial coherence properties of the light studied in a scattering experiment.

Consider the experimental situation depicted in fig. 2.5. A laser of beam diameter a is used to illuminate a cell containing a macromolecular solution. The length of the illuminated volume is L . An observer studies the scattering at point \vec{R} located in the plane defined by the wave vectors

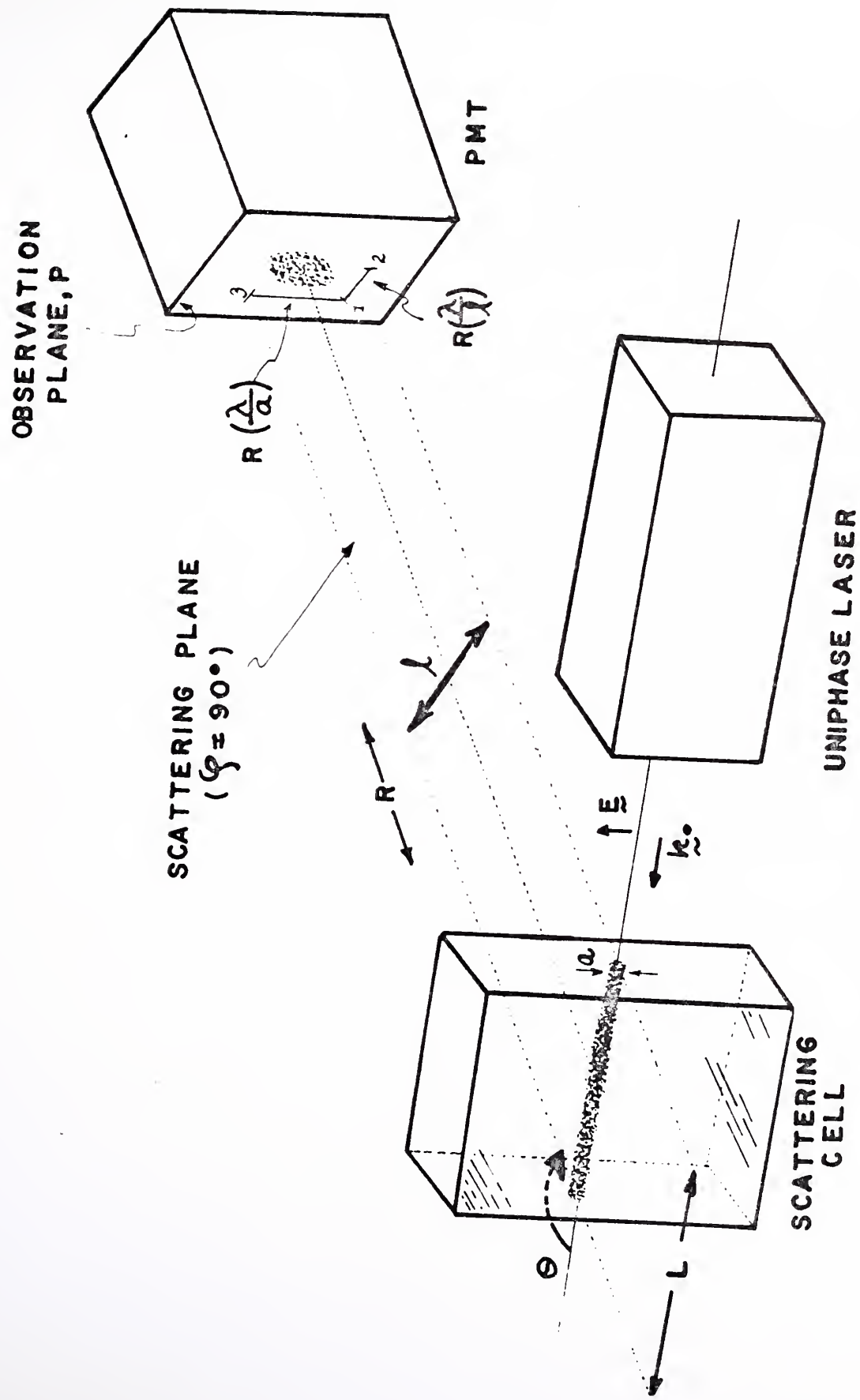


Fig. 2.5 Geometry for Determination of the Coherence Area in the Far Field of the Scattered Light

of the light which have $\phi = 90^\circ$ (the horizontal plane). Consider the case in which the scattering angle, θ , is 90° . The observer at \vec{R} then sees the illuminated volume as a rectangle of length L and height a . The scattered light falls on the observation plane, P .

The solution is illuminated by the plane wave output of a laser. Hence, the scattering volume is coherently illuminated. However, as an observer at \vec{R} moves from point 1 to point 2, the phase of the electric field of the scattered light will change. This, of course, is due to the difference in path length of the light scattered by various portions of the incident beam. In fact, it is well known from physical optics⁽³²⁾ that if the distance from 1 to 2 is approximately $(\lambda/L)R$, the phase of the electric field will change sign; λ/L is called the "diffraction angle" of the beam. Similarly, if the observer moves from 1 to 3, a distance of approximately $(\lambda/a)R$, the electric field will again change sign. Hence, within an area of size $A \approx \frac{\lambda^2}{aL} R^2$ the phase of the electric field of the scattered light will be the same. Such an area is called the "coherence area" of the scattered light, A_{Coh} , and $\frac{\lambda^2}{aL}$ is called the "coherence solid angle", Ω_{Coh} .

It is immediately apparent that the coherence area of the scattered light is a function of the scattering angle, θ . This obtains because the apparent source size is a function of θ . For an observer in the horizontal plane, the apparent length of the illuminated region as seen at the point \vec{R} is $\ell = L \sin \theta + a|\cos \theta|$. Hence, we have that the coherence solid angle for any scattering angle θ is given by

$$\Omega_{Coh} \approx \frac{\lambda^2}{a[L \sin \theta + a|\cos \theta|]}, \quad (2.63)$$

and the coherence area is then

$$A_{Coh} = R^2 \Omega_{Coh} \approx \frac{R^2 \lambda^2}{a \{ L \sin \theta + a |\cos \theta| \}} . \quad (2.64)$$

As we shall discuss in section III.B, the feasibility of experiments employing optical mixing spectrometers depends greatly on the power contained in a single area of coherence. From Eq. (2.40), we have the power scattered into the solid angle $d\Omega$ is, for an isotropic scatterer,

$$\frac{\mathbf{P}_s(d\Omega)}{\mathbf{P}_{Inc}} = 2L \mathbf{R} \sin^2 \phi \, d\Omega . \quad (2.65)$$

Hence, setting $\phi = 90^\circ$ for an observer in the horizontal plane, we see that the power scattered into a coherence solid angle is

$$\frac{\mathbf{P}_s^{Coh}(\Omega_{Coh})}{\mathbf{P}_{Inc}} = 2L \mathbf{R} \frac{\lambda^2}{a \{ L \sin \theta + a |\cos \theta| \}} . \quad (2.66)$$

Equation (2.66) has two distinct regions of interest. The usual experimental situation is $L \gg a$. Hence, for any reasonably large scattering angle, we see that \mathbf{P}_s^{Coh} is independent of the beam length L and varies inversely as the beam diameter, a . The other region of interest is for small scattering angles. In this case \mathbf{P}_s^{Coh} varies as L/a^2 . It is thus readily apparent that appreciably more power per coherence solid angle can be obtained at small scattering angles, a desirable result for the operation of optical mixing spectrometers. However, making the beam dimensions small introduces a spread in the wave vectors making up the incident beam:

(33)

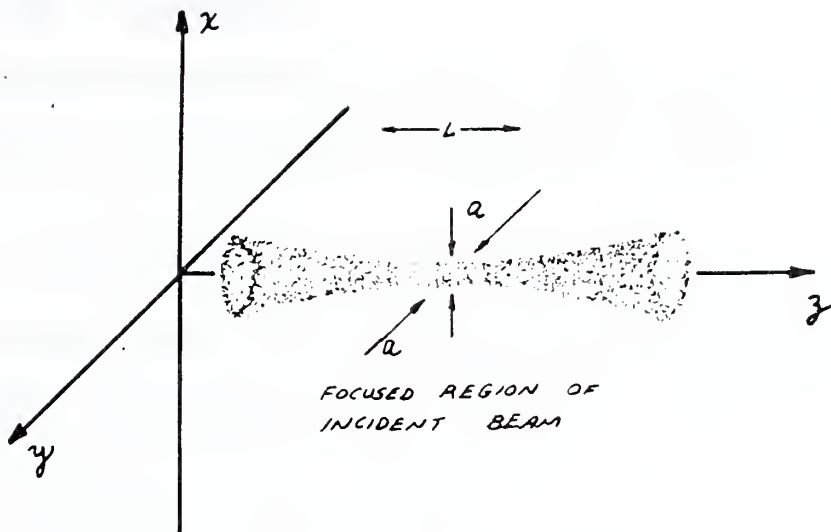


Fig. 2.6 Spread in Wave Vector of Incident Light Due to Finite Beam Dimensions

$$\Delta k_x \sim \frac{1}{a} \quad (2.67a)$$

$$\Delta k_y \sim \frac{1}{a} \quad (2.67b)$$

$$\Delta k_z \sim \frac{1}{L} \quad . \quad (2.67c)$$

Our original assumption of plane wave illumination of course implies

$\Delta k_x = \Delta k_y = 0$. The beam length L and diameter a are usually sufficiently large that no difficulties are encountered due to the implications of Eqs. (2.67 a-c). This becomes progressively less the case as the scattering angle is decreased, particularly for small beam diameters. From Eq. (2.12) we see that $\vec{k} = \vec{k}_s - \vec{k}$. Assuming the only uncertainty in \vec{k} is due to the uncertainty in \vec{k} due to the finite beam diameter, we have

$$\frac{\Delta K}{K} \approx \frac{(1/a)}{2k \sin \theta/2} . \quad (2.68)$$

If we state, for convenience, that the maximum spread in K that we will allow is 1%, Eq. (2.68) sets a criterion for θ and a :

$$a \sin \left(\frac{\theta}{2}\right) \gtrsim \frac{50}{k} . \quad (2.69a)$$

For the 6328 $^{\circ}$ laser line in aqueous solution, $k = n k_o = 1.33 \frac{2\pi}{6328\text{A}}$.

Thus, Eq. (2.69) requires

$$a \sin \left(\frac{\theta}{2}\right) \gtrsim 3.8 \times 10^{-4} \text{ cm.} \quad (2.69b)$$

Equation (2.69b) is indeed restrictive. We see immediately that focusing the beam to its diffraction limit is in general never permissible if we wish a 1% definition in the wave vector of the fluctuation we are studying. As we proceed to the forward direction, the minimum size to which we may focus the beam progressively increases until, for example, at $\theta = 2^{\circ}$, we have $a_{\min} = 0.2\text{mm}$. This is actually quite large, yet we cannot decrease the beam diameter without an unacceptable loss in definition of K . Hence, even though Eq. (2.64) implies the region of coherence in the scattered light can be made arbitrarily large by decreasing the beam diameter and studying the scattered light at small angles, such an experimental procedure must be done within the restrictions imposed by Eq. (2.69b). It is possible that a 1% definition requirement on K may be too stringent under certain circumstances. But the restriction of Eq. (2.68) must still be obeyed, after an appropriate value of $\Delta K/K$ is decided for the particular case being studied.

On the other hand, if it is possible from an experimental point of view to study the scattered light in the extreme backward direction ($\theta \sim 180^{\circ}$),

this problem can be circumvented. If we set $\theta = 180^\circ$ in Eq. (2.69b), we see that the beam diameter must be no smaller than a couple of microns for our restriction $\Delta K/K \leq 1\%$ to be met. For red light, this is only a few times the diffraction limit. Thus, we can focus essentially to the diffraction limit without an unacceptable spread in K if we study the scattered light in the backward direction. This can be of significant interest as we shall discuss when we consider the signal-to-noise ratio obtainable from light mixing spectrometers (section III.B).

Even assuming that the beam diameter is sufficiently large that there is not a large spread in K due to a spread in k , the wave vector of the incident light, it is still possible to have poor definition in K . As Eq. (2.13) indicates, $K = 2k \sin \frac{\theta}{2}$. Hence, even if k is well defined, K may have an uncertainty due to acceptance angle spread given by

$$\left(\frac{\Delta K}{K} \right)_{\Delta\theta} = \left(\frac{1}{2} \operatorname{ctn} \frac{\theta}{2} \right) \Delta\theta. \quad (2.70)$$

For large angles, Eq. (2.70) indicates that nearly an arbitrarily large $\Delta\theta$ (acceptance angle) is permissible since $\operatorname{ctn} \frac{\theta}{2} \rightarrow 0$ as $\theta \rightarrow 180^\circ$. Even for small angles, the restriction at first glance does not appear great, since even if $\Delta\theta$ is about 0.1° (a reasonably large aperture), θ can be as small as 5° without $\left(\frac{\Delta K}{K} \right)_{\Delta\theta}$ exceeding 1%. However, even an aperture of 0.1° will not collect an entire coherence area at 5° scattering angle for a well focused beam ($\sim 0.1\text{mm}$), let alone a beam focused nearer the diffraction limit. Hence, we see the dual problems of spread in observed K values due to finite beam diameter and finite acceptance angle must be traded off against collecting an entire coherence area.

The latter, as we shall see in III.B, is desirable from the point of view

of light-mixing spectrometers.

It is most important to note, however, that these problems are not present for large scattering angles. We have shown that it is permissible to focus the incident light essentially to its diffraction limit without unacceptable spread in wave vector \mathbf{k} of the incident light if we study the scattering for large angles [Eq. (2.69b)]. Hence, we can make the beam diameter of the order of one micron for red laser light and thereby make the region of coherence quite large [Eqs. (2.63) and (2.64)], hence the power per coherence solid angle large [Eq. (2.66)]. We may then make $\Delta\theta$ large enough to accept an entire coherence solid angle if we again study the scattering for large angles where

$$\left(\frac{\Delta K}{K}\right)_{\Delta\theta} \rightarrow 0 \text{ as } \theta \rightarrow 180^\circ.$$

D. Temporal Coherence of the Scattered Light

In the preceding section, we showed that the spatial coherence of the light scattered by a solution is a function only of the geometric configuration of the beam in the cell. The information which can be obtained, therefore, from the spatial coherence properties of the scattered light can yield no information on the macromolecules we wish to study.*

We thus turn now to the temporal coherence of the scattered light. As was demonstrated in Eq. (2.14), the time dependence of the electric field of the scattered light mirrors that of the particular fluctuation in dielectric constant which produced it. The fluctuations in dielectric constant are, of course, random variables. The most convenient way to consider the time dependence of a random variable is to consider the

* If, on the other hand, the size of the source of light is the desired goal, the spatial coherence properties are indeed useful, as demonstrated by the Brown-Twiss experiments to determine stellar diameters,⁽³⁴⁾

amount of correlation such a variable has over a given period of time.

This temporal "correlation function" of a random variable, x , may be defined as

$$R_x(\tau) \equiv \lim_{T \rightarrow \infty} \frac{1}{2T} \int_{-T}^T x(t+\tau)x^*(t)dt. \quad (2.71)$$

An alternative definition is that the temporal correlation function of x is the ensemble average of the quantity $x(t+\tau)x^*(t)$. That is, by definition,

$$R_x(\tau) \equiv \langle x(t+\tau)x^*(t) \rangle. \quad (2.72)$$

By the ergodic hypothesis, Eqs. (2.71) and (2.72) are equivalent.

It is obvious from either of the above definitions that the correlation function is a type of average quantity. Its use is both necessary and convenient. The necessity arises from the fact that the electric field of the scattered light is not integrable in the mean-square, and a frequency decomposition of the electric field via the Fourier transform is therefore not possible. It is clear for physical reasons that the correlation function as defined above must go to zero for large times and thus we do have a function to which Fourier transformation may be applied. Furthermore, the convenience of the correlation function approach is that the Fourier transform of the correlation function is the spectral power density of the fluctuations being considered. This latter result is a statement of the Wiener-Khintchine theorem. ⁽³⁵⁾

If we now turn specifically to the problem of light scattered by a solution of macromolecules, we see that

$$R_{E_s}(\tau) = \langle E_s(t+\tau)E_s^*(t) \rangle, \quad (2.73)$$

$$\text{and } S(\omega) = \int_{-\infty}^{\infty} R_E(\tau) e^{i\omega\tau} d\tau , \quad (2.74)$$

where $S(\omega)$ is the spectral power density of the fluctuations in the electric field.

Let us first consider fluctuations in the electric field of the scattered light due to concentration fluctuations. From Eq. (2.14) and (2.16c) we may write:

$$\vec{E}_s(\vec{k}, t) = \vec{J} e^{-i\omega_0 t} \delta C(\vec{k}, t) , \quad (2.75)$$

$$\text{where } \vec{J} = -\frac{1}{\langle \epsilon \rangle} \vec{k}_s \times (\vec{k}_s \times \vec{E}) \frac{e^{ik_s \cdot \vec{R}}}{4\pi R} \cdot (2\pi)^{3/2} \frac{2n \partial n}{\partial C} \quad (2.76)$$

Hence, we may immediately write, from Eq. (2.73),

$$R_E(\tau) = |\vec{J}|^2 \langle \delta C(\vec{k}, t+\tau) \delta C^*(\vec{k}, t) \rangle e^{-i\omega_0 \tau} . \quad (2.77)$$

To calculate $\langle \delta C(\vec{k}, t+\tau) \delta C^*(\vec{k}, t) \rangle$ we make the reasonable assumption that the time dependence of the correlation function for the random fluctuations in concentration is the same as that of a specified, non-random concentration gradient. This type of assumption was first made formally by Onsager^(36,37) in his "regression hypothesis".

We may now readily calculate $R_{\delta C}(\tau)$ as follows. Let us specify that at a point \vec{r} in the solution, the concentration is uniform until at $t=0$ a gradient in concentration $\delta C(\vec{r}, t)$ is established. The decay of this concentration gradient will be accurately governed by the diffusion equation in the case of a dilute solution of non-interacting molecules:⁽³⁸⁾

$$\frac{\partial}{\partial t} \delta C(\vec{r}, t) = D \nabla^2 \delta C(\vec{r}, t), \quad (2.78)$$

where D is the diffusion constant of the macromolecule.

Upon Fourier transformation, we obtain

$$\frac{\partial}{\partial t} \delta C(\vec{k}, t) = -Dk^2 \delta C(\vec{k}, t) \quad (2.79)$$

whose solution for the given boundary conditions is

$$\delta C(\vec{k}, t) = \begin{cases} \delta C(\vec{k}, 0) e^{-Dk^2 t} & t \geq 0 \\ 0 & t < 0 \end{cases} \quad (2.80)$$

The quantity Dk^2 has units of reciprocal time, and is called the "decay rate", Γ_D . If we further observe that

$$\langle \delta C(\vec{k}, t + \tau) \delta C^*(\vec{k}, t) \rangle = \langle \delta C(\vec{k}, \tau) \delta C^*(\vec{k}, 0) \rangle \quad (2.81)$$

since the concentration fluctuations are assumed to be a stationary random process, we may combine Eqs. (2.77), (2.80) and (2.81) with the Onsager regression hypothesis to obtain

$$R_E(\tau) = |\vec{j}|^2 \langle |\delta C(\vec{k}, 0)|^2 \rangle e^{-\Gamma_D |\tau|} e^{-i\omega_0 |\tau|}, \quad (2.82a)$$

$$\text{or, } R_E(\tau) = R_E(0) e^{-\Gamma_D |\tau|} e^{-i\omega_0 |\tau|}. \quad (2.82b)$$

We use $|\tau|$ instead of τ in Eq. (2.82) by the physical argument that we must "lose correlation" no matter which way we go in time from a given reference time -- that is, $R(\tau)$ must be a symmetric function of τ .

The spectrum of the scattered light may then be obtained from the correlation function by the Wiener-Khintchine theorem [Eq. (2.74)]:

$$\begin{aligned}
 S_{E_s}(\vec{k}, \omega) &= |\vec{J}|^2 \langle |\delta C(\vec{k}, 0)|^2 \rangle \int_0^\infty e^{-\Gamma_D |\tau|} e^{i(\omega - \omega_0) |\tau|} d\tau \\
 &= |\vec{J}|^2 \langle |\delta C(\vec{k}, 0)|^2 \rangle \frac{2\Gamma_D}{\Gamma_D^2 + (\omega - \omega_0)^2} .
 \end{aligned} \tag{2.83}$$

It is usually more convenient to express the spectrum in terms of the experimentally measured quantity, the frequency ν , instead of the angular frequency, $\omega = 2\pi\nu$. Hence, we rewrite Eq. (2.83) as

$$S_{E_s}(\vec{k}, \nu) = |\vec{J}|^2 \langle |\delta C(\vec{k}, 0)|^2 \rangle \frac{1}{\pi} \frac{(\Gamma_D/2\pi)}{\left(\frac{\Gamma_D}{2\pi}\right)^2 + (\nu - \nu_0)^2} . \tag{2.84}$$

We thus see that the spectrum of the light which is scattered due to concentration fluctuations is Lorentzian and is centered at the frequency of the incident light. The half-width at half-maximum (HWHM) of this spectrum in Hz is $\Gamma_D/2\pi$ and since $\Gamma_D = DK^2$, we have

$$\frac{\Gamma_D}{2\pi} = \frac{DK^2}{2\pi} = \frac{D}{2\pi} \left[\frac{4n\pi}{\lambda_0} \sin\left(\frac{\theta}{2}\right) \right]^2 . \tag{2.85}$$

Measurement of the width of the light scattered by concentration fluctuations yields therefore the diffusion constant of the molecule.*

In 1967, Dubin, Lunacek, and Benedek⁽¹⁴⁾ accurately verified the predictions of a Lorentzian profile and K^2 dependence of the scattered light [Eqs. (2.84) and (2.85)]. They studied solutions of several small proteins for which the various assumptions we have made thus far were valid. They

* It is interesting to note that Mandel'shtam anticipated some of the arguments presented here as early as 1926, and suggested light scattering as a means of measuring molecular diffusion constants: Mandel'shtam, L. I., *Zhurnal Russkogo Fiziko Khimicheskogo Obshchestva*, 58, 381 (1926).

also demonstrated that, for larger molecules, a more detailed analysis than presented thus far may be necessary in some cases [e.g., tobacco mosaic virus (TMV) and deoxyribonucleic acid (DNA)] to interpret the observed spectrum. This arises because, for those molecules which are comparable to the wavelength of light, the orientation of the molecule modulates the intensity of the scattered light, and also anisotropic diffusion may be significant for such molecules. The effects of rotational modulation have been treated theoretically in recent works by Pecora⁽³⁹⁻⁴¹⁾ and by Pecora and Steele,⁽⁴²⁾ and experimentally by Cummins, Carlson, Herbert and Woods.⁽⁴³⁾ The role of anisotropic diffusion has been considered from both theoretical and experimental viewpoints by Schoefield, Schaefer, and Benedek.⁽⁴⁴⁾ We shall not discuss these considerations further here, since, as will be demonstrated, the effects of anisotropic diffusion and rotational modulation on the polarized portion of the scattered light were not observable in our experiments.

We may obtain the spectrum of the anisotropy scattering by analogy with the arguments presented thus far for the concentration fluctuation scattering. The anisotropy scattering arises from fluctuations in the optical isotropy of the medium which are produced by the reorientation of the molecules. Pecora⁽³⁹⁾ assumed such reorientation is governed by the rotational diffusion equation,

$$\frac{\partial}{\partial t} p(\Omega_t - \Omega_o, t) = D_R \nabla_s^2 p(\Omega_t - \Omega_o, t) \quad (2.86)$$

where ∇_s^2 is the Laplacian on the surface of a sphere, $p(\Omega_t - \Omega_o, t)$ is the probability that if the orientation of the molecule is within $d\Omega$ about the solid angle Ω_o at time $t = 0$, its orientation will be within $d\Omega$ about

Ω_t at time t , and D_R is the rotational diffusion coefficient. He then proceeded to assume that rotational and translational motion are uncoupled, a reasonable assumption if rotational relaxation times are short compared with translational relaxation times. From the time dependence of the diffusion equation, we would expect a Lorentzian spectrum (i.e., an exponential correlation function) for reorientational scattering. Under the above assumptions, Pecora indeed predicted such a correlation function, and obtained for the spectrum

$$S_{E_s}(\nu) \propto \frac{1}{\left(\frac{\Gamma_R}{2\pi}\right)^2 + (\nu - \nu_0)^2}, \quad (2.87a)$$

where Γ_R , the rotational relaxation rate, is given by⁽³⁹⁾

$$\Gamma_R = 6 D_R \quad (2.87b)$$

and we may write $R_{E_s}(\tau)$ as

$$R_{E_s}(\tau) = R_{E_s}(0) e^{-\Gamma_R |\tau|} e^{-i \omega_0 |\tau|}. \quad (2.87c)$$

Pecora's prediction that $\Gamma_R = 6 D_R$ is in agreement with the result of Benoit⁽⁴⁵⁾ which was used in interpreting electric birefringence data. We notice that the predicted spectrum is independent of scattering angle, as we would expect, since it arises from reorientation of the molecules. This prediction is in agreement with experimental and theoretical work in anisotropy scattering in liquids and recent experimental work in a liquid crystal.⁽¹⁰⁾ Wada, Suda, Tsuda and Soda⁽⁴⁷⁾ have measured the rotary diffusion coefficient of TMV by analyzing the spectrum of the depolarized

scattered light using heterodyne spectroscopy. (47)

Hence, within the limitations of our simplified model, we see that the concentration fluctuation scattering can yield the translational diffusion coefficient D , and anisotropy scattering the rotary diffusion coefficient, D_R . As shown in section II.B.2.b, $I_C \gg I_A$ for solutions of macromolecules. Hence, analysis of that portion of the scattered light with the same polarization as the incident need not include any correction for the anisotropy scattering, which is negligibly small. Conversely, if we look only at the depolarized light, we can completely eliminate the large contribution from the concentration fluctuations and study only pure anisotropy effects and thereby obtain D_R .

To get an idea of the spectroscopic techniques which are required to resolve the two components of the spectrum of the scattered light, let us consider an idealized biological macromolecule as a sphere of diameter 100\AA . This would be typical of the proteins and other globular molecules. We then observe that for spheres (48)

$$D = \frac{k_B T}{6\pi n r} \quad (2.88)$$

$$D_R = \frac{k_B T}{8\pi n r^3} \quad (2.89)$$

where k_B is Boltzmann's constant, T is the absolute temperature, n is the solvent viscosity, and r the molecular radius. Hence, for $r = 50\text{\AA}$ we have at 20°C that

$$D = 4.3 \times 10^{-7} \text{ cm}^2/\text{sec} \quad \text{and} \quad D_R = 1.3 \times 10^6 / \text{sec.}$$

These calculations agree well with the measured values (49,50) for hemoglobin, a protein of about this size, which are $6.9 \times 10^{-7} \text{ cm}^2/\text{sec}$ and $6 \times 10^6 \text{ sec}^{-1}$

respectively.

Now, from Eq. (2.85), we see that the maximum width ($\theta = 180^\circ$) of the light scattered by an aqueous solution of such a molecule due to concentration fluctuations is only about 550 Hz, a remarkably narrow line. Since the 6328Å laser line has a frequency of $v_0 \approx 5 \times 10^{14}$ Hz, the observation of a 550 Hz profile requires a resolving power ($v_0/\Delta v$) at least 10^{13} to display the line. This is far greater than the resolving power obtainable from a grating spectrograph ($< 10^6$) or Fabry-Perot etalon spectrometers ($< 10^9$). The observation of this portion of the spectrum requires the recently developed techniques of light mixing spectroscopy, which will be discussed in section III.B.

On the other hand, the spectrum of the anisotropy scattering from a molecule like hemoglobin presents a different problem. From Eq. (2.87) we see that the width of the anisotropy scattered light is $\Gamma_R/2\pi = 3D_R/\pi \approx 1 \times 10^6$ Hz. This is just barely within the resolving power of the very good spherical Fabry-Perot interferometers available today, and just beyond the range of mixing spectroscopy. The latter statement is a result of signal-to-noise requirements, as we shall discuss in the next chapter, wherein we shall also establish feasibility criteria for the observation of the spectra described above.

We have seen that the characteristic lifetime (reciprocal decay rate) of the fluctuations in concentration is of the order of milliseconds, while that of the fluctuations in anisotropy is of the order of microseconds. Hence, at least for macromolecules of the size we consider here, we can view the molecules as able to reorient themselves much faster than they can achieve translation. For such molecules, then, Pecora's assumption⁽³⁹⁾

of uncoupled rotational and translational motion is valid and our simple model is adequate.

Equations (2.88) and (2.89) indicate that while D is a relatively weak function of the molecular dimension, D_R is quite a strong function of this dimension. Hence, an increase in effective radius of only a factor of 2.15 reduces D_R an order of magnitude, bringing the anisotropy spectrum of a molecule with $r \approx 100\text{\AA}$ out of the resolving range of even the best spherical Fabry-Perot interferometer which is available, not even mentioning the problem of frequency stabilizing a laser to much better than 100 kHz.

On the other hand, for molecules only about a factor of 2 smaller in diameter than our reference molecule (that is, $r \sim 25\text{\AA}$), $\Gamma_R/2\pi$ becomes about 10 MHz, a profile which is readily resolved by a spherical Fabry-Perot and which is well beyond the present limits of mixing spectroscopy. Hence, it would appear that both mixing and filter (Fabry-Perot) techniques will be useful in observing the spectrum of that portion of the scattered light which is scattered due to optical anisotropy.

E. Applications of the Information in the Spectrum of the Scattered Light

1) Determination of Bacteriophage Molecular Weights

As we have discussed in section II.B.1, the intensity of light scattered by macromolecules can be used to determine molecular weights. In practice, however, it is found that when the molecules become comparable to the wavelength of light, the utility of the method becomes marginal. The extrapolations to zero concentration and zero scattering angle which are required for these large molecules are plagued particularly by scattering from dust and stray light. Because such alternative methods as osmotic pressure determination also tend to become marginal at high molecular weights, the present knowledge of

the weights of large viruses is poor indeed.

There is one method among the classical techniques which is readily applicable if the diffusion coefficient of the molecule is known. However, since it has been extremely difficult to measure D for the very large phages, the method of "sedimentation-diffusion"⁽⁵¹⁾ has also borne little fruit in this problem. We have seen, however, that D can be determined by spectral analysis of the light scattered by macromolecules. Hence, the method of sedimentation-diffusion has renewed possibilities.

The method bears great resemblance to the Millikan oil drop experiment. We accelerate the macromolecule we are studying in a viscous medium such as water, to its terminal velocity, v_t , in a strong gravitational field, g. The field must be quite strong to render diffusive motion of the molecule negligible. This is quite readily done for large molecules such as viruses in the analytical ultracentrifuge.

The particle reaches its terminal velocity v_t when the net force on it is zero. As indicated in Fig. 2.7 below, there are the frictional drag, fv_t , where f is the frictional coefficient, and the buoyant force F_B , both acting upward, and the "weight" of the particle, mg, acting downward (m is the mass of a single molecule). At equilibrium we have

$$mg = fv_t + F_B . \quad (2.90)$$

The buoyant force, F_B , is simply the weight of the solvent displaced by the macromolecule. We call the volume of solvent displaced per gram of solute the "partial specific volume" of the molecule, \bar{v} .



Fig. 2.7 Forces Acting on a Particle Accelerated to its Terminal Velocity in a Viscous Medium

Hence, if ρ is the solvent density, we see $F_B = \rho \bar{v} mg$. Hence,

$$mg = fv_t + \rho \bar{v} mg$$

or

$$m = \frac{v_t}{g} \frac{f}{(1 - \rho \bar{v})} \quad (2.91)$$

Every parameter in Eq. (2.91) is readily measured to give m , except f . However, the frictional coefficient f is related to the diffusion coefficient D by the relation⁽⁵²⁾

$$D = \frac{kT}{f} . \quad (2.92)$$

Hence, from Eq. (2.91) we see that

$$m = \frac{v_t}{g} \frac{kT}{D} \frac{1}{(1 - \rho v)} \quad (2.93)$$

The ratio $\frac{v_t}{g}$ is readily measured in the ultracentrifuge, and is usually called S, the sedimentation rate (expressed in units of 10^{-13} sec). Hence, using this substitution for v_t/g and multiplying both sides of Eq. (2.93) by Avogadro's number N_o , we have that the molecular weight per mole of the molecule is given by

$$M = \frac{S}{D} \frac{N_o kT}{(1 - \rho v)} \quad (2.94)$$

This expression has proved quite useful in measurements of molecular weights, with the ability to measure D usually the chief limitation. When D is less than about $1 \times 10^{-7} \text{ cm}^2/\text{sec}$, its measurement by classical techniques becomes quite laborious.⁽⁵³⁾ As the present work demonstrates, it is in this regime when the methods of light scattering become most effective.

This thesis presents for the first time a combination of determining D by spectral analysis of the scattered light and S by the techniques of the ultracentrifuge to measure molecular weights. We have thereby extended the technique of sedimentation-diffusion to molecules of molecular weight up to 200 million, about an order of magnitude extension beyond previous results. Furthermore, the technique is shown to be applicable even to much larger molecules if such are found of interest.

2) The Chemical Denaturation of Lysozyme

In Eq. (2.92) we noted that the translational diffusion coefficient D is inversely proportional to the frictional coefficient, f. The exact form of f has been obtained for spheres⁽⁵⁴⁾ and ellipsoids

of revolution.⁽⁵⁴⁾ In the case of asymmetric molecules, f is of course a function of the direction of motion of the molecule. However, for the vast majority of macromolecules, the rotary relaxation time is so short, compared with the translational relaxation time, that the molecule can be considered as a rapidly rotating object moving from point to point rather slowly. Hence, we measure an average diffusion coefficient, that is, one which is averaged over all orientations. In addition, in an actual experiment we are studying large numbers of molecules whose orientations are randomly distributed. Hence, experimental values of f determined through a measurement of either D or S yield an angular-averaged value for the parameter. This is true even at the high velocities molecules reach when accelerated in the ultracentrifuge, that is, kT is sufficiently large to prevent preferred orientations even at high velocities.⁽⁵⁵⁾

Since the frictional coefficient of the molecule is a function of its size and shape, measurement of D or S alone can give information on these quantities and, in addition, on changes in such quantities. However, for very small molecules, S is quite small. Hence, even at the gravitational fields available in large ultracentrifuges, diffusive motion competes strongly with sedimentation motion. It therefore becomes quite difficult to extract specific information from such experiments on very small molecules.

The technique of measuring D by light scattering offers a rapid measurement by spectral analysis, even in the case of the small proteins. In specific, this thesis presents a study of the change in D (and hence f , and the molecular conformation) of the protein lysozyme upon chemical denaturation by guanidine hydrochloride. The

analogous experiment of measuring S has not appeared in the literature, evidently because of the difficulties discussed above.

References for Chapter II

1. Landau, L. D., and Lifshitz, E. M., "Electrodynamics of Continuous Media", Addison-Wesley Publishing Co., Inc., Reading, Mass., 1960, p. 273.
2. Landau, L. D., and Lifshitz, E. M., "The Classical Theory of Fields", Addison-Wesley Publishing Co., Inc., Reading, Mass., 1962, p. 200.
3. Zimm, B., J. Chem. Phys., 16, 1099 (1948).
4. Fabelinskii, I. L., Usp. Fiz. Nauk, 63, 355 (1957). English translation: AEC Translation 3973, Part I, Advan. Phys. Sci., 63, 474 (1957).
5. Edsall, J. T., Advances in Colloid Sci., 1, 269 (1942).
6. ref. 1, pp. 43-45.
7. Goldstein, H., "Classical Mechanics", Addison-Wesley Publishing Co., Inc., Reading, Mass., 1950, pp. 107-109.
8. van de Hulst, H. C., "Light Scattering by Small Particles", John Wiley and Sons, Inc., New York, 1957, p. 80.
9. Trumpp, B., Z. für Physik, 88, 226 (1934).
10. Litster, J., and Stinson, T. W., III, J. Appl. Phys., to be published in March, 1970.
11. Cabannes, J., "La Diffusion Moléculaire de la Lumière", Presses Univ. France, Paris, 1929.
12. ref. 4, p. 503.
13. Lord Rayleigh, Phil. Mag., 35, 373 (1918).
14. Dubin, S. B., Lunacek, J. H., and Benedek, G. B., Proc. Nat. Acad. Sci., 57, 1164 (1967).
15. Dubin, S. B., unpublished results.
16. Halwer, M., Nutting, G. C., and Brice, B. A., J. Am. Chem. Soc., 73, 2786 (1951).

17. Edsall, J., Edelhoch, H., Lontie, R., and Morrison, P., J. Am. Chem. Soc., 72, 4641 (1950).
18. Geiduschek, E. P., J. Polymer Sci., 13, 408 (1954).
19. Doty, P., and Stein, S., J. Polymer Sci., 3, 763 (1948).
20. This is discussed in greater detail in chapter III.
21. Wada, A., private communication.
22. Lauffer, M., J. Phys. Chem., 42, 935 (1938).
23. Jennings, B., and Jerrard, H., J. Chem. Phys., 44, 1291 (1966).
24. Putzeys, P., and Brosteaux, J., Bull. Soc. Chim. Biol., 18, 1681 (1936).
25. Tanford, C., "Physical Chemistry of Macromolecules", John Wiley and Sons, Inc., New York, 1961, pp. 359, 395.
26. ref. 25, p. 359.
27. Edsall, J., and Foster, J., J. Am. Chem. Soc., 70, 1860 (1948).
28. Doty, P., and Edsall, J., Adv. Protein Chem., 6, 35 (1951).
29. Putzeys, P., and Brosteaux, J., Trans. Faraday Soc., 31, 1314 (1935).
30. Forrester, A. T., Parkins, W. E., and Gerjuoy, E., Phys. Rev., 72, 728 (1947).
31. Griffin, L. R., Phys. Rev., 73, 922 (1948).
32. ref. 2, p. 165.
33. ref. 2, p. 164.
34. Brown, H., and Twiss, R., Nature, 178, 1046 (1956).
35. Kittel, C., "Elementary Statistical Physics", John Wiley and Sons, Inc., New York, 1958, p. 136.
36. Onsager, L., Phys. Rev., 37, 405 (1931).
37. Onsager, L., Phys. Rev., 38, 2265 (1931).
38. ref. 25, p. 347.
39. Pecora, R., J. Chem. Phys., 40, 1604 (1964).
40. Pecora, R., J. Chem. Phys., 43, 1562 (1965).

41. Pecora, R., J. Chem. Phys., 48, 4126 (1968).
42. Pecora, R., and Steele, W. A., J. Chem. Phys., 42, 1872 (1965).
43. Cummins, H. Z., Carlson, F. D., Herbert, T. J., and Woods, G., Biophys. J., 9, 518 (1969).
44. Schoefield, P., Schaefer, D., and Benedek, G., to be published.
45. Benoit, H., Ann. Phys., 6, 561 (1951).
46. Shapiro, S. L., and Broida, H. P., Phys. Rev., 154, 129 (1967).
47. Wada, A., Suda, N., Tsuda, T., and Soda, K., J. Chem. Phys., 50, 31 (1969).
48. ref. 25, pp. 327, 349, 435.
49. ref. 25, p. 358.
50. Setlow, R. B., and Pollard, E. C., "Molecular Biophysics", Addison-Wesley Publishing Co., Inc., Reading, Mass., 1962, p. 106.
51. ref. 25, pp. 379-381.
52. ref. 25, p. 349.
53. Markham, R., in Maramorosch, K., and Koprowski, H. (eds.), "Methods in Virology", vol. 2, Academic Press, New York, 1967, p. 280.
54. ref. 25, p. 327.
55. Putnam, F., J. Polymer Sci., 12, 391 (1954).

Chapter III

EXPERIMENTAL APPARATUS, METHODS, AND MATERIALS

"Everybody knows as much as he works."

Saint Francis

A. Introduction

As we discussed in section II.D, the spectral linewidths we can expect to observe in scattering experiments in macromolecular solutions are quite small, and the new techniques of light-mixing spectroscopy will be required to resolve them. We discuss in detail in section III.B the operation of the "self-beating" spectrometer employed in this thesis. Particular attention is paid to the problem of realizable signal-to-noise ratios and hence the feasibility of a given experiment. The "self-beating" spectrometer is contrasted with the spherical Fabry-Perot interferometer, and the utility of the latter in studies of anisotropy scattering is suggested. In addition, we discuss the desirability and feasibility of determining the correlation function of the scattered light instead of its power spectrum. The section concludes with a description of the optical and electronic experimental setup.

Section III.C concludes the chapter with a detailed discussion of all experimental samples employed in this thesis, together with a description of solvents, buffers, sample cleaning, and cell cleaning and filling techniques.

B. The Square-Law Spectrometer⁽¹⁻⁵⁾

1) Theory of Operation

The problem which arises when we attempt to observe the spectrum

of light scattered by concentration fluctuations or the spectrum of the anisotropy scattering lies in the extremely high resolving power required. If we could translate the spectrum to a much lower center frequency from that of the incident light, the required resolving power would then of course be much smaller as well. Such a translation requires a non-linear element and we are, in fact, provided with a perfect square-law detector in the photomultiplier tube (PMT). The photocurrent $i(t)$ is proportional to the intensity of the scattered light $I(t)$, and hence to the square of the electric field. We therefore investigate the correlation function for the fluctuations in the photocurrent, $R_i(\tau)$, and we shall see that the square-law device (phototube) does indeed give the desired translation in frequency of the information we seek.

We begin by calculating the correlation function for the square of the electric field. If the electric field is a Gaussian random variable (GRV) (i.e., if the fluctuations in concentration and optical isotropy which produce the scattering are GRV's), we may write⁽⁶⁾

$$\begin{aligned} \langle E_s(\tau)E_s^*(\tau)E_s(0)E_s^*(0) \rangle &= \langle |E_s(0)|^2 \rangle^2 \\ &+ \langle E_s(\tau)E_s^*(0) \rangle \langle E_s^*(\tau)E_s(0) \rangle + \langle E_s(\tau)E_s(0) \rangle \langle E_s^*(\tau)E_s^*(0) \rangle . \end{aligned} \quad (3.1)$$

Since $E_s(\tau) \propto e^{-i\omega\tau}$, we see that the third term on the right in Eq. (3.1) vanishes and we have simply

$$\begin{aligned} \langle |E_s(\tau)|^2 |E_s(0)|^2 \rangle &= \langle |E_s(0)|^2 \rangle^2 \\ &+ \langle E_s(\tau)E_s^*(0) \rangle \langle E_s^*(\tau)E_s(0) \rangle . \end{aligned} \quad (3.2)$$

Now, since $I_s(t) = \left(\frac{c}{8\pi}\right) |E_s(t)|^2$, Eq. (3.2) yields

$$R_I(\tau) = \left(\frac{c}{8\pi}\right)^2 \left[R_{E_s}^2(0) + |R_{E_s}(\tau)|^2 \right]. \quad (3.3)$$

We have therefore been able to obtain an expression for the correlation function of the fluctuations in the intensity of the scattered light in terms of the correlation function of the fluctuations in the electric field. We now wish to extend our arguments to obtain the correlation function for the fluctuations in the photocurrent, $R_i(\tau)$.

We begin by observing that the photocurrent $i(t)$ resulting from light of intensity $I_s(t)$ and frequency ν falling on an area A of the photomultiplier tube is given by definition of the involved quantities as

$$i(t) = \left(\frac{I_s(t)A}{hv} \right) \gamma Ge, \quad (3.4)$$

where h is Planck's constant

G is the PMT gain

γ is the PMT quantum efficiency

e is the electric charge.

By definition, the number of photoelectrons ejected per second from the photocathode is

$$\frac{dn}{dt} = \left(\frac{I_s(t)A}{hv} \right) \gamma, \quad (3.5)$$

and the magnitude of each pulse which results from a photoelectron proceeding down the PMT dynode chain is simply Ge .

Equation (3.4) is valid over the short-time or longer average, that is, $i(t)$ mirrors the envelope function of $I_s(t)$. We must add

that this time dependence is valid only if $E_s(t)$ is uniform over the illuminated area, A . Since light falling on another region of the phototube is not necessarily correlated with that in the area we consider (i.e., the two points do not lie within a coherence area), [see Eq. (2.64)] the time dependence of Eq. (3.4) is valid only within a region no larger than a coherence area, A_{Coh} . We will consider the case which arises when A is greater than A_{Coh} after obtaining results pertinent to this simplified case first.

It would be tempting to obtain the correlation function for the fluctuations in the photocurrent, $R_i(\tau)$, using Eq. (3.4) to relate $i(t)$ and $I_s(t)$. In fact, this is almost correct, but neglects the fact that $i(t)$ is not a continuous function of time whose fluctuations arise solely from variations in $I_s(t)$ around the average intensity, $\langle I_s(t) \rangle$, but rather is made up of pulses of charge Ge . These pulses are essentially delta functions in time*, hence the correlation function for the photocurrent has an additional term due to this so-called "shot effect". This portion of the correlation function is given by⁽⁷⁾ $Ge i_o \delta(\tau)$. We may then write the complete correlation function for the photocurrent using Eqs. (3.3) and (3.4), and the shot term, as

$$R_i(\tau) = \left(\frac{AYGec}{8\pi\hbar\nu} \right)^2 \left[R_{E_s}^2(0) + |R_{E_s}(\tau)|^2 \right] + Ge i_o \delta(\tau). \quad (3.6)$$

Since

$$\begin{aligned} R_{E_s}^2(0) &= \langle |E_s(0)|^2 \rangle \\ &= \left(\frac{8\pi}{c} \right)^2 \langle I_s \rangle^2, \end{aligned} \quad (3.7)$$

* Their width in time is actually their dispersion as they travel down the dynode string of the photomultiplier tube, about 10^{-9} sec, typically.

we have, using Eq. (3.4):

$$R_i(\tau) = i_o^2 + \frac{|R_E(\tau)|^2}{\frac{R_E(0)}{s}} i_o^2 + G e i_o \delta(\tau) , \quad (3.8)$$

where i_o is the average photocurrent, $i_o = \langle i(t) \rangle$. Since the correlation function for the fluctuations in the electric field of the scattered light may be written as

$$R_E(\tau) = R_E(0) e^{-\Gamma_D |\tau|} e^{-i\omega_o |\tau|} \quad (2.82b)$$

$$\Gamma_D = D K^2 \quad (2.80)$$

for concentration fluctuation scattering, and as

$$R_E(\tau) = R_E(0) e^{-\Gamma_R |\tau|} e^{-i\omega_o |\tau|} \quad (2.87c)$$

$$\Gamma_R = 6 D_R \quad (2.87b)$$

for anisotropy scattering, we may rewrite Eq. (3.8) as

$$R_i(\tau) = i_o^2 + i_o^2 e^{-2\Gamma|\tau|} + G e i_o \delta(\tau) \quad (3.9)$$

where $\Gamma = \Gamma_D = D K^2$ for concentration fluctuations

or $\Gamma = \Gamma_R = 6 D_R$ for anisotropy fluctuations.

The most significant property of Eq. (3.9) is that it does not contain ω_o . Indeed, upon Fourier transformation, we obtain the spectrum of the photocurrent as

$$S_i(\omega) = 2\pi i_o^2 \delta(\omega) + 2i_o^2 \left[\frac{2\Gamma}{\omega^2 + (2\Gamma)^2} \right] + G e i_o , \quad (3.10)$$

where Γ has the same dual meaning as in Eq. (3.9). Substituting $\omega = 2\pi\nu$, we obtain

$$S_i(\nu) = i_o^2 \delta(\nu) + \frac{1}{\pi} i_o^2 \left[\frac{\left(\frac{2\Gamma}{2\pi}\right)}{\nu^2 + \left(\frac{2\Gamma}{2\pi}\right)^2} \right] + Gei_o , \quad (3.11)$$

where, by our assumptions of spatial coherence, Eq. (3.11) is valid only if the illuminated area A is less than or equal to the coherence area, A_{Coh} . We therefore see that whereas the spectrum of the light is Lorentzian of width $\Gamma/2\pi$, centered at the optical frequency ν_o , [see Eqs. (2.84) and (2.87a)], the spectrum of the photocurrent is Lorentzian of width $2\Gamma/2\pi$ but now centered at D.C. Since we have already indicated that $\Gamma_D/2\pi$ can be expected to be typically around 1 kHz and $\Gamma_R/2\pi$ around 1 MHz, we see that detection of the photocurrent spectrum may be quite feasible indeed, since high quality filters operating in the audio range (0 to ~ 1 MHz) are commercially available.

Before we consider further the detectability of the spectrum of the photocurrent, it is important to remove one restriction we have placed on the derivation of Eq. (3.11) -- namely, that all the light falling on the phototube is spatially coherent. A straightforward physical argument allows us to understand this problem. Let us assume the illuminated area of the phototube, A , is not smaller than a coherence area, but rather exactly equal to a coherence area, A_{Coh} . Then, Eq. (3.11) is still valid, with i_o in this case given by Eq. (3.4) as*

$$i_o = i_{Coh} = \frac{I_s A_{Coh}}{h\nu} \gamma Ge. \quad (3.12)$$

* For convenience we write $\langle I_s(t) \rangle = I_s$.

Let us now assume that N such coherence areas of the photocathode are illuminated, i.e., $N = A/A_{Coh}$. We then see that the average photocurrent, i_o , is $N i_{Coh}$. Hence, the first term on the R.H.S. of Eq. (3.11), which is proportional to i_o^2 , increases by a factor of N^2 . Next, if we consider the part of $R_i(\tau)$ due to the fluctuations in the scattered light, we may write

$$\left| \left(R_{E_s}(\tau) \right)_A \right|^2 = \left| \sum_{j=1}^N \left(R_{E_s}(\tau) \right)_{A_{Coh}} \right|^2 \\ = N \left| \left(R_{E_s}(\tau) \right)_{A_{Coh}} \right|^2 ,$$

where the above result simply states that each coherence area adds independently to the correlation function of the photocurrent. Hence, the second term on the R.H.S. of Eq. (3.11) increases only as N . Finally, since the shot portion of the spectrum is proportional only to the D.C. photocurrent, which results from the random emission of the photoelectrons from the photocathode, the third term on the R.H.S. of Eq. (3.11) increases as N . Hence, combining Eqs. (3.11) and (3.12) with the argument above, we have

$$S_i(v) = N^2 i_{Coh}^2 \delta(v) + \frac{N}{\pi} i_{Coh}^2 \left[\frac{\left(\frac{2\Gamma}{2\pi}\right)}{v^2 + \left(\frac{2\Gamma}{2\pi}\right)^2} \right] + N G e i_{Coh} . \quad (3.13a)$$

Since $N i_{Coh} = i_o$, we may then write

$$S_i(v) = i_o^2 \delta(v) + \frac{1}{\pi} \frac{i_o^2}{N} \left[\frac{\left(\frac{2\Gamma}{2\pi}\right)}{v^2 + \left(\frac{2\Gamma}{2\pi}\right)^2} \right] + G e i_o . \quad (3.13b)$$

We recall that Eq. (3.13b) is valid by our development above only if

$A > A_{Coh}$. If $A < A_{Coh}$, Eq. (3.11) must be used. We summarize these two results by writing

$$S_i(v) = \begin{cases} i_o^2 \delta(v) + \frac{1}{\pi} \frac{i_o^2}{n} \left[\frac{\left(\frac{2\Gamma}{2\pi}\right)}{v^2 + \left(\frac{2\Gamma}{2\pi}\right)^2} \right] + Gei_o & n \geq 1 \\ i_o^2 \delta(v) + \frac{1}{\pi} i_o^2 \left[\frac{\left(\frac{2\Gamma}{2\pi}\right)}{v^2 + \left(\frac{2\Gamma}{2\pi}\right)^2} \right] + Gei_o & n \leq 1 \end{cases} \quad (3.14)$$

The spectrum is an average quantity, because it is simply the Fourier transform of the correlation function, which is a time (or ensemble) average quantity by definition. If we call the second term in Eq. (3.14) the "signal" [$\mathbf{S}(v)$] because it contains the information we seek (i.e., Γ) and the third term the "noise" [$\mathbf{N}(v)$] because it contains no useful information, we may rewrite Eq. (3.14) as

$$S_i(v) = i_o^2 \delta(v) + \langle \mathbf{S}(v) \rangle + \langle \mathbf{N}(v) \rangle . \quad (3.15)$$

The $\langle \rangle$ signs in Eq. (3.15) indicate that the "signal" and "noise" are both random variables and the spectrum reflects the average values of these quantities.

From Eq. (3.14) the noise contribution $\langle \mathbf{N}(v) \rangle$ is seen to be "flat", i.e., independent of v . Because the electron pulses are not true delta functions in time [as we assumed in deriving Eq. (3.14)], but rather have a width of around 10^{-9} sec due to their dispersion in the dynode string of the PMT, the shot noise is actually flat to only around 1 GHz. However, since the frequency range we consider here is

< 1 MHz, we can truly consider the spectrum of the shot noise to be flat.

The essential features of Eqs. (3.14 - 3.15) may now be displayed in Fig. 3.1 below:

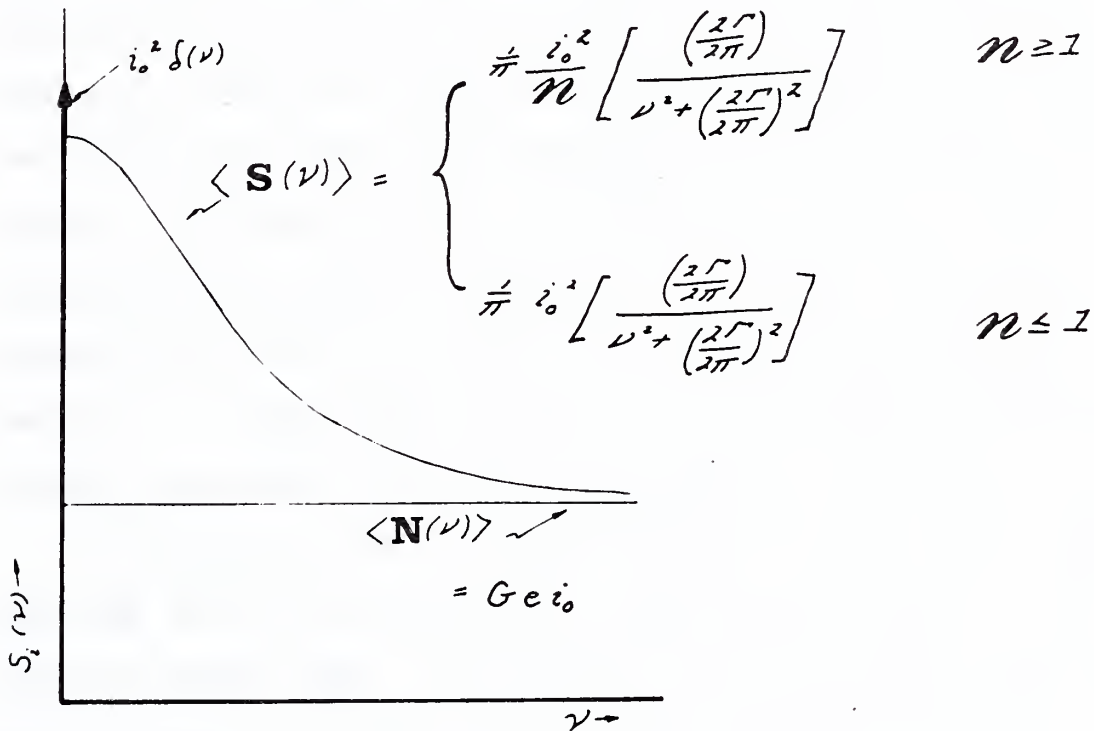


Fig. 3.1 The Power Spectrum of the Photocurrent

Because the phototube has been used as a non-linear element to mix the scattered light with itself, the spectrum displayed in Fig. 3.1 has been termed the "self-beat" spectrum of the photocurrent.⁽²⁾ An alternative method, not employed in this thesis, is to mix the scattered light with an intense coherent local oscillator. This is referred to as "heterodyne mixing spectroscopy",^(1,4,5) and gives essentially the same results

as above, except the spectrum of the photocurrent now is Lorentzian of width $\Gamma/2\pi$ and still centered at zero frequency if the spectrum of the incident light is Lorentzian of width $\Gamma/2\pi$. In general, self-beating spectroscopy is more readily performed because problems of scattered light-local oscillator wavefront mismatch are not present,⁽⁵⁾ nor does one have to contend with noise present on the very strong local oscillator.⁽⁵⁾ On the other hand, heterodyning is often unavoidable. For example, at very small angles it is difficult to remove all light elastically scattered from windows, etc. In addition, the predetection signal-to-noise ratio is a factor of four larger in the heterodyne method.⁽⁵⁾ In this thesis, the ease of the self-beating technique outweighed the increased signal-to-noise advantage of heterodyne detection.

It is clear from Fig. 3.1 that if $\langle \mathbf{S}(\nu) \rangle$ is always small compared with $\langle \mathbf{N} \rangle$ we will have difficulty in discerning the signal. In fact, the ratio $\langle \mathbf{S}(0) \rangle / \langle \mathbf{N} \rangle$ will be useful to give us an idea of the signal's detectability, and Gerjony, Forrester, and Parkins⁽⁸⁾ suggested a similar expression for any experiment in which the primary competition to the "signal" is the "shot noise". The ratio has come to be called the "predetection" signal-to-noise ratio⁽³⁻⁵⁾ because it does not refer to the instrumental bandwidth before detection, or how long we accumulate the information contained in this bandwidth. We can say somewhat arbitrarily that a predetection signal-to-noise ratio of about 1 is desirable as a minimum value we would like experimentally, although experiments involving much smaller values are still feasible. We will proceed in section III.B.2 to calculate exactly what values we might expect for macromolecular solutions.

By definition, we set

$$\left(\frac{\text{SIG}}{\text{NOISE}} \right)_{\text{PRE}} = \frac{\langle \mathbf{S}(0) \rangle}{\langle \mathbf{N} \rangle} . \quad (3.16)$$

We then have, from Eqs. (3.14) and (3.15), that

$$\left(\frac{\text{SIG}}{\text{NOISE}} \right)_{\text{PRE}} = \frac{i_o}{\text{GeV}} \times \begin{cases} \frac{1}{n} & n \geq 1 \\ 1 & n \leq 1 \end{cases} . \quad (3.17)$$

We now take the average of Eq. (3.4) to obtain

$$i_o = \begin{cases} \frac{I_s A}{h \nu} \gamma \text{ Ge} & A \leq A_{\text{Coh}} \\ & (n \leq 1) \\ \frac{n I_s}{h \nu} A_{\text{Coh}} \gamma \text{ Ge} & A \geq A_{\text{Coh}} \\ & (n \geq 1) \end{cases} . \quad (3.18)$$

Combining Eqs. (3.17) and (3.18) yields

$$\left(\frac{\text{SIG}}{\text{NOISE}} \right)_{\text{PRE}} = \begin{cases} \frac{I_s A}{h \nu} \frac{\gamma}{\Gamma} & A \leq A_{\text{Coh}} \\ \frac{I_s A_{\text{Coh}}}{h \nu} \frac{\gamma}{\Gamma} & A \geq A_{\text{Coh}} \end{cases} . \quad (3.19)$$

Equation (3.19) indicates that the value of the predetection signal-to-noise ratio can never exceed that obtained by collecting a single coherence area. Although it may be desirable to increase the illuminated area A of the photocathode to obtain sufficient photocurrent to swamp other sources of noise (e.g., dark current, residual amplifier noise, etc.) this does not improve or reduce the value of $\left(\frac{\text{SIG}}{\text{NOISE}} \right)_{\text{PRE}}$.

On the other hand, it may be necessary to reduce A to a value less than A_{Coh} due to acceptance angle considerations (see section II.C). This would indeed reduce our predetection signal-to-noise ratio as indicated by Eq. (3.19).

Before using Eq. (3.19) to calculate the value of $\frac{\langle \mathbf{S}(0) \rangle}{\langle \mathbf{N} \rangle}$ expected experimentally (section III.B.2), it is interesting to point out that combining Eqs. (3.5) and (3.19) we see that

$$\left(\frac{\text{SIG}}{\text{NOISE}} \right)_{\text{PRE}} = \begin{cases} \left\langle \frac{dn}{dt} \right\rangle_{\text{Coh}} \frac{1}{\Gamma} \frac{A}{A_{Coh}} & A \leq A_{Coh} \\ \left\langle \frac{dn}{dt} \right\rangle_{\text{Coh}} \frac{1}{\Gamma} & A > A_{Coh} \end{cases} \quad (3.20)$$

where $\left\langle \frac{dn}{dt} \right\rangle_{\text{Coh}}$ is the average number of photoelectrons per second which arise from an area of the photocathode of size A_{Coh} . For $\langle \mathbf{S}(0) \rangle / \langle \mathbf{N} \rangle$ to be 1, we see that we need one photoelectron ejected per correlation time τ of the field of the scattered light ($\tau = 1/\Gamma$) if $A \geq A_{Coh}$, and (A_{Coh}/A) photoelectrons per time τ if $A \leq A_{Coh}$. This gives physical insight into the relationship between the nature of the incident light and the operation of the spectrometer. We see immediately that no amount of "electronic wizardry" can improve the ratio $\langle \mathbf{S}(0) \rangle / \langle \mathbf{N} \rangle$ since it is related solely to the number of photoelectrons we can obtain in a time, τ . On the other hand, an optical regenerative amplifier which could increase I_s would increase $\left\langle \frac{dn}{dt} \right\rangle_{\text{Coh}}$ and hence $\left(\frac{\text{SIG}}{\text{NOISE}} \right)_{\text{PRE}}$ as would raising the quantum efficiency, γ , or the intensity of the incident light, I_{Inc} . Of course, within the restriction of a given value for I_s , γ , and I_{Inc} , we can still raise $\langle \mathbf{S}(0) \rangle / \langle \mathbf{N} \rangle$ by making A_{Coh} as large as possible and insuring that the collecting solid

angle is at least as large as Ω_{Coh} . These adjustments must be made within the restrictions on beam diameter and acceptance solid angle discussed in section II.C.

On the other hand, the ratio $\langle \mathbf{S}(0) \rangle / \langle \mathbf{N} \rangle$ does not indicate the actual signal-to-noise as it is usually defined. We now define the "post detection" signal-to-noise ratio, ⁽³⁻⁵⁾ $\left(\frac{\text{SIG}}{\text{NOISE}} \right)_{\text{POST}}$. This requires the introduction of experimental parameters and hence is not so intrinsic a quantity as $\left(\frac{\text{SIG}}{\text{NOISE}} \right)_{\text{PRE}}$. It does indicate, however, the actual detectability of the signal, and therefore is most useful. This ratio is defined as the average value of the signal, $\langle \mathbf{S}(\nu) \rangle$, divided by the rms value of the fluctuations in the signal and shot noise terms, that is:

$$\left(\frac{\text{SIG}(\nu)}{\text{NOISE}} \right)_{\text{POST}} = \frac{\langle \mathbf{S}(\nu) \rangle}{\langle (\delta[\mathbf{S}(\nu)] + \mathbf{N}(\nu))^2 \rangle^{1/2}} \quad (3.21)$$

We will discuss the experimental methods which result in the observed $\left(\frac{\text{SIG}(\nu)}{\text{NOISE}} \right)_{\text{POST}}$ in the next section. Experimentally, we will observe a finite section of the spectrum of the photocurrent of width $\Delta\nu_1$. If we average the power we observe within $\Delta\nu_1$ for a time T , then the post-detection signal-to-noise is given by ⁽⁹⁾

$$\left(\frac{\text{SIG}(\nu)}{\text{NOISE}} \right)_{\text{POST}} = \frac{\langle \mathbf{S}(\nu) \rangle}{\langle \mathbf{S}(\nu) \rangle + \langle \mathbf{N}(\nu) \rangle} \sqrt{\frac{\nu_1}{\nu_2}} \quad (3.22)$$

where $\nu_2 = \frac{1}{T}$ and is called the "post-detection bandwidth". If we define a frequency-dependent predetection signal to noise ratio as

$$\left(\frac{\text{SIG}(\nu)}{\text{NOISE}} \right)_{\text{PRE}} = \frac{\langle \mathbf{S}(\nu) \rangle}{\langle \mathbf{N}(\nu) \rangle}, \quad (3.23)$$

then

$$\left(\frac{\text{SIG}(\nu)}{\text{NOISE}} \right)_{\text{POST}} = \frac{\left(\frac{\text{SIG}(\nu)}{\text{NOISE}} \right)_{\text{PRE}}}{\left(\frac{\text{SIG}(\nu)}{\text{NOISE}} \right)_{\text{PRE}} + 1} \cdot \sqrt{\frac{\nu_1}{\nu_2}} \quad (3.24)$$

The interesting implications of this result have been pointed out by Lastovka⁽¹⁰⁾ and Benedek.⁽⁹⁾ If the predetection signal-to-noise ratio is high, the post-detection ratio becomes independent of all parameters except ν_1 and ν_2 . In such cases, it serves no advantage to increase I_{Inc} , γ , A_{Coh} , etc., a rather unintuitive result.

We now turn in section III.B.2 to the experimental setup of a square-law spectrometer and the calculation of realizable signal-to-noise ratios in light scattering experiments from solutions of macromolecules.

2) Experimental Configuration and Evaluation of Signal-to-Noise Ratio

Figure 3.2 below depicts the experimental setup of a self-beating spectrometer with sufficient detail to allow us to evaluate the signal-to-noise ratio obtainable in our experiments.

The laser must have uniphase output (TEM_{00}) to insure the spatial coherence required for mixing, as we have already discussed. The focusing lens renders a beam in the cell of diameter a and length L . If d is the initial diameter of the beam as it leaves the laser, and f is the focal length of the lens, then⁽¹¹⁾

$$a \approx \left(\frac{f}{d} \right) \lambda \quad (3.25)$$

$$L \approx \left(\frac{f}{d} \right)^2 \lambda, \quad (3.26)$$

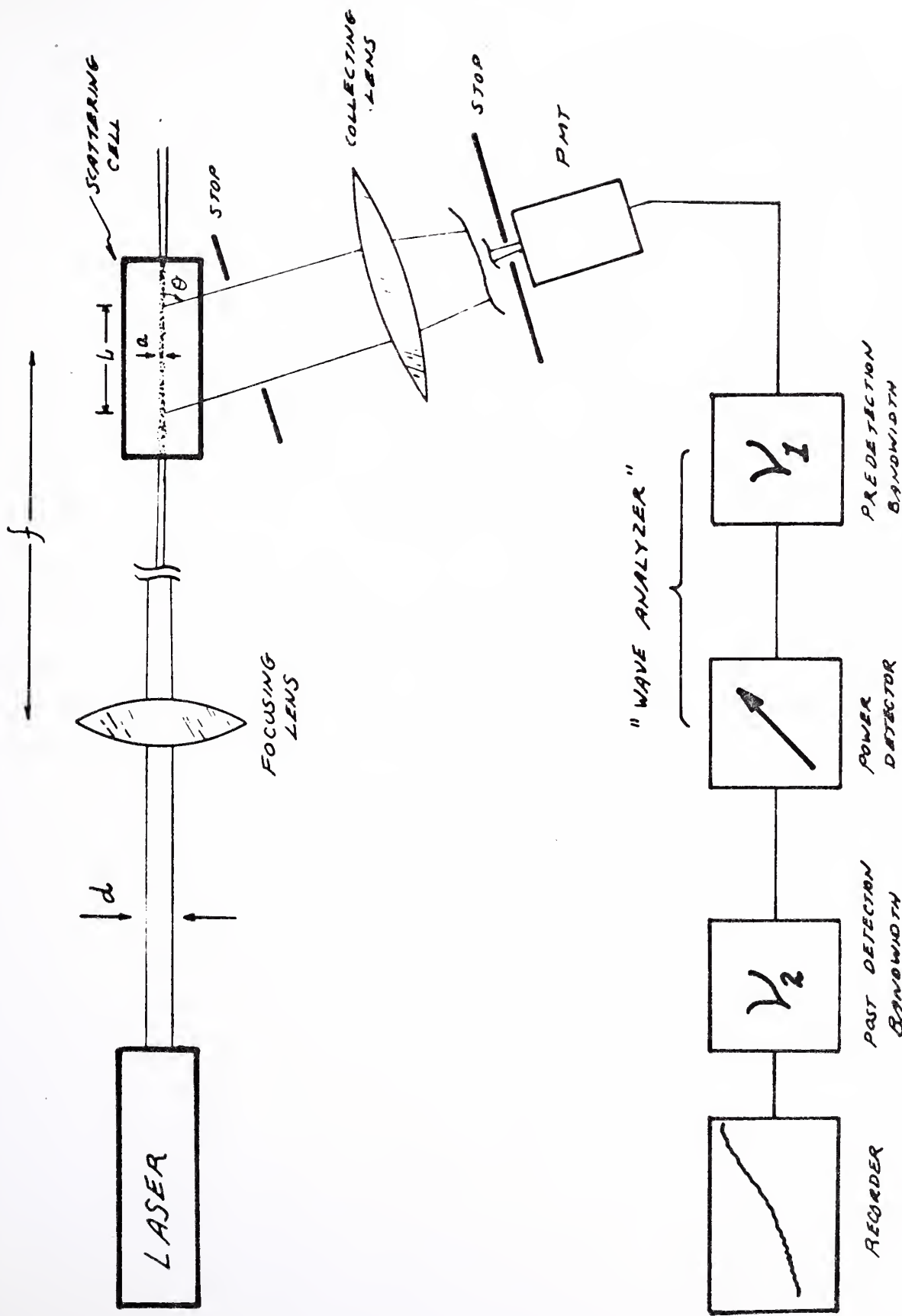


Fig. 3.2 Block Diagram of Self-Beating Spectrometer

where, within this approximation, λ can be taken as the wavelength of light in the medium.

To insure that no stray light is seen by the collecting lens, an aperture is placed immediately after the cell. The scattered light then falls on a collecting lens which maps all parallel light scattered at an angle θ onto the photomultiplier tube. An aperture before the PMT insures an acceptance solid angle which complies with the requirements of section II.C.

The photocurrent is then analyzed by the spectrometer which in block form consists of a predetection filter of width v_1 , a power detector, and then is displayed on the strip chart recorder after being accumulated for a time $T = \frac{1}{v_2}$.

We may now evaluate the expected signal-to-noise ratio. For convenience, we will assume that we can arrange the scattering geometry so as to allow collection of at least one coherence area. Then, recognizing that $I_s A_{\text{Coh}}$ is simply P_s^{Coh} , we may combine Eqs. (2.66) and (3.19) as

$$\left(\frac{\text{SIG}}{\text{NOISE}} \right)_{\text{PRE}} = \left(\frac{\gamma}{hv\Gamma} \right) P_{\text{Inc}}^{2L} R \frac{\lambda^2}{a(L \sin \theta + a|\cos \theta|)} . \quad (3.27)$$

We may express L and a in terms of Eqs. (3.25) and (3.26) and thus rewrite Eq. (3.27) as

$$\left(\frac{\text{SIG}}{\text{NOISE}} \right)_{\text{PRE}} = \left(\frac{\gamma}{hv\Gamma} \right) P_{\text{Inc}}^{2R} \frac{\lambda}{\left(\frac{f}{d} \right) \sin \theta + |\cos \theta|} . \quad (3.28)$$

We recognize that $hv = \frac{hc}{n\lambda}$, and we can use specific expressions for Γ_D and Γ_R [Eqs. (2.85) and (2.87b)], to obtain

$$\left(\frac{\text{SIG}}{\text{NOISE}} \right)_{\text{PRE}} = \left\{ \begin{array}{l} \frac{n\gamma}{8\pi^2 hc} \frac{1}{\sin^2(\frac{\theta}{2})} \frac{\mathbf{P}_{\text{Inc}} \mathbf{R}}{D} \frac{\lambda^4}{(\frac{f}{d}) \sin \theta + |\cos \theta|} \\ \quad [\text{Concentration fluctuation scattering}] \end{array} \right. \quad (3.29)$$

$$\left. \begin{array}{l} \frac{n\gamma}{3hc} \frac{\mathbf{P}_{\text{Inc}} \mathbf{R}_a}{D_R} \frac{\lambda^2}{(\frac{f}{d}) \sin \theta + |\cos \theta|} \\ \quad [\text{Anisotropy scattering}] \end{array} \right\} \quad (3.30)$$

where \mathbf{R}_a is the Rayleigh ratio of the depolarized light.

The results of Eqs. (3.29) and (3.30) are worthy of comment. We see immediately from (3.29) that the predetection signal-to-noise ratio in a concentration fluctuation experiment is independent of the wavelength of the incident light. That is, the familiar $(1/\lambda)^4$ dependence of the Rayleigh ratio [Eq. (2.34)] is completely canceled by the λ^4 present in Eq. (3.29). Thus, one's intuitive feeling that the $(1/\lambda)^4$ dependence of the intensity of Rayleigh scattering would imply improved $\left(\frac{\text{SIG}}{\text{NOISE}} \right)_{\text{PRE}}$ for shorter wavelengths is not valid in the case of concentration fluctuations.

The physical origins of this result are clear. The predetection signal-to-noise ratio, as shown in Eq. (3.20), is a measure of the number of photoelectrons ejected per correlation time ($\tau = \frac{1}{F}$). Since τ decreases as λ^2 for concentration fluctuations, the value of $\left(\frac{\text{SIG}}{\text{NOISE}} \right)_{\text{PRE}}$ also decreases as λ^2 . Similarly, since the number of photons in a beam of given power decreases as the wavelength decreases, the number of photoelectrons also decreases as λ . Finally, although the coherence solid angle Ω_{Coh} [Eq. (2.63)] is seen to be independent of λ upon applying Eqs. (3.25) and (3.26), the length of the beam, L , over which scattered

light is focused decreases as λ [Eq. (3.26)]. Hence, four factors of λ appear in the numerator of $\left(\frac{\text{SIG}}{\text{NOISE}}\right)_{\text{PRE}}$, completely canceling the $(1/\lambda)^4$ dependence of \mathbf{R} . However, the value of the correlation time $(1/\Gamma)$ increases as $\sin^2(\frac{\theta}{2})$, so that the $\left(\frac{\text{SIG}}{\text{NOISE}}\right)_{\text{PRE}}$ can still be enhanced at small angles, and the K^2 dependence of the spectrum of the scattered light does more good than harm from an experimental point of view.

Since Γ_R (anisotropy scattering) is independent of K , Eq. (3.30) reveals that in this type of scattering, we do get a $(1/\lambda)^2$ enhancement of the signal-to-noise ratio as we decrease λ . However, since Γ_R is independent of angle, we get no pronounced improvement in the small angle regime except through the fact that the coherence areas become large. This is indicated by the factor of $\{(\frac{f}{d}) \sin \theta + |\cos \theta|\}$ in the denominator of Eqs. (3.29) and (3.30). This factor is a symmetric function of the scattering angle, and we thus see that, due to coherence area enlargement alone, the signal-to-noise ratio increases for both small and large values of θ , having a minimum at $\theta = 90^\circ$. In the case of anisotropy scattering, for example, where there is no $\sin^2(\frac{\theta}{2})$ dependence of the spectrum, the same signal-to-noise ratio can be obtained at an angle θ and the supplementary angle $\pi - \theta$. Since stray light is peaked in the forward direction, it might therefore be desirable to study the spectrum for large angles under these conditions. Even in the case of concentration fluctuation scattering, it might be desirable to study the spectrum at large angles to eliminate problems of lack of definition in K as discussed in section II.C. Of course, in the case of concentration fluctuations, small-angle scattering has the additional advantage the Γ_D becomes small, and this is not the case for large angles.

Although there thus does not seem to be much reason to use short

wavelength incident light, there is in reality much reason to do so for reasons not related to the $(1/\lambda)^4$ dependence of Rayleigh scattering.

Presently, phototubes are available with a quantum efficiency, γ , several times larger in the blue than in the red, for example. Similarly, high power short wavelength lasers are becoming increasingly common and inexpensive. Hence, indirect reasons may well motivate the use of short wavelength incident light.

We now examine numerically the value of $\left(\frac{\text{SIG}}{\text{NOISE}}\right)_{\text{PRE}}$ we anticipate in the experiments to be performed in this thesis, and consider other experiments in light of these results. Since lysozyme has a larger value of D and smaller scattering cross-section than any of the other molecules we consider, it will have the lowest value of $\left(\frac{\text{SIG}}{\text{NOISE}}\right)_{\text{PRE}}$ and hence will serve as an appropriate example in the case of concentration fluctuations. We recall from section II.C that we may study the spectrum for scattering angles as small as about 5° , if we restrict the beam diameter to be about 0.1 mm or larger. Since self-beating spectroscopy is extremely difficult below this angle, due to stray light, we will set $a = 0.1$ mm and calculate $\left(\frac{\text{SIG}}{\text{NOISE}}\right)_{\text{PRE}}$ for angles larger than 5° . For red light, Eq. (3.25) then indicates the focal ratio (f/d) must be about 160 and we used a value of 165 in the actual experiment. We may now evaluate Eq. (3.29) for $\left(\frac{\text{SIG}}{\text{NOISE}}\right)_{\text{PRE}}$ using the values given in Table 3.1 below:

Table 3.1

Physical Parameters to Evaluate $\left(\frac{\text{SIG}}{\text{NOISE}}\right)_{\text{PRE}}$

$n_w = 1.33^{(1)}$	$R_{\text{Lys}, 1\%} = 20 \times 10^{-6} \text{ cm}^{-1}^{(3)}$
$\gamma = 0.053^{(2)}$	$P_{\text{Inc}} = 50 \text{ mw}^{(4)}$
$f/d = 165$	$D = 10.6 \times 10^{-7} \text{ cm}^2/\text{sec}^{(5)}$
	$\lambda = \lambda_o/n = 4750\text{\AA}^{(6)}$

- (1) For convenience, we treat the solution index as that of water
- (2) Derived from cathode radiant given in specification sheet,
7265 PMT (RCA)
- (3) Equation (2.38)
- (4) Incident power available from a Spectra-Physics He-Ne model
125 laser
- (5) Chapter V
- (6) $\lambda_0 = 6328\text{A}^\circ$

Since $(f/d) \sin \theta \gg |\cos \theta|$ for all angles down to 5° , we may write Eq. (3.29), upon substitution of the values in Table 3.1 above, as

$$\left(\frac{\text{SIG}}{\text{NOISE}} \right)_{\text{PRE}} = \frac{216}{\sin^2(\frac{\theta}{2})} \quad \frac{1}{165 \sin \theta}$$

or

$$\left(\frac{\text{SIG}}{\text{NOISE}} \right)_{\text{PRE}} = \frac{1.3}{\sin^2(\frac{\theta}{2}) \sin \theta} \quad . \quad (3.31)$$

As we discuss in Chapter V, this is somewhat larger (a factor of 5) than was observed experimentally.

We see from Eq. (3.31) that a predetection signal-to-noise ratio of about 1/1 is feasible even in the case of lysozyme. Hence, our proposed experiments on the bacteriophages are seen to be readily done from a signal-to-noise point of view.

Equation (3.31) reveals, in addition, the severe difficulties to be encountered if we try to study the anisotropy spectrum of proteins with the light mixing techniques. For we have already shown (section II.B.2.b) that we expect the depolarization ratio (p_v) for proteins to be around

10^{-4} in round numbers. Hence, even if the anisotropy spectrum had the same width as the concentration fluctuation spectrum, the predetection signal-to-noise ratio would be four orders of magnitude smaller.

A value of $\left(\frac{\text{SIG}}{\text{NOISE}}\right)_{\text{PRE}} \sim 10^{-4}$ would be bad enough, but in addition, we expect Γ_R to be typically three or four orders of magnitude larger than Γ_D (see section II.D), bringing $\left(\frac{\text{SIG}}{\text{NOISE}}\right)_{\text{PRE}}$ to the value of $\sim 10^{-8}$. This is a formidable obstacle, indeed.

There are, of course, ways to improve the signal-to-noise ratio we actually observe, i.e., $\left(\frac{\text{SIG}}{\text{NOISE}}\right)_{\text{POST}}$. For example, let us assume that $\Gamma_R/2\pi$ is about 1 MHz. If we use a predetection bandwidth, v_1 , of about 1/4 MHz (to avoid distortion of the measured lineshape $v_1/[2(2\Gamma_R/2\pi)] \leq 1/10$ as we discuss in section III.B.4), and integrate the signal for, say, 10 sec. (larger values of $T = 1/v_2$ become difficult to use, since experimental stability over long times then becomes a problem), we see from Eq. (3.24) that the post-detection signal-to-noise is enhanced by a factor of $\sqrt{v_1/v_2} = 1.6 \times 10^3$. In addition, since Γ_R is independent of K , we can focus the beam arbitrarily small, even to the diffraction limit, and thereby gain another two orders of magnitude in our value of $\left(\frac{\text{SIG}}{\text{NOISE}}\right)_{\text{POST}}$. We are still left with $\left(\frac{\text{SIG}}{\text{NOISE}}\right)_{\text{POST}} \sim 10^{-3}$, an unsatisfactory value.

At this point, the potential of the spherical Fabry-Perot etalon interferometer becomes clear. As we mentioned in section II.D, line-widths of the order of 1 MHz are definitely within the resolving power of such instruments. Also, and quite significant, the Fabry-Perot requires far fewer photoelectrons per second to yield the same post-detection signal-to-noise ratio. Lastovka⁽¹²⁾ has made a detailed analysis of the relative merits of the two systems. In the range of 1 MHz, the Fabry-Perot gives three to four orders of magnitude improved signal-to-noise ratio

under the same experimental conditions. We thus see that those molecules whose values of $\Gamma_R/2\pi$ can be resolved by a Fabry-Perot, can be experimentally studied with feasible signal-to-noise values. Such experiments require a single-frequency laser and, perhaps, pulse counting equipment, and are thus non-trivial. On the other hand, the vastly improved signal-to-noise ratio expected would justify the effort in those cases in which the anisotropy scattering has a spectral width of the order of one MHz and, as shown in section II.D, this would be a typical value.

Nevertheless, there are many molecules, quite interesting from the viewpoint of biology or polymer chemistry, which are far larger than the proteins. An often-studied example is tobacco mosaic virus (TMV). D_R has been measured for this virus by various techniques, a typical value being (corrected to 20°C, water)

$$D_R = (295 \pm 12)/\text{sec} , \quad (3.32)$$

as measured by the technique of electric birefringence.⁽¹³⁾ From eqs. (2.87b) and (3.13b), we see that the width (HWHM) of the spectrum of the photocurrent would then be

$$\frac{2\Gamma_R}{2\pi} \approx 563 \text{ Hz} @ 20^\circ\text{C} , \quad (3.33)$$

a far smaller value than for the proteins which we have discussed.

We will discuss the interpretation of D_R in terms of hydrodynamic models of TMV with the use of hydrodynamic equations due to Broersma⁽¹⁴⁾ and others in Chapter V. For the moment, Eq. (3.32) allows us to get some idea of the expected predetection signal-to-noise we might obtain in a self-beat experiment on the depolarized light scattered by TMV.

We may use Eq. (3.30) to obtain $\left(\frac{\text{SIG}}{\text{NOISE}}\right)_{\text{PRE}}$, if we can reasonably

estimate the Rayleigh ratio for the depolarized part of the scattered light, which we denote \mathbf{R}_a . As shown in section II.B.2.b, for polarized incident light, we may write

$$\mathbf{R}_a = \mathbf{R} \rho_v, \quad (3.34)$$

where \mathbf{R} is the Rayleigh ratio for the light scattered by concentration fluctuations. If we consider a dilute solution of TMV and study the scattering for small angles, we have

$$\mathbf{R} = \mathbf{K} CM \quad (2.35)$$

where $\mathbf{K} \approx 1.3 \times 10^{-7} (\text{cm/g})^2$. For a 0.01% solution of TMV the molecular weight of which is about 50 million, we see that

$$\mathbf{R} \approx 650 \times 10^{-6} \text{ cm}^{-1}. \quad (3.35)$$

Thus, since we showed in section II.B.2.b that ρ_v for TMV is about 0.0023, we have

$$(\mathbf{R}_a)_{\text{TMV, 0.01\%}} \approx 1.5 \times 10^{-6}. \quad (3.36)$$

This is a reasonably large value, indeed, being about 8% as large as the Rayleigh ratio of the light scattered by concentration fluctuations in a 1% lysozyme solution [$\mathbf{R}_{\text{Lys, 1\%}} = 20 \times 10^{-6}$, see Eq. (2.38) in section II.B.1.].

If we use the value of D_R in Eq. (3.32) and the value of \mathbf{R}_a in Eq. (3.36), we may then calculate $\left(\frac{\text{SIG}}{\text{NOISE}} \right)_{\text{PRE}}$ using Eq. (3.30) to obtain a value of about 10/1 at 90° scattering angle, where we neglect the dependence of \mathbf{R} on scattering angle. It is clear, therefore, that TMV is an

ideal example to study the anisotropy scattering from a signal-to-noise point of view. On the other hand, the rotary relaxation time of TMV is sufficiently long that the assumption of uncoupled translation and rotation made in section II.D to derive the spectrum of the anisotropy scattering is not ideally met. We will discuss this point in Chapter V.

It is appropriate to conclude this section with several general observations regarding experimentally realizable values of $\left(\frac{\text{SIG}}{\text{NOISE}}\right)_{\text{PRE}}$. First, all calculations made in this section assume a 50 mw laser output at $\lambda_0 = 6328\text{\AA}$. This is a reasonable value of He-Ne lasers presently available. In recent months, however, argon-ion lasers have become commercially available with outputs approaching one watt in the blue and green sections of the visible spectrum. This factor of 20 increase in power, coupled with the factor of two or three gained in quantum efficiency for these shorter wavelengths, decidedly improves the value of $\left(\frac{\text{SIG}}{\text{NOISE}}\right)_{\text{PRE}}$ that can be expected, and the possibility of self-beat spectroscopy of the anisotropy spectrum of proteins becomes far better. There is every reason to believe that this upward spiral in power available in commercial lasers will continue, and photosurfaces with improved quantum efficiency appear regularly as well.

In addition, one may ask whether there might be advantages in studying the correlation function of the photocurrent fluctuations directly, rather than the spectrum. Since these two quantities are simply related by the Fourier transform, we might expect, at first thought, that the signal-to-noise obtainable in either form of experiment would be the same. Indeed, if we use an n-channel wave analyzer (i.e., study $S_1(v)$ for n discrete values of v simultaneously] and an n-channel autocorrelator [i.e.

study $R_i(\tau)$ for n discrete values of τ simultaneously], we can obtain essentially the same value of the signal-to-noise ratio in either case, for a given time of observation.⁽¹⁵⁾ However, with the advent of digital integrated circuits, it is apparent that it is more practical to construct an n -channel autocorrelator than an n -channel wave analyzer. Two autocorrelators are already available commercially,⁽¹⁶⁾ but neither is a true digital device and therefore neither allows the determination of the correlation function on the individual pulses of the photocurrent. For an autocorrelator to be useful in light scattering, it is almost a necessity to perform autocorrelation on the individual photocurrent pulses (i.e., the correlator must be digital) as we can see by the following discussion. We have shown that the correlation function for the photocurrent, for a Lorentzian input spectrum, is:

$$R_i(\tau) = i_o^2 + i_o^2 e^{-2\Gamma|\tau|} + Gei_o \delta(\tau) \quad (3.9)$$

if the illuminated region of the photocathode is $\leq A_{Coh}$. We may generalize this result for $A \geq A_{Coh}$ exactly as we did to obtain $S_i(v)$ [Eq. (3.10)] and we then obtain the complete result:

$$R_i(\tau) = \begin{cases} i_o^2 + i_o^2 e^{-2\Gamma|\tau|} + Gei_o \delta(\tau) & 0 < n \leq 1 \\ i_o^2 + \frac{i_o^2}{n} e^{-2\Gamma|\tau|} + Gei_o \delta(\tau) & n \geq 1 \end{cases} \quad (3.37)$$

where $n = \frac{A}{A_{Coh}}$ = # of coherence areas we collect. This result is quite significantly different from the corresponding result for $S_i(v)$ [Eq. (3.14)]. For if we define the "signal" as $S(\tau)$ and the "noise" as $N(\tau)$, we may write

$$\langle \mathbf{S}(\tau) \rangle = \begin{cases} i_0^2 e^{-2\Gamma|\tau|} & 0 < n \leq 1 \\ \frac{i_0^2}{n} e^{-2\Gamma|\tau|} & n \geq 1 \end{cases} \quad (3.38)$$

$$\langle \mathbf{N}(\tau) \rangle = i_0^2 \quad . \quad (3.39)$$

We may now display Eq. (3.37) in Fig. 3.3 below:

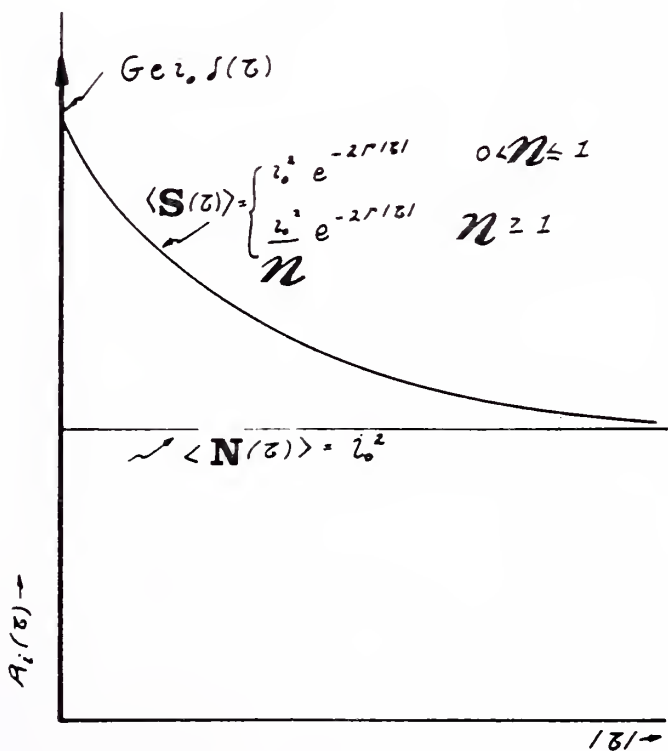


Fig. 3.3 The Correlation Function of the Photocurrent

We then have

$$\frac{\langle \mathbf{S}(0) \rangle}{\langle \mathbf{N}(0) \rangle} = \begin{cases} 1/1 & 0 < n \leq 1 \\ 1/n & n \geq 1 \end{cases}, \quad (3.39)$$

where $\frac{\langle \mathbf{S}(0) \rangle}{\langle \mathbf{N}(0) \rangle}$ is the τ -space analogue of the predetection signal-to-noise ratio, Eq. (3.16). We thus see that the signal-to-noise value does not saturate at $n = 1$, as it does in a spectral determination, but actually decreases as n increases above 1 and is constant for $0 < n \leq 1$.

We are thus compelled to operate using no more than one coherence area, i.e., $A_{\text{Max}} = A_{\text{Coh}}$. This implies, in a light-scattering experiment, relatively few pulses per second in the photocurrent. If this number, dn/dt , is still much larger than the dark current, we are in no trouble with a digital autocorrelator. With the devices that have analogue-to-digital converters at the input, on the other hand, we must operate so far down on the dynamic range of the input amplifier to avoid input clipping that electronic noise intrinsic to the correlator becomes a serious problem. This then represents a distinct disadvantage of an analogue autocorrelator relative to a wave analyzer, which is also an analogue device.

The considerations above make a multi-channel wave analyzer attractive at this time. At least one such device which would be appropriate to experiments in light scattering is available commercially. ⁽¹⁷⁾

It seems reasonable to assume that much progress in the commercial availability of both multi-channel autocorrelators and multi-channel wave analyzers will be made in the coming years.

3) Optical Alignment and Detection

As we showed in section III.B.1, no gain is achieved in the experimental signal-to-noise ratio, after collecting at least one coherence area, by increasing the amount of scattered light which is collected. This allows us to use the relatively simple collection system indicated in Fig. 3.4 below for most of the work presented in this thesis. The laser is focused into the scattering cell in accordance with the requirements of Section II.C. Stop #1 immediately in front of the laser serves to block the large amount of stray light which is emitted by the laser. In all experiments except that on TMV, a Spectra-Physics model 125 laser was employed, delivering 50 mw @ $\lambda_0 = 6328\text{\AA}$, TEM_{00}^0 . In the TMV study, a Coherent Radiation Labs model 52 laser became available, from which about 700 mw @ $\lambda_0 = 5145\text{\AA}$ TEM_{00}^0 was obtained. Before being focused, the laser light is rotated to a convenient angle by a front surface deflecting mirror. The optical bench containing all optics between points A and B in Fig. 3.4 is then rotated until the incident beam executes the path indicated in the figure. We describe below the method of determining this angle.

Despite careful cleaning, a small amount of light is elastically scattered by both the mirror and the focusing lens, and stops #2 and #3 serve to prevent this light from entering the scattering cell. In all experiments standard fluorescence cells were used to hold the sample (Lux Scientific Inst. Corp., New York, N.Y.). These were made of near ultra-violet glass and allowed a path length of 2 cm. In all cases, this length was sufficient to collect scattered light over the entire focused region of the incident beam. After exiting the cell, most of the transmitted beam is reflected into a light trap by a No. 3 metallic film neutral density filter. A small portion (10^{-3}) of the transmitted light is allowed to fall on a silicon solar

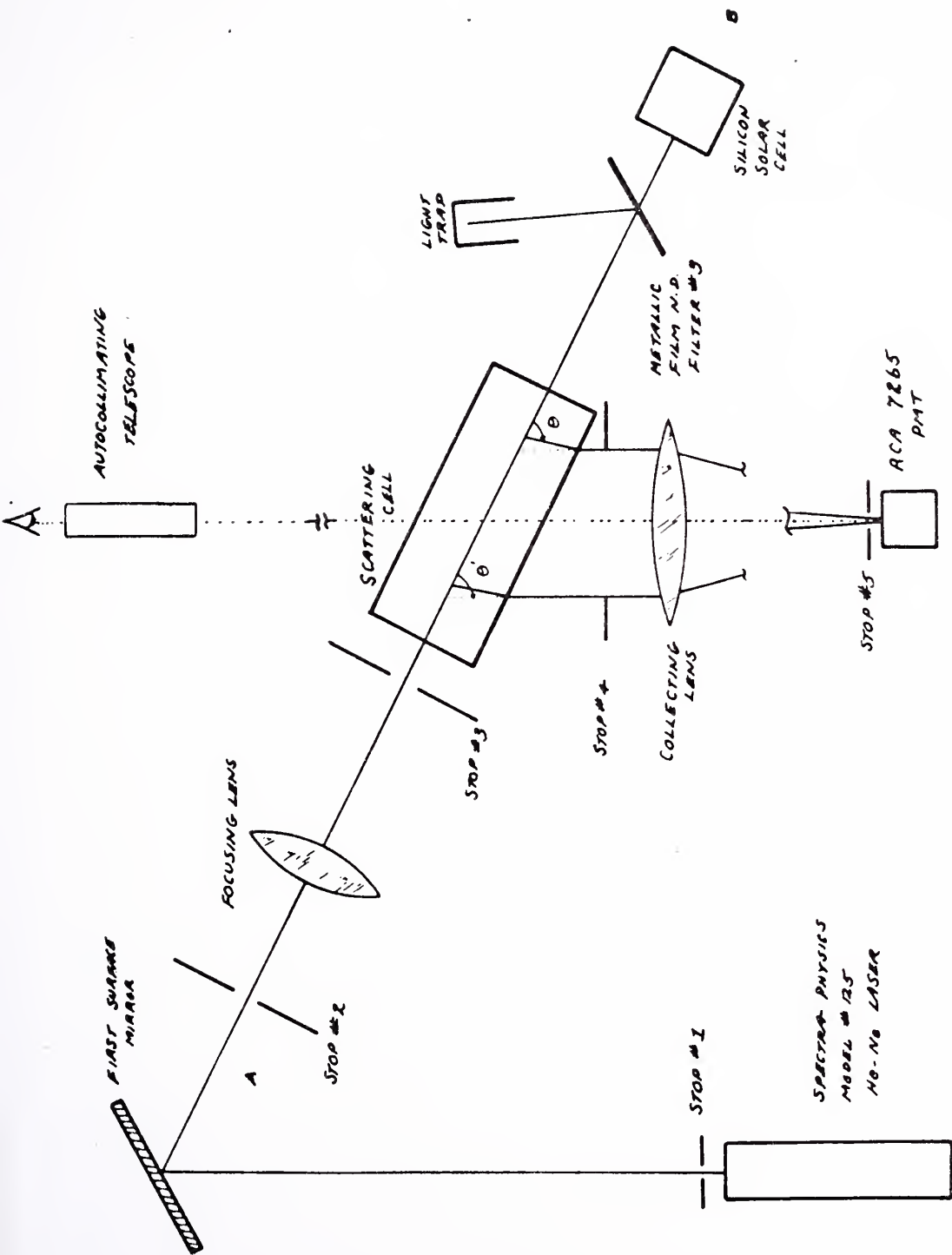


Fig. 3.4 Block Diagram of Optical Setup Employed in Concentration Fluctuation Scattering

cell, the output of which is used to servo the laser power as described in section III.B.5.

Parallel light scattered at an angle θ relative to the incident beam is focused by the collecting lens onto the surface of an RCA 7265 photomultiplier tube. Stop #4 prevents stray light, particularly that scattered at the entrance and exit faces by the incident beam, from reaching the PMT.

We observe from Fig. 3.4 that the apparent scattering angle in this geometry is θ' . We readily obtain θ from θ' by Snell's law if the index of refraction of the sample being studied is known. This was measured for each sample using a Bausch and Lomb Abbé refractometer.*

The apparent scattering angle, θ' , was measured with an accuracy of $20'$ by the following technique. An autocollimating telescope was aligned parallel to the optical axis of the collecting lens, which was arranged to have stop #5 (the PMT aperture) at its focus. This alignment was achieved by focusing the collimator at infinity and then moving it until stop #5 was centered on the cross-hairs of the telescope. The scattering cell was removed and replaced by a front surface mirror mounted on a rotating table calibrated in degrees and readable to within $20'$. The table was rotated until autocollimation was achieved with the alignment telescope. This rendered the mirror perpendicular to the optical axis of the alignment telescope. The table was then rotated until it sent the incident laser beam back through the small aperture in stop #3. The apparent scattering angle θ' could then be read off the calibrated table.

An aperture, stop #5, was placed in front of the phototube to restrict

* The use of this instrument was kindly afforded us by Prof. Maurice Fox, Department of Biology, MIT.

the angular acceptance, $\Delta\theta$. Lastovka⁽¹⁸⁾ has shown that, if an acceptance angle $\Delta\theta$ is collected about the mean angle θ , then the observed spectrum is broadened, as given by

$$\frac{\Gamma_{OBS}}{2\pi} = \frac{\Gamma}{2\pi} \left[1 + \left(\frac{\Delta\theta}{\theta} \right)^2 \right] \quad (3.40)$$

if the spectral width of the scattered light varies as K^2 . For such experiments presented in this thesis, $(\Delta\theta/\theta)^2$ never exceeded 10^{-3} and was generally $< 10^{-4}$. Hence, acceptance angle broadening played no role in our observed spectra.

In the case of our study of the depolarized light scattered by TMV, $(\Delta\theta/\theta)^2 \approx 10^{-2}$ but here, too, the effect was absolutely negligible since Γ_R is independent of K [Eqs. (2.87a) and (2.87b)]. Indeed, the acceptance angle played no role in our work except to allow us to collect sufficient light to swamp the phototube dark current and noise inherent in the wave analyzers (section III.B.5).

The scattering geometry depicted in Fig. 3.4 has been used with no difficulty for scattering angles as small as about 30° , and as large as about 170° . If we try to study the scattering for angles smaller than about 30° with this technique, problems with stray light become severe. In the TMV experiment, we wish to study the anisotropy spectrum, whose form [Eqs. 2.87a) and (2.87b)] was stated under the assumption that the molecules could rotate, but not translate. If we restrict our attention to very small scattering angles, we can have this assumption approximately met in the TMV experiment, as will be discussed in greater detail in Chapter V. The optical arrangement was modified for this experiment to allow studying the scattered light in the vicinity of $\theta = 2^\circ$. The exper-

mental setup is essentially as in Fig. 3.4, except for the collection optics⁽¹⁹⁾ which are shown below in Fig. 3.5:

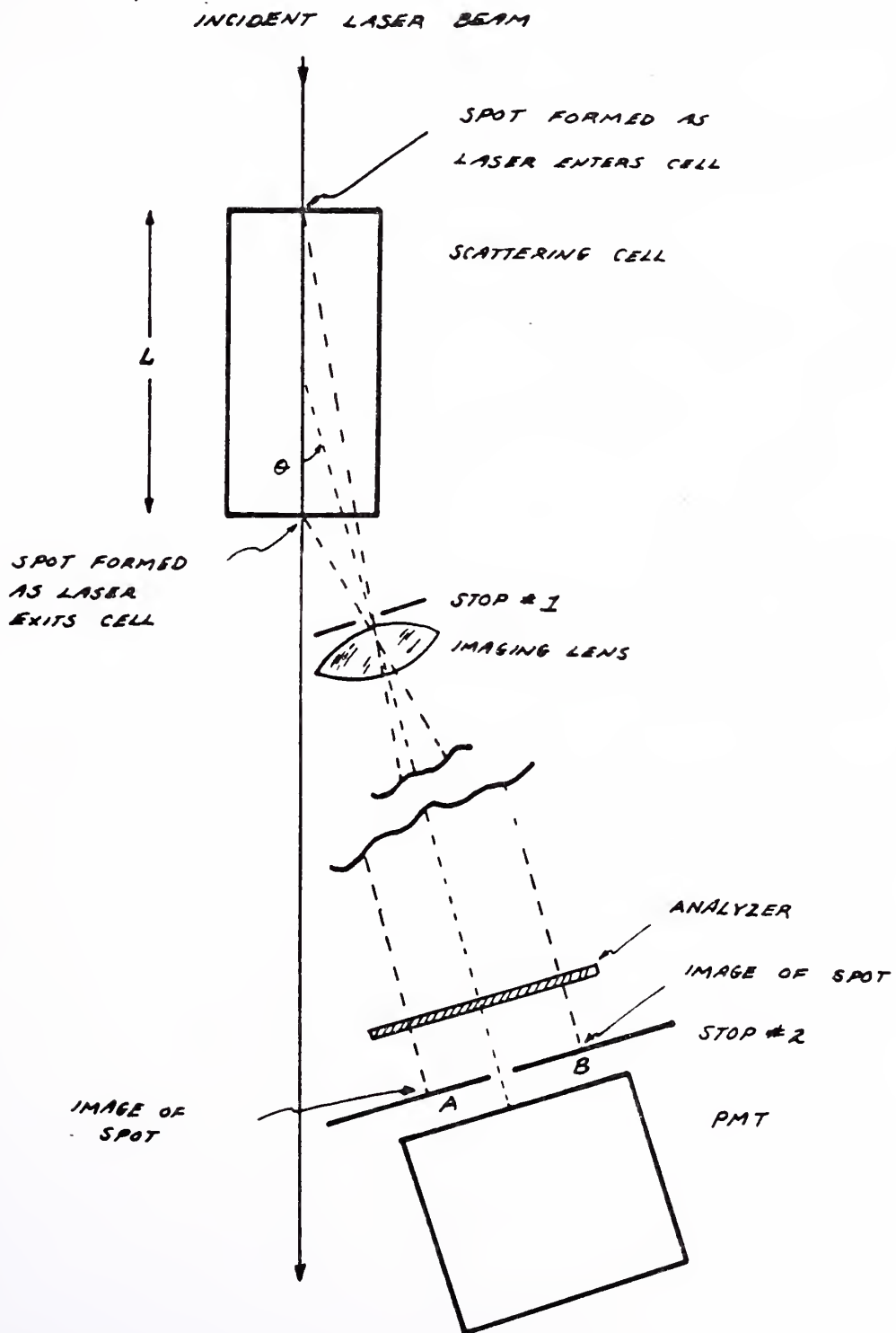


Fig. 3.5 Block Diagram of Optical Setup Employed in Anisotropy Scattering

The imaging lens is used to image the entire scattering cell onto stop #2 immediately in front of the photomultiplier tube. The image is enlarged by the magnification of the lens, M. A small aperture (stop #1) restricts the acceptance angle of the imaging lens and hence a sharp image of the cell appears at the focal plane of the PMT, and stop #2 is used to block the well-defined images of the spots caused by the laser entering and exiting the scattering cell. Since the magnification of the lens is M, we have

$$AB = ML \sin \theta . \quad (3.41)$$

We may then solve Eq. (3.41) for the scattering angle, to obtain

$$\theta = \sin^{-1} \left(\frac{AB}{ML} \right) . \quad (3.42)$$

The angle is thus easily determined by measuring the distance between the spot images on the PMT focal plane, and the cell length. With this system, angles between 1° and 3° were easily obtained and the principal source of stray light -- the spots on the cell at laser entrance and exit faces -- was eliminated. Stops #1 and #2 combined gave a $(\Delta\theta/\theta)^2$ value better than 10^{-2} in all cases.

The analyzer placed in front of the PMT is now adjusted to look only at the depolarized light. Since elastically scattered stray light will be mostly polarized like the incident beam, this filter aids greatly in the elimination of stray light problem. However, some of the stray light is depolarized as well, and hence stop #2 is still essential to prevent such light from reaching the PMT.

By using a Glan-Thompson prism as an analyzer, that component of the scattered light with the same polarization as the incident light can be reduced to less than 10^{-4} of its original value before reaching the PMT.

Since ρ_v for TMV is only about 0.0023, as shown in II.B.2.b, even 10^{-4} of the polarized component leaking through the prism could partially mask the small depolarized component we seek to study. This problem could be rendered more serious if the incident light was not completely polarized. We have, however, a very simple means of determining whether leaking of the polarized component of the scattered light (i.e., that part due to concentration fluctuations) gives any appreciable contribution to the total photocurrent we measure, i_o . Dubin, Lunacek, and Benedek⁽²⁰⁾ showed that D , the translational diffusion constant for TMV, is $(0.40 \pm 0.02) \times 10^{-7} \text{ cm}^2/\text{sec}^*$. Using this and Eqs. (2.85) and (3.14), we see that the concentration fluctuation spectrum in the photocurrent has a width $(2\Gamma_D/2\pi) \approx 1 \text{ Hz}$ at a scattering angle of 3° . Since the bandwidth of the D.C. chopper-stabilized microammeter used to monitor the D.C. photocurrent, i_o , on this experiment (see section III.B.4) is about the same value, most of the power in the translational diffusion spectrum fits under the bandwidth of the current meter and hence i_o would fluctuate grossly if any of the light falling on the PMT were due to translational diffusion spectrum. On the contrary, when the experimental setup was aligned and the Glan-Thompson prism adjusted for minimum transmission, peak-to-peak excursions in i_o were measured at less than 1%.

To summarize, then, sufficient precautions were taken to guarantee that we observed only the depolarized light scattered by TMV and hence performed a true self-beating experiment. We will contrast our results in Chapter V with those of Wada, Suda, Tsuda and Soda⁽²¹⁾ who performed the same experiment, using the heterodyne mixing technique.^(1,4,5)

In all experiments described in this thesis, the experimental apparatus was completely surrounded by a plastic box onto which all dust was

* Corrected to 25°C , water

electrostatically precipitated. Contribution to the scattered light from scattering by airborne dust is generally negligible except when studying very small scattering angles. Hence, in studying the depolarized light scattered by TMV, it was particularly necessary to eliminate the dust problem by the above technique.

We now proceed to consider in detail the electronic detection system employed in these experiments (III.B.4).

4) Electronic Detection

The spectrum of the photocurrent was analyzed by essentially the same techniques as first employed by Ford and Benedek.⁽²²⁾ The equipment is diagrammed below in Fig. 3.6.

The PMT was operated at typically 2000 volts delivered by a Fluke 415B high voltage power supply. In the study of lysozyme, the tube was operated at the design maximum of 2400 volts to obtain sufficient photocurrent to swamp residual noise in the wave analyzer. To avoid high-frequency roll-off due to cable capacitance, the photocurrent was fed into a low-impedance preamplifier* before spectral analysis. The low input and low output impedances of the preamp allowed convenient cable lengths of several feet at input and output. The preamp permitted an extremely flat frequency response, with the roll-off at 150 kHz being only about 1%.

The fluctuations in the photocurrent were then analyzed by either a General Radio 1900 A wave analyzer (for spectra up to about 2 kHz wide), or by a Hewlett-Packard 310-A for wider spectra. The adjustable predetection bandwidths (see section II.B.2) available on these analyzers (3, 10 and 50 Hz for the G R 1900 A, and 200, 1000, and 3000 Hz for the HP 310-A) allowed us

* This preamplifier was designed by Joe Lunacek of this laboratory.

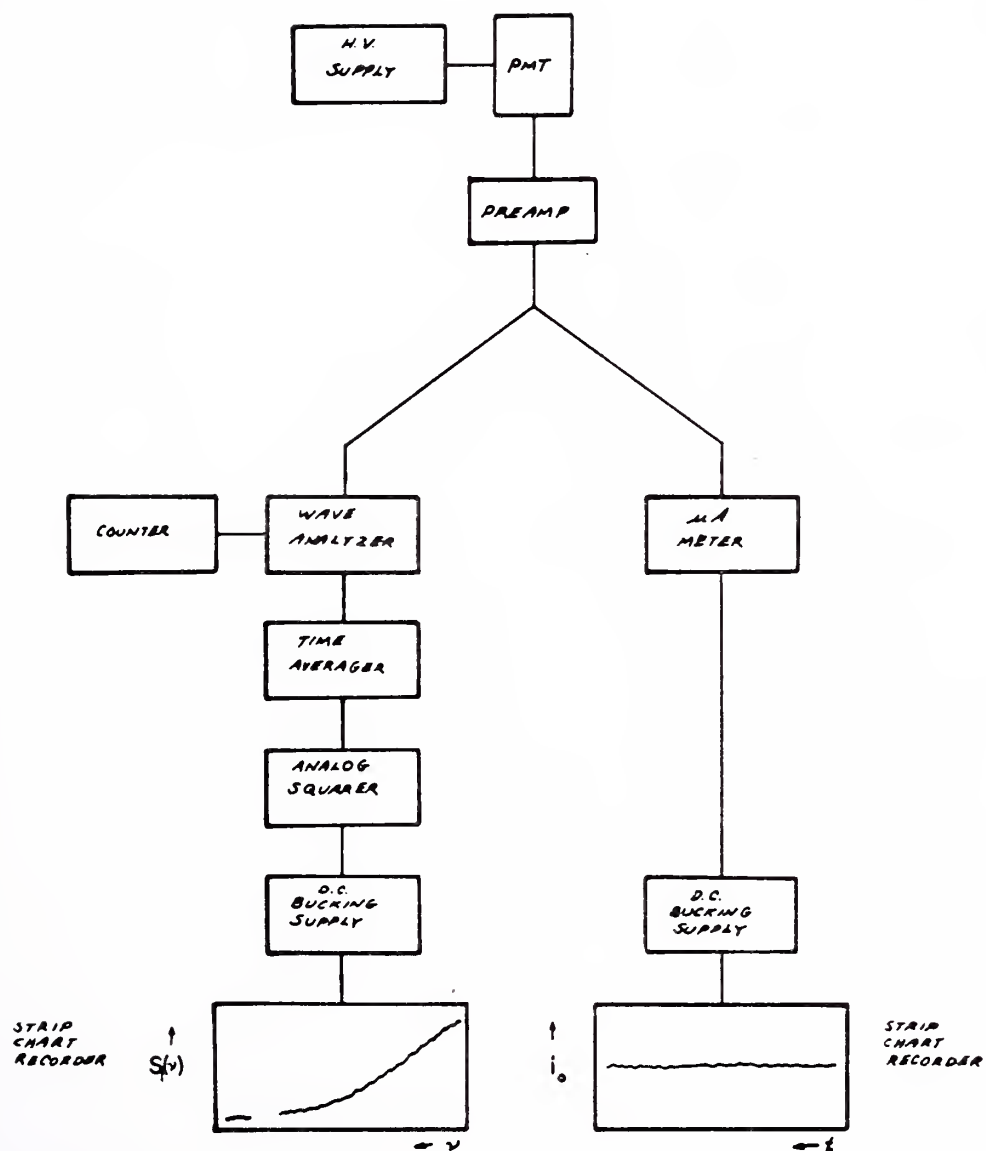


Fig. 3.6 Electronic Detection System

to prevent any line shape distortion by insuring that $S_1(v)$ was essentially constant over the bandwidth v_1 . In fact, in our experiments, the ratio of v_1 to the full width of the self-beat spectrum never exceeded 1/12. Under these conditions, the observed spectrum will be Lorentzian (for a Lorentzian input spectrum) with an observed linewidth broadening less than 0.7% due to the finite predetection bandwidth.⁽²³⁾ In general, the ratio of v_1 to the full width of the photocurrent spectrum was less than 1/12, so that 0.7% is the maximum error we observed due to this effect.

Because the detector in the wave analyzer delivers an output proportional to the voltage contained in the bandwidth v_1 , the output is squared (after being averaged for a time $T = 1/v_1$ by a double RC filter) before being displayed on the strip chart recorder. We thus record the power spectrum of the fluctuations in the photocurrent. This is a particular convenience in the case of $\left(\frac{\text{SIG}}{\text{NOISE}}\right)_{\text{PRE}} \approx 1$, since it allows one to "buck out" the shot noise $\langle \mathbf{N}(v) \rangle$ and enlarge the display of $\langle \mathbf{S}(v) \rangle$. Since $S_1(v) = \left(\frac{1}{2\pi}\right) I_0 \delta(v) + \langle \mathbf{S}(v) \rangle + \langle \mathbf{N}(v) \rangle$, as given by Eq. (3.15), we see that even if we "buck off" the residual level from a square-root spectrum, the strip chart recorder displays $\sqrt{\langle \mathbf{S}(v) \rangle + \langle \mathbf{N}(v) \rangle} - \sqrt{\langle \mathbf{N}(v) \rangle}$, that is, the display is still a function of the shot noise level, and hence each point must be corrected for the shot noise.

It thus simplifies data analysis, since the strip chart recorded displays the actual power spectrum instead of the square-root power spectrum. An electronic squaring module (Consolidated Electrodynamics model 19-302) was employed to square the wave analyzer output.

The complete system response (output amplitude versus frequency) of the phototube-preamp-wave analyzer-time averager-squarer units was easily calibrated by utilizing the fact that the shot effect spectrum is flat to about

1 GHz (see section III.B.1). We therefore illuminate the PMT with a light bulb driven by a well-regulated D.C. supply. By attenuating the light with sufficient neutral density filters, the shot noise level $\langle N(n) \rangle = Gei_0$, Eq. (3.14), can be made adequately large to be measured on the same wave analyzer scale as the experimental runs used. We then record the system response to the shot noise and easily calibrate the frequency response to within 0.1%. This calibration procedure was particularly significant in the case of the HP 310-A analyzer which had an intrinsic response non-linearity of about 4% in the range $v = 2000$ Hz to $v = 12,000$ Hz. The experimental traces were then corrected with this calibration curve. The correction was quite important in the lysozyme study, in which $\left(\frac{\text{SIG}}{\text{NOISE}}\right)_{\text{PRE}}$ did not exceed about 1/1. Hence, a system response non-linearity of, say, 4%, could affect the signal term 8% or more for the cases in which $\left(\frac{\text{SIG}}{\text{NOISE}}\right)_{\text{PRE}} < 1$. For example, if the shot noise level is 100 units and $\langle S(0) \rangle$ only 50 units, a 4% amplitude non-linearity in the wave analyzer at $v = 0$ is six units in the total display of the power spectrum, or 12% of $\langle S(0) \rangle$. This problem obviously worsens for $v > 0$, since $\langle S(v) \rangle$ is then decreasing. This consideration led to the effort expended in the wave analyzer amplitude response calibration we have described here.

The light-bulb-generated shot noise traces also allowed us to measure system stability. The photocurrent i_0 drifted less than 0.1% in ten hours if the phototube was illuminated by a light bulb powered by a regulated D.C. supply, and the shot noise level at any frequency was also stable to better than 0.1% over this time scale. Hence, the temperature dependence of the photocathode's quantum efficiency and any drift in the gain G due to high voltage power supply drift or heating effects in the dynode resistor string

were negligible for runs of less than ten hours' duration (the average run did not exceed about two hours). Since the laser intensity was servoed to better than 0.05% for indefinite periods (section III.B.5), we thus see that no experimental drift or instability could affect our observed results.

The D.C. photocurrent (i_o) was also monitored continuously during experimental runs. By "bucking out" 99% of i_o and enlarging the remaining 1% to full-scale deflection on a strip chart recorder, very slight changes in i_o during the course of an experimental run could be detected. In light of the discussion in the previous paragraph, such fluctuations could arise only from drifts in the scattered intensity. Such drifts were observed only in the study of lysozyme, and arose due to particulate contamination drifting through the incident beam. This problem occurred despite the most careful cleaning of the sample and sample cell (see section III.C.2), and is due to the very small scattered intensity obtained from lysozyme. It was found that, if the drift in i_o did not exceed 0.2%, then the observed spectra were quite reproducible. Hence, before running an experimental determination of the spectrum of lysozyme, i_o was observed for about one hour. The photocurrent usually drifted considerably, about 1 or 2%, in this period, and then stabilized to better than 0.2% after an hour, as the few troublesome dust particles settled out. The determination of the spectrum was then performed. Under these circumstances, the illuminated volume in the scattering cell appeared uniformly intense, even at very low angle inspection, and no particulate contamination was observed when the beam was blown up to about 2 mm and examined with a 20X microscope. If these two requirements were not met, experiments were not performed, and the cell was refilled (section III.C.2).

The experimental spectra were recorded by slowly sweeping the center frequency of v_1 , the predetection bandwidth. Typically, one to two hours were required to sweep from $v < \frac{1}{4} (2\Gamma/2\pi)$ to $v > 6(2\Gamma/2\pi)$, i.e., from less than 1/4 of the self-beat line width to more than six self-beat line widths. An alternative method is to sweep through this frequency range very quickly, storing the output in a CAT. Sweeps are repeated for a sufficient number of times until the averaged signal-to-noise is adequate. This method does not improve the observed signal-to-noise over that of the slow-sweep technique used in this thesis, but does have the advantage of being relatively immune to long-term drifts in laser power, phototube gain, etc. The fast-sweep technique has been successfully employed by Rimai, Hickmott, Cole, and Carew⁽²⁴⁾ in a study of the thermal denaturation of ribonuclease.

The frequency calibration of each wave analyzer was checked, using a Hewlett-Packard 5245 L electronic counter. The GR 1900 A was accurate to better than 1/2% over the entire range used, and better than 1/4% between the range of 0 to 500 Hz., the most important region (\lesssim experimental line width) for spectra studied on this device. The HP 310-A was frequency-calibrated to better than 1% over the entire range used.

5) The Lasers

In the experiments on the bacteriophages and lysozyme, a Spectra-Physics model 125 He-Ne laser was employed. Since the output optical power of the laser is a weak but distinct function of the plasma discharge current, a convenient way to servo the laser power is through adjustment of the plasma current. This was done using the system diagrammed in Fig. 3.7, on the next page. The laser power is monitored by a silicon solar cell onto which passes 10^{-3} of the incident light. The remaining fraction of the laser power is reflected by a No. 3 metallic film neutral density

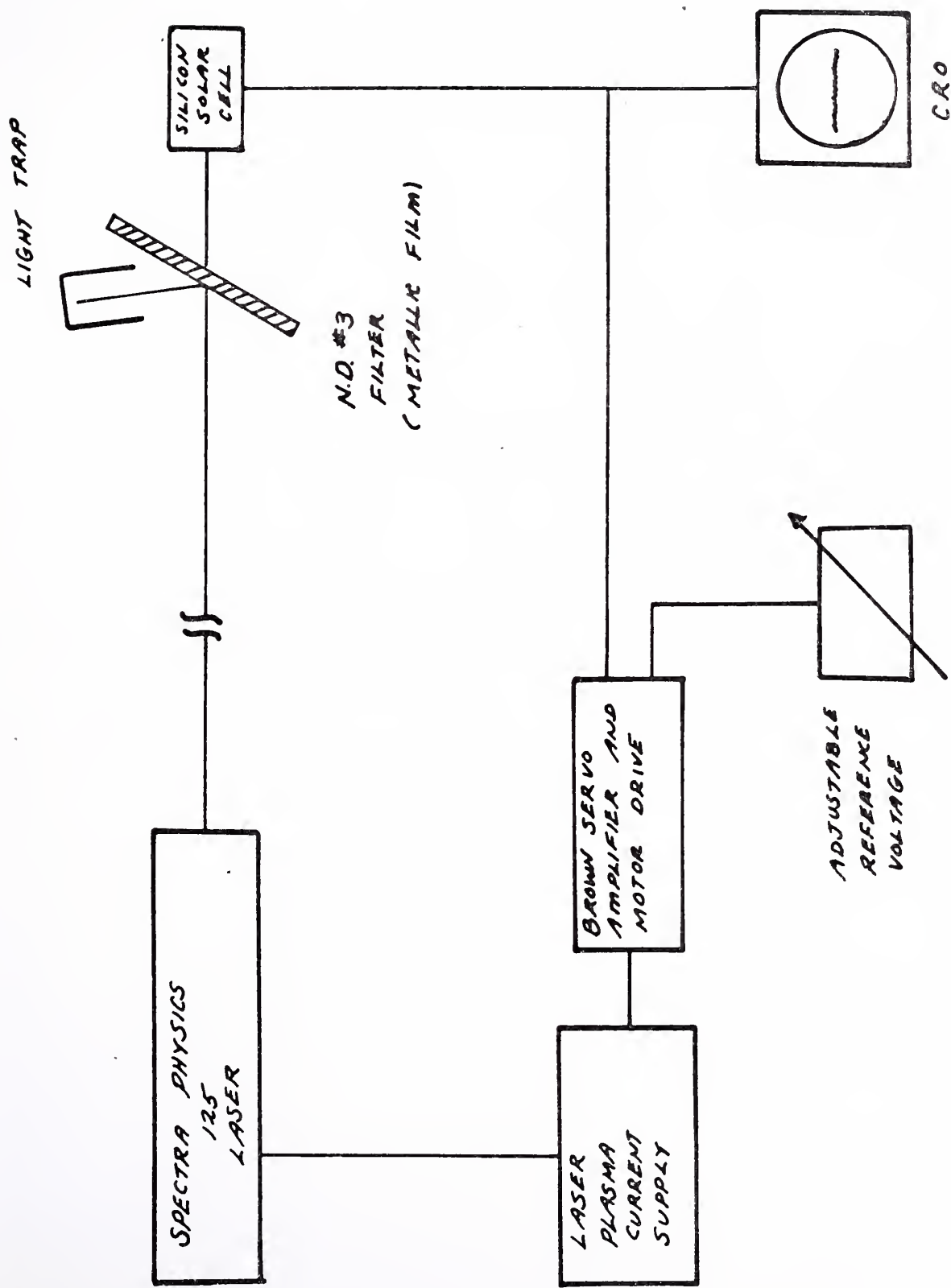


Fig. 3.7 Block Diagram of the Laser Servo

filter into a light trap. The output of the solar cell is compared with an adjustable reference voltage, and their difference is fed into a Brown servo amplifier. The amplifier drives a servo motor which, in turn, controls a resistor which sets the plasma current regulation point in the laser plasma current supply. The response time of this system (~ 1 sec) was more than adequate to servo slow laser power drifts and long-term stability of 0.05% was regularly maintained indefinitely.

Short-time fluctuations ("noise") on the laser output was negligible. This was determined by applying the laser output directly onto the PMT, sufficiently attenuated to give the same i_0 at the same PMT gain as was used in experimental runs. The resulting self-beat spectrum was simply that due to the shot term, i.e., $\langle N(v) \rangle = Gei_0$.

As the laser tube ages, the model 125 laser has a tendency to support plasma oscillations. One such oscillation can occur strongly at about 150 kHz and results in a modulation of the laser output at this frequency. Hence, the output of the solar cell was monitored visually on an oscilloscope to insure that no such oscillations were in fact occurring. As the tube aged, the tendency for plasma oscillation could be eliminated by gradually increasing the normal plasma current, although this, in turn, reduced the dynamic range of the laser servo as the point of optical power saturation was approached. In all cases, a trade-off between servo dynamic range and plasma oscillation elimination could be obtained, which resulted in satisfactory servoing as well as in sufficient quieting of the laser output.

The Coherent Radiation Labs model No. 52 argon-ion laser employed in the study of tobacco mosaic virus was not servoed. The laser output was

stable to about 5% over the experimental runs, and was recorded on a strip chart recorder. This calibration of the laser power was then used to normalize the observed self-beat spectra of the scattered light via Eq. (3.14). The output of this laser was determined to be noise-free in the same fashion as was the model 125 laser as described above.

C. Experimental Samples and Sample Preparation

We describe in this section the samples employed in this thesis. Since the solvents, buffers, sample cleaning, and cell cleaning and filling techniques varied so greatly among the various samples used, it is most convenient to discuss all these points under the heading of the individual samples.

1) The Bacteriophages

All bacteriophage samples employed in this thesis (T4, T5, T7 and λ) were supplied to us completely prepared by Professor David Freifelder of Brandeis University. The bacteriophages were grown on E. coli by standard techniques,⁽²⁵⁾ and were received by us at a concentration of ~ 1 mg/cc.

The determinations of the diffusion coefficients of the various phages were made by diluting these samples in their appropriate solvents, as given in Table 3.2 below. Dilutions were made using solvents which had been prefiltered through a 0.22μ Millipore cellulose ester filter.⁽²⁶⁾

The scattering cells were cleaned in Alconox and rinsed in distilled water. Approximately 100 cc of distilled water, prefiltered with a 0.22μ Millipore cellulose ester filter, was forced through the cell using a standard hypodermic syringe. The water remaining in the cell was forced out, and the cell dried by a stream of dry nitrogen or air, prefiltered with a 0.22μ filter also. Since the system was closed, this process excluded dust from the cell and rendered it ready for filling.

Table 3.2Solvents Employed in the Determination of Bacteriophage Diffusion Coefficients

Bacteriophage	Solvent
T4	0.5M NaCl 0.001 M MgCl ₂ 0.01 tris maleate buffer (pH = 7.8)
T5	0.1 M NaCl 0.01 M MgSO ₄ 0.001 M CaCl ₂ 0.01 M tris maleate buffer (pH = 7.0)
T7	same as T4
λ	0.01 M MgSO ₄ 0.01 M tris maleate buffer (pH = 7.0)

Dilute phage solutions were filtered into the scattering cell through specially prepared 0.22 μ Millipore filters. Since the phages have a tendency to adsorb onto the cellulose ester filters, the filters were prewashed in a 0.1% bovine serum albumin (BSA) solution and then rinsed in distilled water.⁽²⁷⁾ This was done by forcing the appropriate solutions (0.1% BSA and then distilled water) through the filter with a syringe. This process partially neutralizes electrostatic interaction between phage and filter and no phage loss was encountered in the filtering process as determined by optical density measurement before and after filtration.

The filled cells showed no particulate contamination, as determined both by low-angle observation of the scattered light and by observing the enlarged beam (about 2 mm) through a twenty power microscope.

Some experimenters^(27,28) add a small amount of deoxyribonuclease (~ 10 mg/cc) to destroy any free DNA which might be present in the phage solutions. However, since this enzyme does not function at the high salt concentration used for several phages as listed in Table 3.2, we employed the following technique. The solvent viscosity, and the viscosity of the phage-solvent solution, were all measured to an accuracy of 1/4% using a Cannon-Manning semi-micro viscometer.⁽²⁹⁾ The phage solution viscosities were measured before and after the experimental runs. In all cases, the viscosity of the solvent alone was found to be identical to that of the phage solution being studied. Since the presence of the free DNA distorts experimental results by increasing the solution viscosity markedly, we conclude that there was no free DNA present in any of our experimental solutions. Since all solutions were filtered with a 0.22μ Millipore filter, it is reasonable to conclude that any free DNA initially present was removed by the filter. We then observe that no DNA leaked from the phages in the course of an experimental run, since the initial and final solution viscosities were identical. We have observed, in addition, that such phage solutions do not show any increase in viscosity over a period of even several weeks, casting doubt on the significance of this problem under any circumstances.

All experimental runs were performed within one hour of sample preparation, except in the case of T 7. Results for this phage were found to be erratic and unreproducible unless the diluted phage solu-

tion was allowed to stand for about 10 hours (at 7°C) after dilution. The source of this problem is not understood, but it is noteworthy that the optical density of a T7 phage solution which has been diluted will slowly rise and then level off.⁽³⁰⁾ Evidently, some type of phage-solvent or phage-glass interaction occurs upon dilution, but its effects are gone after waiting several hours.

All phage solutions were found to be quite stable even at room temperature. However, to retard bacterial growth, the unused phage solutions were stored at 7°C. The concentration of diluted phage solutions was determined by measuring the optical density (O.D.)* at 260 m μ with a Zeiss spectrophotometer, and then using the approximate relation⁽²⁷⁾

$$C_{\text{phage}} \text{ (mg/cc)} = \frac{1}{12} \text{ O.D.}_{260 \text{ m}\mu} . \quad (3.43)$$

The sedimentation coefficients of the bacteriophages were determined using a Beckman Model E analytical ultracentrifuge. Since this technique has been described in detail elsewhere,⁽³¹⁾ we shall not give a specific description here. However, a few points are important to make, as given below.

Because of particle interactions, the sedimentation coefficient is a function of the phage concentration.⁽³²⁾ It is therefore desirable to study the sedimentation coefficient for several values of the concentration and extrapolate to C = 0. All our values of S were determined

* By definition, O.D. = $\log_{10} \frac{I_{\text{Inc}}}{I_{\text{Trans}}}$, where I_{Inc} is the intensity of the light incident upon the measuring cell and I_{Trans} is the intensity of the transmitted light after traversing a cm path length in the cell.

for values of $C \leq 100 \mu\text{g/cc}$, and these values were extrapolated to zero concentration (see Chapter V). Working at such low concentrations requires the use of ultraviolet absorption optics, and these were used in our studies.

The sedimentation coefficient of T4 was determined in a slightly different solvent from that of the diffusion coefficient. This presents no difficulty, however, since all results were normalized to standard conditions (20°C , water) as described in Chapter IV. The solvent in which S was determined for T4 was 0.1M NaCl , 0.01M MgSO_4 , 0.001M CaCl_2 and $0.01\text{M tris maleate buffer (pH = 7.0)}$.

No temperature controls were employed in either the diffusion or sedimentation determinations. In the former case, the temperature was measured with a glass stem thermometer (accurate to 0.1°C) and was constant to within 0.2°C over the course of an experimental run. In the sedimentation coefficient determinations, a thermistor built into the centrifuge rotor was used to determine the temperature. In these runs the temperature (unregulated) was constant to better than 0.1°C and the thermistor and bridge assembly were calibrated against a glass stem thermometer (accuracy of 0.1°C). With this knowledge of solution temperature (always in the range of 23 - 25°C in our work), and the viscometric determination of solvent viscosity, all experimental data were corrected to 20°C and water, as described in Chapter IV.

2) Lysozyme

Chicken egg white lysozyme was obtained from Worthington Biochemical Corporation (Freehold, New Jersey). This preparation comes salt-free and purified by $2\times$ crystallization. All of our experiments were

performed on lysozyme from one Worthington LYSF preparation (lot #8AA).

The solvent used to study lysozyme must be buffered to an acid pH to avoid dimerization and higher order aggregation, which occur above about pH = 5. (33,34) Accordingly, all experimental runs were made at pH = 4.2 ± 0.1, using a 0.1 M sodium acetate-acetic acid buffer. (35) This buffer serves to set the pH at the desired level and to maintain this pH independent of any external conditions.

The guanidine hydrochloride (GuCl) used to denature the lysozyme was obtained from Mann Research Laboratories (New York, New York) and was of "ultra pure" grade. All experiments were done using a single supply of GuCl (Mann lot #U-2491). Since the GuCl is about 1% hydrated, the concentration of GuCl in our solutions could not be determined to better than 1% by simply weighing out a given amount of GuCl. Accordingly, the concentrations were determined refractometrically, using the index versus concentration data of Kielley and Harrington. (36) The experimental procedure was to make a large stock solution of 0.1M Na Ac .- acetic acid buffer. The index of refraction of this solution was measured, and hence the contribution to the index of the sodium acetate-acetic acid was determined. The GuCl solutions were then prepared from this stock solution, and the concentration of GuCl was determined by measuring the index of refraction, upon correction for the contribution due to the sodium acetate-acetic acid.

One per cent protein solutions (0.01 g lysozyme per cc of solution) were then made in volumetric flasks. The index of this final solution was also measured in order to determine the scattering angle θ (see section III.B.3), and scattering wave vector K [see Eqs. (2.13a) and (2.13b)].

Despite its grade of "ultra pure", the Mann GuCl was found to contain a small amount of particulate contamination, which could be seen clearly as a residue on a Millipore filter. It was found to be advantageous to preclean the buffered GuCl solution before the addition of the lysozyme. Two filtrations of the solution through a 50 m μ cellulose ester filter removed all trace of the residue. The lysozyme was then added, and, after the cell was cleaned as described below, the lysozyme solution was final-filtered into the scattering cell through a 0.22 μ Millipore filter.

Cell cleaning in the lysozyme experiment became something of a ritual, because any trace of particulate matter left in the cell, although perhaps innocuous in itself, became a nucleation site for the formation of bubbles or GuCl crystals. At the high concentrations of GuCl used in this experiment (0M-6M), it appeared that micro crystals of GuCl would form and then redissolve quite readily. This conclusion was reached after observing that distilled water could be filtered sufficiently well that no particulate contamination was visible under any circumstances, and the cleaned water would remain in this state (in a sealed scattering cell) for several days. This was not the case for GuCl solutions unless the cell was painstakingly precleaned. Similar problems at high salt concentrations have been observed by other workers.⁽³⁷⁾

An additional problem arose with the use of the sodium acetate-acetic acid buffer. When this solution was prepared, many large bubbles were clearly visible. The number and size of these bubbles gradually decreased to zero if the scattering cell was sufficiently clean.

Both of the above problems point out a situation not immediately apparent from our theoretical discussion in section III.B.2. In Eqs.

(3.29) and (3.30), we see that the predetection signal-to-noise ratio is proportional to the incident power, P_{Inc} , and the Rayleigh ratio, R . Hence, for all other things held constant, we might expect two experiments with the same value of the product ($P_{Inc} \cdot R$) to have the same amount of "difficulty". Experimentally this is by no means the case, since experiments in which R is very small are plagued by scattering from sources other than the experimental sample, e.g., dust, particulate contamination, or stray light. An experiment limited by such factors is not necessarily aided by an increase in P_{Inc} . Of course, if P_{Inc} is sufficiently large, we can study the spectrum of the scattered light in the extreme backward direction where dust effects are much less important, due to the angular dependence of light scattered by large particles. In general, however, it is desirable to make the scattering cell and sample solution as clean as possible.

The scattering cell was first cleaned by immersion in chromic acid. After careful rinsing in distilled water, the cell was then cleaned ultrasonically in glacial acetic acid for 15 minutes. This step was essential to the elimination of the bubble problem described above. Four liters (approximately 500 cell volumes) of distilled water were then forced through the cell in a closed system under pressure, being filtered through a $0.22\ \mu$ Millipore filter. To insure a high flow rate (about 250 cc/minute), large size (14 cm diameter) filters were employed. Filtered dry nitrogen was then used to dry the cell. The 1% lysozyme solution, prepared using precleaned buffered GuCl as described above, was then filtered several times through a $0.22\ \mu$ Millipore filter and admitted to the scattering cell. This technique gave essentially perfect results, if distilled water instead of the lysozyme solution was

admitted into the cell. In the case of the protein solution, however, the success rate was about one in three. A successful filling of the cell is one in which no angular dissymmetry could be detected in the scattered light, and no particulate contamination could be detected in the enlarged (2 mm) beam under investigation with a 20x microscope.

Because an occasional particle or two would pass through the beam in the course of an experimental run, operation at very small scattering angles was impossible. It was found that the effect of scattering from such particles was sufficiently small if a scattering angle θ of approximately 60° was chosen. As shown in section III.B.2, enhanced signal-to-noise could be achieved by working at very large angles, thereby utilizing the increased coherence area size (angles smaller than 60° being ruled out by the dust problem). However, Eq. (3.31) indicates that to enjoy the same $\left(\frac{\text{SIG}}{\text{NOISE}}\right)_{\text{PRE}}$ as we obtain at $\theta = 60^\circ$, we would have to study the scattered light at about 170° , where the increase in coherence area size counteracts the increase in spectral linewidth to yield the same signal-to-noise ratio (see section III.B.2 for a detailed discussion of this point). This is far more difficult than at $\theta = 60^\circ$, particularly due to the difficulty in masking the spots as the incident beam enters and exits the cell. We therefore settled upon approximately 60° as an appropriate scattering angle for this experiment.

All experiments were performed at room temperature without temperature controls. However, when the equipment had been operating for about one hour, the temperature in the experimental area was stable to better than 0.2°C in the course of an experimental run, approximately three hours. All data were obtained between 23°C and 25°C , and corrected to standard conditions as described in the next chapter. Experimental runs

were begun within two hours of sample preparation, and the length of the run was typically three hours, although some runs lasting as long as 10 hours were performed.

3) Tobacco Mosaic Virus

The tobacco mosaic virus employed in this experiment was kindly supplied to us by Dr. Helga Doty of Harvard University. It was prepared by the method of Boedtker and Simmons.⁽³⁸⁾ This method has been shown by a study in the electron microscope by Hall⁽³⁹⁾ to give a reasonably monodisperse preparation of TMV (85% of the particles have lengths between 2800 Å and 3200 Å). Our own electron microscopic investigation showed our sample to be somewhat poorer than this. The virus was supported on a carbon substrate and stained with uranyl acetate. The microscope was calibrated with a 2160 lines/mm replica grating and the distribution of lengths of 141 viruses we measured for our sample is shown in Fig. 3.8, on the next page.

This distribution peaks at approximately 3000 Å, which is considered to be the length of the biologically significant molecule. Smaller forms are presumably broken versions of the 3000 Å species, and larger forms, end-to-end aggregates.

Although the distribution presented in Fig. 3.8 is far from monodisperse, light scattering experiments are somewhat immune to this length nonuniformity. At the small scattering angles we employed (1.5°- 3.0°), the scattering form factor for rods even 5000 Å long is unity.⁽⁴⁰⁾ Hence, the intensity of the scattered light varies simply as the product of number of molecules of a given length and the square of their molecular weight. Hence, the short rods contribute little to the scattered light.

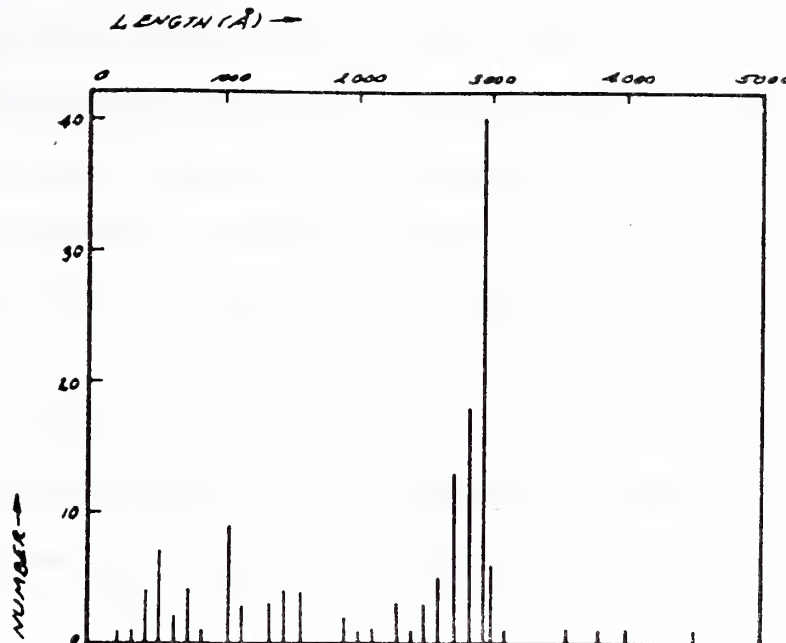


Fig. 3.8 Length Distribution in Sample of Tobacco Mosaic Virus

On the other hand, even the few large molecules present (length $> 3000\text{\AA}$) can make a significant contribution. We discuss this in detail in Chapter V.

The virus was suspended in distilled water for these experiments. It was stored over chloroform to retard bacterial contamination. The cell cleaning and filling techniques were those employed in the study of the bacteriophages (section III.C.1) except that a 0.45μ Millipore filter was used in the cell filling. No virus adsorption occurred using untreated cellulose ester filters.

Since the scattering experiments were performed at such a small angle, absolute freedom from particulate contamination was mandatory.

Since the scattering of light due to rods of TMV's length is so strongly peaked in the forward direction, dust contamination cannot be detected by low-angle examination of the scattered light. However, observation of the enlarged beam with a 20x microscope revealed no trace of particulate contamination. As was the case with distilled water described in section III.C.2, no difficulty was found in cleaning the salt-free TMV solution.

Experiments were performed at a virus concentration of 0.01%. Spectra were obtained at room temperature in about one hour, all results being corrected to standard conditions as described in Chapter IV.

References for Chapter III

1. Forrester, A. T., J. Opt. Soc. Am., 51, 253 (1961).
2. Ford, N. C., Jr., and Benedek, G. B., Phys. Rev. Letters, 15, 649 (1965).
3. Benedek, G. B., "Thermal Fluctuations and the Scattering of Light", Brandeis Summer Institute for Theoretical Physics, 1966, Gordon and Breach, and Co., (in press).
4. Benedek, G. B., "Optical Mixing Spectroscopy, with Applications to Problems in Physics, Chemistry, Biology, and Engineering", in "Polarization, Matter, and Radiation", Presses Universitaire de France, Paris, 1969, pp. 49-84.
5. Lastovka, J. B., Ph. D. Thesis, MIT, 1967 (unpublished).
6. Davenport, W. B., Jr., and Root, W. L., "Random Signals and Noise", McGraw-Hill Book Company, Inc., New York, 1958, p. 168.
7. Ref. 6, section 7-4.
8. Gerjuoy, E., Forrester, A. T., and Parkins, W. E., Phys. Rev., 73, 922 (1948).
9. Ref. 4, p. 60.

10. Ref. 5, p. 246.
11. Born, M., and Wolf, E., "Principles of Optics", Pergamon Press, Oxford, 1965, pp. 415, 441.
12. Ref. 5, p. 349.
13. O'Konski, C. T., and Haltner, A. J., J. Am. Chem. Soc., 78, 3604 (1956).
14. Broersma, S., J. Chem. Phys., 32, 1626 (1960).
15. Degiorgio, V., and Lastovka, J., to be published.
16. Information may be obtained from Princeton Applied Research Corp., Princeton, New Jersey, and Hewlett-Packard Corp., Palo Alto, Cal.
17. Federal Scientific Corp., New York, N. Y.
18. Ref. 5, p. 463.
19. This optical arrangement was devised by Joseph Lunacek, with whose collaboration the experiment on TMV was performed.
20. Dubin, S. B., Lunacek, J. H., and Benedek, G. B., Proc. Nat. Acad. Sci., 57, 1164 (1967).
21. Wada, A., Suda, N., Tsuda, T., and Soda, K., J. Chem. Phys., 50, 31 (1969).
22. This experimental setup has come to be called the "self-beating" spectrometer; see Ref. 2.
23. Ref. 5, p. 481.
24. Rimai, L., Hickmott, J. T., Cole, T., and Carew, E. B., to be published in the Biophys. J.
25. Davison, P. F., Freifelder, D., and Holloway, B. W., J. Mol. Biol., 8, 1 (1964).
26. Millipore Filter Corporation, Bedford, Massachusetts.
27. Davison, P. F., and Freifelder, D., J. Mol. Biol., 5, 635 (1962).
28. Dyson, R. D., and Van Holde, K. E., Virology, 33, 559 (1967).
29. Cannon Instrument Co., State College, Pa.
30. Freifelder, D., private communication.

31. Markham, R., in Maramorosch, K., and Koprowski, H. (eds.), "Methods in Virology", Vol. 2, Academic Press, New York, 1967, Chapter 1.
32. Ref. 31, p. 17.
33. Sophianopoulos, A. J., and Van Holde, K. E., J. Biol. Chem., 239, 2516 (1964).
34. Bruzzesi, M. R., Chianconi, E., and Antonini, E., Biochemistry, 4, 1796 (1965).
35. Walpole, G. S., J. Chem. Soc., 105, 2501 (1914).
36. Kielley, W., and Harrington, W. F., Biochim. Biophys. Acta, 41, 401 (1960).
37. Wada, A., private communication.
38. Boedtker, H., and Simmons, N., J. Am. Chem. Soc., 80, 2550 (1958).
39. Hall, C., J. Am. Chem. Soc., 80, 2556 (1958).
40. Geiduschek, E. P., and Holtzer, A., Advances in Biol. and Med. Phys., 6, 431 (1958) (see p. 443).

Chapter IV

DATA REDUCTION

"Water water everywhere, nor any drop to drink."

The Ancient Mariner, Samuel Taylor Coleridge

A. Introduction

Although the corrections and normalizations required to obtain the desired information from the raw data were generally small, it is desirable to describe this data reduction procedure in detail. In the study of lysozyme, these corrections were sometimes quite large, and in addition, a careful analysis of the data yielded a determination of the translational diffusion coefficient of guanidine hydrochloride as well.

The adjustment of the data consisted of two parts: (1) the determination of the spectral shape and linewidth, and hence the desired diffusion coefficient; (2) the reduction of these data and the sedimentation rate data to standard conditions, that is, the values S and D would have at 20°C if their solvents had the viscosity and density of water at that temperature.

B. Determination of Spectral Shape and Linewidth

1. The Bacteriophages and Tobacco Mosaic Virus

Equation (3.14) indicates that the power spectrum of the fluctuations in the photocurrent due to concentration fluctuation scattering or anisotropy scattering is Lorentzian (plus the constant shot effect term) with half-width of half maximum given by $\frac{2\Gamma}{2\pi}$ where

$$\Gamma_D = DK^2 , \quad (2.80)$$

$$\text{and } \Gamma_R = 6 D_R . \quad (2.87b)$$

We thus can obtain D and D_R by making a best least squares Lorentzian fit to the experimental data. The GR 1900A wave analyzer was used in

these experiments and was flat to better than $\frac{1}{2}\%$ out to 45 kHz. Hence, since the spectral width in both the phage and TMV experiments never exceeded about 700 Hz, we could determine the shot noise level, $\langle \mathbf{N}(\nu) \rangle$ by observing the spectral power density at 45 kHz (always more than about 70 linewidths of $\langle \mathbf{S}(\nu) \rangle$), and fitting $\langle \mathbf{S}(\nu) \rangle$ to a Lorentzian spectrum above this shot level.⁽¹⁾ In the case of the bacteriophages and TMV, the solvent made only a minuscule contribution to the total scattered intensity, and was negligible in the interpretation of the results.

2. Lysozyme

As we showed in Eq. (2.38), a 1% lysozyme solution has a value of the Rayleigh ratio of only $\mathbf{R} = 20 \times 10^{-6} \text{ cm}^{-1}$. Since water, the weakest scatterer among the pure liquids, has a value for \mathbf{R} 3% as large as this, it is readily apparent that the lysozyme experiment represents an example of exactly how far self-beating spectroscopy can be pushed in the study of macromolecules. It is noteworthy, for example, that even though many pure liquids scatter comparably to lysozyme (see Table 2.2), the central component in a pure liquid has never been studied by self-beating spectroscopy. This is true despite the fact that the central component of the scattered light often contains most of the scattered intensity (i.e., is comparable to or larger than the Brillouin components and anisotropy scattering).

In light of these remarks, it is clear that we must pay appropriate attention to the light scattered by the denaturant, guanidine hydrochloride (GuCl). The high concentration of GuCl employed as a denaturant in the lysozyme experiments will make a significant contribution

to the total scattered intensity. In addition, the spectrum of the light scattered by GuCl is of a width which will be observable in our experiments. We proceed below to analyze this effect in detail.

In aqueous solution, GuCl consists chiefly of guanidine and the chloride ion. Since we know the molecular weight of each of these entities (59.1 and 35.5 respectively), we could calculate their Rayleigh ratios from Eq. (2.34) if we knew their respective values of $\frac{\partial n}{\partial C}$. From the data of Kielley and Harrington⁽²⁾ we know that $\frac{\partial n}{\partial C}$ for guanidine hydrochloride is 0.17 cc/g, and from the International Critical Tables⁽³⁾ we have $\frac{\partial n}{\partial C}$ for the chloride ion as about 0.22 cc/g. The value of $\frac{\partial n}{\partial C}$ for lysozyme itself is 0.1888 cc/g (see Table 2.1). Hence, since we will show the GuCl contribution to be a small (but observable) correction term in our lysozyme results, it will be adequate to consider $\frac{\partial n}{\partial C}$ to be the same for all species present. Then, Eq. (2.34) allows us to calculate the relative contributions of these scatterers by simply considering their respective products of molecular weight times concentration, that is:

$$R_{Lys,1\%} : R_{Gu,1M} : R_{Cl,1M} = (MC)_{Lys,1\%} : (MC)_{Gu,1M} : (MC)_{Cl,1M}, \quad (4.1a)$$

where we consider a 1M GuCl solution for reference. Hence, we see that for this 1M GuCl reference solution,

$$R_{Lys,1\%} : R_{Gu,1M} : R_{Cl,1M} = 1 : 0.025 : 0.009. \quad (4.1b)$$

We thus see that the guanidine and chloride contributions combined, in a 1M GuCl solution, scatter about 3.4% as much light as lysozyme. At 6 M GuCl (the highest value we studied), the salt is then scatter-

ing 20% as much light as the lysozyme. This effect is indeed not negligible, both because the width of the spectrum of the light scattered by GuCl is not so broad as to be unobserved, and, as we shall show below, its contribution is actually enhanced by the operation of the self-beating spectrometer.

We will make a helpful simplification by treating the diffusion coefficients of both guanidine and chloride as the same. Equation (4.1b) indicates that the guanidine scatters 3/4 of the light scattered by GuCl anyway, so that if D_{Cl} is somewhat different from D_{Gu} , it is of no great concern. We then consider GuCl as a single entity with diffusion constant D_G whose scattered intensity [from Eq. (4.1b)] is 3.4% as large as that of a 1% lysozyme solution for each mole of GuCl present in a liter of solution.

That this assumption is reasonable is evidenced by the fact that sodium chloride has the same diffusion constant as urea,⁽⁴⁾ a molecule with essentially the same molecular weight as guanidine and a similar structure. In any case, as we shall show, the entire effect of the GuCl scattering on the observed width of the lysozyme spectrum is not very large, so this approach is adequate.

We now proceed to calculate the spectrum of the light scattered by the lysozyme-GuCl system and the spectrum of the photocurrent obtained by self-beating this light. We begin by writing the correlation function of the scattered light:

$$R_E S(\tau) = R_E S^L(\tau) + R_E S^G(\tau) \quad (4.2)$$

where $R_E S^L(\tau) = R_E S^L(0) e^{-\Gamma_L |\tau|} e^{-i\omega_0 |\tau|}$ (2.82)

$$R_E^G(\tau) = R_E^G(0) e^{-\Gamma_G |\tau|} e^{-i\omega_0 |\tau|} \quad (2.82)$$

$$\Gamma_L = D_L K^2 \quad (2.85)$$

$$\Gamma_G = D_G K^2 \quad (2.85)$$

D_L = translational diffusion constant of lysozyme

D_G = translational diffusion constant of GuCl as
defined above

To simplify the appearance of equations we are about to obtain, we define

$$A \equiv R_E^L(0) \quad (4.3a)$$

$$B \equiv R_E^G(0) \quad (4.3b)$$

We may then write the spectrum of the scattered light [from Eq. (2.84)] as

$$S_E(v) = \frac{A}{\pi} \frac{(\Gamma_L/2\pi)}{\left(\frac{\Gamma_L}{2\pi}\right)^2 + (v - v_o)^2} + \frac{B}{\pi} \frac{(\Gamma_G/2\pi)}{\left(\frac{\Gamma_G}{2\pi}\right)^2 + (v - v_o)^2} . \quad (4.4)$$

As we would of course expect, the spectrum of the scattered light is simply the sum of two Lorentzians of relative integrated intensity A/B.

To calculate the spectrum of the photocurrent, we first obtain its correlation function. From Eq. (3.8), this is given by

$$R_i(\tau) = i_0^2 + \frac{|R_E(\tau)|^2}{R_E^2(0)} + G e i_0 \delta(\tau) . \quad (3.8)$$

Substituting our expressions above for $R_E(\tau)$, we obtain

$$R_1(\tau) = i_0^2 + \frac{A^2 e^{-2\Gamma_L |\tau|} + 2ABe^{-(\Gamma_L + \Gamma_G)|\tau|} + B^2 e^{-2\Gamma_G |\tau|}}{(A+B)^2} + G e i_0 \delta(\tau). \quad (4.5)$$

Whence, upon taking the Fourier transform to obtain the spectrum, we see that the signal portion of the spectrum of the photocurrent is given by

$$\langle \mathbf{S}(\nu) \rangle = \frac{A^2}{(A+B)^2} \frac{1}{\pi} \frac{\left(\frac{2\Gamma_L}{2\pi}/2\pi\right)}{\left(\frac{2\Gamma_L}{2\pi}\right)^2 + \nu^2} + \frac{2AB}{(A+B)^2} \frac{1}{\pi} \frac{\left(\frac{(\Gamma_L + \Gamma_G)}{2\pi}\right)}{\left(\frac{(\Gamma_L + \Gamma_G)}{2\pi}\right)^2 + \nu^2} + \frac{B^2}{(A+B)^2} \frac{1}{\pi} \frac{\left(\frac{2\Gamma_G}{2\pi}\right)}{\left(\frac{2\Gamma_G}{2\pi}\right)^2 + \nu^2} \quad (4.6)$$

Equation (4.6) is a rather significant statement and is worthy of some general observations. We see that, if the spectrum of the scattered light is the sum of two Lorentzians [Eq. (4.4)], then the signal term in the photocurrent is the sum of three Lorentzians. These three include the self-beat spectrum of each of the two Lorentzian spectra present in the light itself, and, in addition, the "cross-beat" spectrum of these two terms. This cross-beat term is also Lorentzian, but with a width equal to the average of the widths of the two Lorentzian spectra present in the scattered light.

The presence of this cross-beat term may seem rather unintuitive. After all, a filter spectrometer such as the Fabry-Perot or grating spectrograph does not produce this intermediate term. However, the physical origins of the result are clear. In the mixing spectrometer,

we are observing the fluctuations in the photocurrent which themselves mirror the fluctuations in the intensity of the scattered light, not its electric field. These fluctuations arise because the interference pattern, due to light scattered by different molecules, moves across the face of the phototube with a frequency characteristic of the relative velocity of the molecules. If we look along a direction defined by a given value of \vec{K} , we see three such characteristic velocities: (1) the relative velocity between molecules of species A; (2) the relative velocity between molecules of species B; and (3) the relative velocity between a molecule of type A and one of type B. All of these motions cause movement of the interference pattern in the far field (i.e., fluctuations in the intensity), hence are mirrored as fluctuations in the photocurrent.

Equation (4.6) indicates how a heterodyne beat spectrometer operates. We simply let one of the "Lorentzian" spectra be very intense and arbitrarily narrow (i.e., a "local oscillator"). Then, the primary term in Eq. (4.6) is the cross-beat term, since the local oscillator self-beat spectrum is essentially a delta function and thus unobservable and the self-beat spectrum of the scattered light is of very low intensity relative to the cross-beat term.

The results of Eq. (4.6) also indicate why dust contamination or coherent stray light is so serious a problem in a self-beating experiment. Although the self-beat term of the dust or stray light may itself be too narrow to be observable, its cross-beat with the scattered light will produce a spectrum half as wide as the desired self-beat term of the scattered light, and hence will be quite noticeable. Thus, the

notion that the only effect of large particulate contamination is "to introduce an abnormally intense signal around zero frequency",⁽⁵⁾ as has been suggested in the literature, is erroneous.

A careful analysis of Eq. (4.6) also indicates that the intensity of the cross-beat term of the photocurrent is enhanced due to a factor of 2 multiplying it. A numerical example will show clearly why this can be a serious problem. Let there be two Lorentzian spectra contained in the spectrum of the scattered light. This is the case in the lysozyme-GuCl experiment as described above. The integrated intensity of the light scattered by lysozyme spectra is A and its spectral width is $\Gamma_L/2\pi$. The light scattered by GuCl has an intensity B and width $\Gamma_G/2\pi$. We can readily estimate the ratio of Γ_G/Γ_L since

$$\frac{\Gamma_G}{\Gamma_L} = \frac{D_G}{D_L} . \quad (4.7)$$

As we will show in the next chapter, $D_L = 10.6 \times 10^{-7} \text{ cm}^2/\text{sec}$ at 20°C in water. This number is not available for GuCl, but for urea (a molecule with essentially the same molecular weight as guanidine and of similar structure) we have⁽⁴⁾

$$D_{\text{Urea}} = 128 \times 10^{-7} \text{ cm}^2/\text{sec.} \quad (20^\circ\text{C, water}) \quad (4.8)$$

We thus anticipate that D_G is about an order of magnitude larger than D_L . Since the intensity of the light scattered by GuCl is never more than about 20% as intense as that by lysozyme (6M GuCl), and since its spectrum is an order of magnitude wider, we might expect its effects to be unobservable. Equation (4.6) indicates quite to the contrary, however.

For we see that the ratio of the intensity of the second term of the photocurrent spectrum (i.e., the lysozyme-GuCl cross-beat spectrum) to that of the first term (i.e., the lysozyme self-beat spectrum) is given by

$$\frac{I_{\text{Cross-beat}}}{I_{\text{Lys Self-beat}}} = \frac{2AB}{A^2} = 2 \left(\frac{B}{A} \right). \quad (4.8)$$

This ratio is twice as large as the ratio of the intensity of the light scattered by GuCl to that scattered by lysozyme. In addition, the ratio of the width of the cross-beat spectrum to that of the lysozyme self-beat term is given by

$$\frac{\left(\frac{\Gamma_L + \Gamma_G}{2\pi} \right)}{\left(\frac{2\Gamma_L}{2\pi} \right)} \approx \frac{1}{2} \frac{\Gamma_G}{\Gamma_L}. \quad (4.9)$$

That is, the cross-beat term is only about five times as wide as the lysozyme self-beat term. At 6 M GuCl, then, the cross-beat spectrum is 41% as intense as the lysozyme self-beat term, and only about five times wider. This is indeed an observable effect, and allowed us to make a determination of D_G with rather surprising precision.

The final term in Eq. (4.6), the self-beat spectrum of GuCl, is on the other hand completely negligible, for it is only $(B/A)^2$ as intense as the lysozyme self-beat spectrum (which is thus only 4% even at 6 M GuCl) and is an order of magnitude wider. We thus may rewrite Eq. (4.6) for the lysozyme experiment in a very simple fashion. As we have shown, GuCl scatters 3.4% as much light as lysozyme for every mole of GuCl present per liter of solution. Hence,

$$\frac{B}{A} = 0.035 \times [\text{GuCl}], \quad (4.10)$$

where $[\text{GuCl}]$ is the molar concentration of guanidine hydrochloride.

Thus, Eq. (4.6) yields

$$\langle \mathbf{S}(v) \rangle \propto A^2 \frac{\left(\frac{2\Gamma_L}{2\pi}\right)}{\left(\frac{2\Gamma_L}{2\pi}\right)^2 + v^2} + 0.07[\text{GuCl}] A^2 \frac{\left(\frac{\Gamma_L + \Gamma_G}{2\pi}\right)}{\left(\frac{\Gamma_L + \Gamma_G}{2\pi}\right)^2 + v^2}. \quad (4.11)$$

A fitting program for a single Lorentzian spectrum involves two adjustable parameters -- the area and width of the spectrum. Equation (4.11) involves three such parameters, namely: $\Gamma_L/2\pi$ and $\Gamma_G/2\pi$ and A . If we were unable to fix the ratio B/A via Eq. (4.10), we would have a dubious possibility of obtaining meaningful results, since, with finite signal-to-noise, a four-adjustable-parameter fit may not even converge uniquely. By performing a three-parameter fit⁽¹⁾ via Eq. (4.11), we were able to obtain a single converging fit to the data and thus learned both Γ_L and Γ_G . The significance of the presence of GuCl never exceeded about a 15% change in the determined value for $(\Gamma_L/2\pi)$. That is, if a simple two-parameter fit was used, $(\Gamma_L/2\pi)$ was determined to be 15% larger than with the three-parameter fit at a GuCl concentration of 6 M. For lower GuCl concentrations, the effect was proportionately smaller. As we shall show in the data presentation in Chapter V, the two-parameter fit was clearly inadequate to describe the experimental data, while the three-parameter fit gave essentially perfect agreement.

There was, in addition, another very small correction (about 2%) made on $\Gamma_L/2\pi$. This arose due to the fact that approximately 4% of the

transmitted incident beam was reflected back into the cell at the glass-air interface on the exit window. The light scattered by this reduced intensity beam is then observed at the angle supplementary to the scattering angle for the main beam. Since the spectral width varies as K^2 , the ratio of the width of the light scattered at the supplementary scattering angle to that of the light scattered at the primary scattering angle is known. Hence, no new adjustable parameters are incorporated into the fitting program. Since the scattering angle chosen for these experiments was about 60° , the ratio of $\frac{[K(\pi-\theta)]^2}{[K(\theta)]^2}$ was about three. Thus, the cross-beat spectrum between the light scattered by lysozyme at $\theta \approx 60^\circ$ and $\theta \approx 120^\circ$ was about twice as wide as the self-beat spectrum of lysozyme and 8% as intense. Incorporating this final perturbation into the fitting program⁽¹¹⁾ changed our determined value for $\Gamma_L/2\pi$ about 2% for all experiments, and therefore was not of great significance.

One of the purposes of the lysozyme study was to determine if there was more than one type of lysozyme present at any GuCl concentration. If there were, the spectrum of the photocurrent would not be as given in Eq. (4.11) and we thus could, in principle, conclude that there were two or more species present. However, as we discuss in Chapter V, the value of D_L changed only from $10.6 \times 10^{-7} \text{ cm}^2/\text{sec}$ at 0 M GuCl (i.e., completely native protein) to $7.3 \times 10^{-7} \text{ cm}^2/\text{sec}$ at 6 M GuCl (i.e., completely denatured protein). This change occurred over a range of about 2.5 M GuCl (beginning at about 2.5 M and being complete at about 5 M GuCl). Even if we assume that somewhere in this range we had equal numbers of lysozyme molecules with the two extreme

diffusion coefficients (the best case for determining the presence of two species), the resulting spectrum of the photocurrent could still be fit by Eq. (4.11). We show this to be the case quite readily as follows. Consider a mixture of equal numbers of lysozyme molecules, one set with $D = D_1$, the other with $D = 1.5 D_1$. Then, since each type has the same molecular weight, the spectrum of the signal portion of the photocurrent is given by Eq. (4.6) as

$$\langle \mathbf{S}(\nu) \rangle \propto \frac{(2\Gamma_1/2\pi)}{\left(\frac{2\Gamma_1}{2\pi}\right)^2 + \nu^2} + 2 \frac{\left(\frac{\Gamma_1 + \Gamma_2}{2\pi}\right)}{\left(\frac{\Gamma_1 + \Gamma_2}{2\pi}\right)^2 + \nu^2} + \frac{\left(\frac{2\Gamma_2}{2\pi}\right)}{\left(\frac{2\Gamma_2}{2\pi}\right)^2 + \nu^2}, \quad (4.12)$$

where $\Gamma_1 = D_1 K^2$

$$\Gamma_2 = D_2 K^2 = 1.5 D_1 K^2.$$

Since Eq. (4.12) is the sum of three Lorentzians, it would appear reasonable that it would itself be non-Lorentzian. Yet, as shown in Fig. 4.1, a single Lorentzian fit describes Eq. (4.11) very well indeed. The solid line in the figure is the display of Eq. (4.12) with $\Gamma_1/2\pi$ normalized to unity. The open circles represent the best least squares fit of a single Lorentzian curve, with

$$(\Gamma_{\text{Best}}/2\pi) = 2.45 (\Gamma_1/2\pi) \quad (4.13)$$

The open circles very well describe the generated curve. The rms deviation of the best fit curve (circles) is only 0.19% of the value of the curve at zero frequency. That is, if we measure the rms deviation of the spectrum $\langle \mathbf{S}(\nu) \rangle$ from the best fit $F(\nu)$ at N discrete values of ν , then

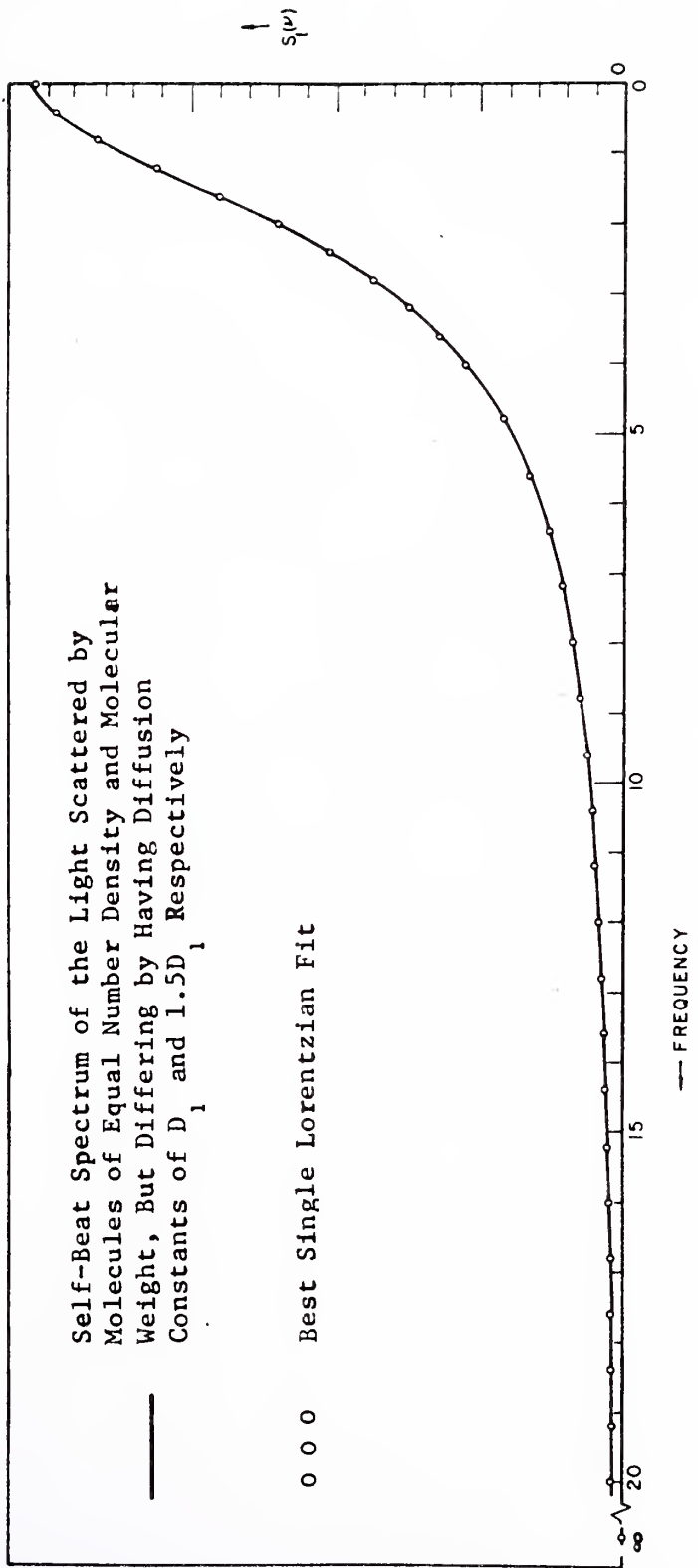


Fig. 4.1 Self-Beat Spectrum of the Light
Scattered by a Two-Component
Mixture

$$\% \text{ rms error} = \frac{\left[\sum_{i=1}^N \left(\frac{\langle S_i(v) \rangle - F_i(v)}{F_i(0)} \right)^2 \right]^{1/2}}{F_i(0)} \times 100, \quad (4.14)$$

where, in the case of Fig. 4.1, the rms error = 0.19%. This fit cannot be distinguished from the generated curve itself without essentially infinite signal-to-noise ratio. We also notice that the best fit curve has a width which is very nearly the average value of the expected self-beat spectra widths of the two individual types of molecules. That is, the self-beat spectrum of the molecule with $D = D_1$ would have a width $\frac{2\Gamma}{2\pi} = 2 D_1 K^2$, and that of the other type would be $\frac{2\Gamma}{2\pi} = 2 D_2 K^2 = 3 D_1 K^2$. Hence, the average value of these two widths is $2.5 D_1 K^2$ and Eq. (4.13) indicates that the best least squares fit of the curve has a width of $\frac{\Gamma_{\text{Best}}}{2\pi} = 2.45 D_1 K^2$. We have generated Eq. (4.12) for several values of the ratio of D_2/D_1 ranging from one to four, and made single Lorentzian best fits to the curves thus obtained. In Fig. 4.2, we display the ratio of the width of the best single Lorentzian fit to the average value of the two self-beat widths. That is, we show $\left(\frac{\frac{\Gamma_{\text{Best}}}{2\pi}}{\frac{2\Gamma_1 + 2\Gamma_2}{2\pi}} \right)$ as a function of D_2/D_1 , where $\Gamma_1 = D_1 K^2$ and $\Gamma_2 = D_2 K^2$. In the same display, we show the rms deviation of the best single Lorentzian fit as a percentage of its amplitude at zero frequency. Even for $D_2/D_1 = 2.5$, this deviation is only about 1%. Clearly, it is not possible to distinguish such mixtures by this technique unless D_2/D_1 is substantially larger than 2.5.

Figure 4.2 may be used to gain information about mixtures if either the ratio of D_2/D_1 is known or the relative percentage of each species present. Hence, in those cases in which one of these numbers is known,

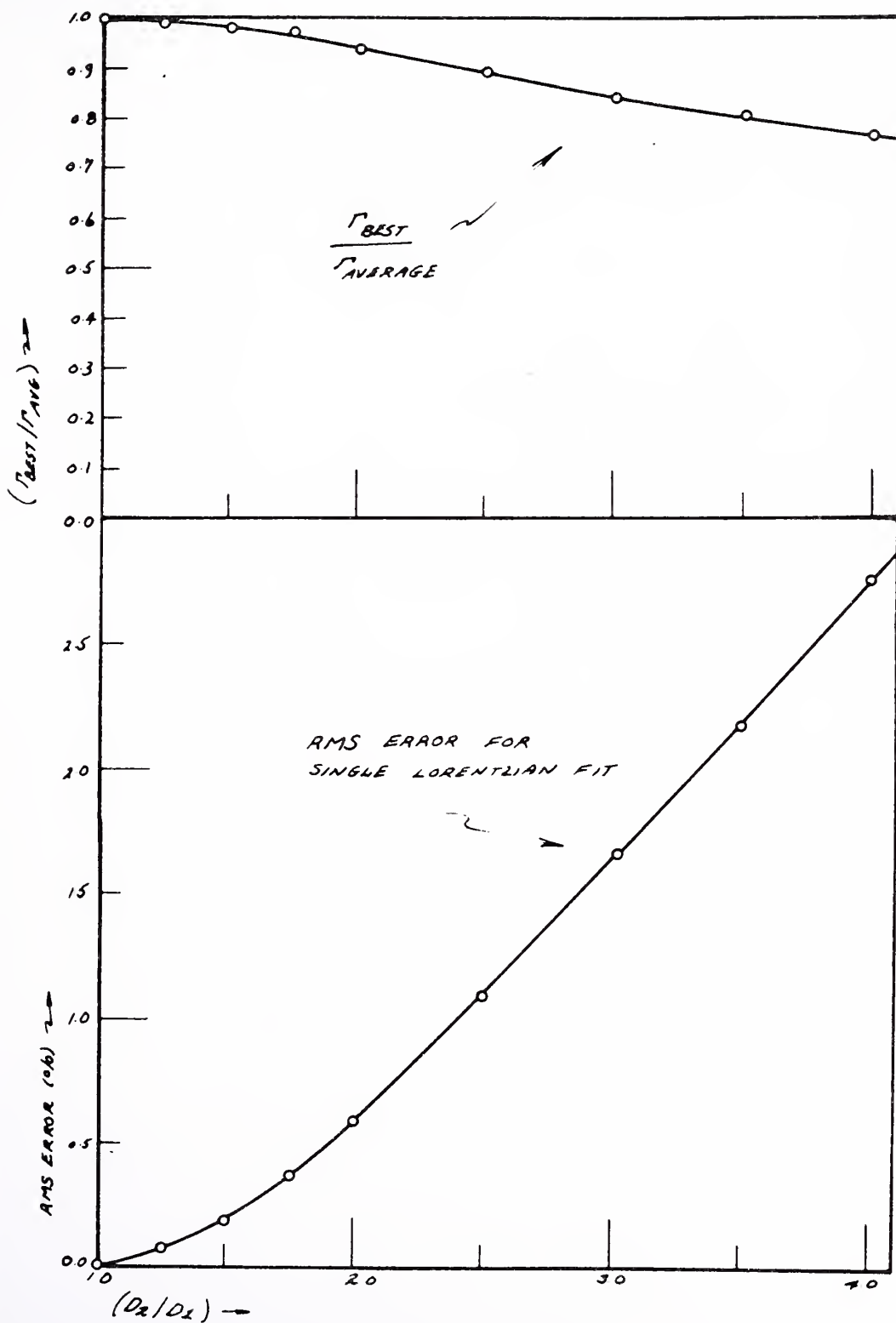


Fig. 4.2 Width and RMS Deviation of Best Single Lorentzian Fit to the Self-Beat Spectrum of the Light Scattered by Various Two-Component Mixtures

we can determine the other comparing the best fit to the experimental with the results of Fig. 4.2. We will, in fact, use this result to determine the percentage of denatured lysozyme molecules present in a lysozyme-GuCl solution as a function of [GuCl].

In light of the above comments, we treated our data on lysozyme as if only one type of lysozyme was present for any value of [GuCl], and fitted all data according to Eq. (4.11). Since there would be only two terms present in a heterodyne beat experiment on such a mixture (namely, the heterodyne spectra of the two species), one might expect it to be somewhat easier to detect a non-Lorentzian profile with this technique. In the appendix to this thesis, we show that essentially no improvement would be obtained in the present experiment by employing the heterodyne method. Also, we consider the heterodyne spectra obtained from various distributions of conformations and molecular weights and show that such distributions lead to a spectrum of the photocurrent even in a heterodyne study, which is indistinguishable from a single Lorentzian profile.

C. Reduction to Standard Conditions (Temperature, Viscosity and Density)

1.) Diffusion Constants

We may write the diffusion constant as

$$D = \frac{kT}{f} . \quad (2.92)$$

The frictional coefficient f may, in turn, be written as⁽⁶⁾

$$f = \eta(T)G \quad (4.15)$$

where η is the solvent viscosity and G is the form factor for the particular molecule being studied. Hence, if we measure the diffusion constant D at a given temperature, T , in a solvent of viscosity $\eta(T)$,

we must normalize the value to a standard temperature and viscosity. These are usually chosen to be 20°C and the viscosity of water at that temperature, respectively. Hence, if D is measured at a temperature T in a solvent with viscosity η , then

$$D_{20,w} = D(\eta, T) \frac{(293.16^\circ K)}{T} \times \frac{\eta}{\eta_{20,w}} \quad (4.16)$$

where the viscosity of water at 20°C is indicated as $\eta_{20,w}$.

As described in Section III.C.1, we measured the bacteriophage solvent viscosities routinely in our check for the presence of free DNA. Our determinations, using a Cannon-Manning semi-micro capillary viscometer, agreed within experimental error (1/4%) with the values obtained by assuming that the solvent viscosity was an additive property of the various constituents* and using the values for these constituents quoted in the International Critical Tables.⁽³⁾ The temperature dependence of the solvent viscosity for all solvents used in the phage study was found to be the same as that of water. This normalization correction never exceeded a few per cent in the case of the phages.

In the lysozyme study, however, the solvent viscosity was appreciably greater than water at a given temperature; in fact, 60% greater at 6 M GuCl. We therefore made a careful study of the solvent viscosity for several concentrations of GuCl prepared with the 0.1 M sodium acetate-acetic acid buffer (see section III.C.2). The

* By "additive", we simply mean that if an x molar solution of constituent A is a % more viscous than water, and a y molar solution of constituent B is b% more viscous than water, than a solution which is x molar in A and y molar in B will be (a+b)% more viscous than water. This approximation is quite good in the range we studied.

capillary viscometer yields the kinetic viscosity of the salt-water solution (η/ρ where ρ = solution density)⁽⁷⁾ and we thus obtained the actual viscosity of the solution by using the GuCl density data of Kielley and Harrington,⁽²⁾ correcting for the slight increase in ρ due to the buffer. Our results at 25°C were uniformly 1/2% higher than those of Kawahara and Tanford⁽⁸⁾ on GuCl alone. This difference probably arises due to the presence of the buffer ions. By increasing their values by 1/2%, this reference may be used for the values we employed to normalize our data.

Since our studies on lysozyme were performed between about 23° and 25°C, it was necessary, in addition, to measure the temperature dependence of the solvent viscosity for various concentrations of GuCl, again prepared with the 0.1 M sodium acetate-acetic acid stock buffer. These data are plotted in Fig. 4.3 in a form which is normalized to the value at 25°C. We see that up to 1M GuCl, the temperature dependence of the solvent viscosity is the same as water, but above that value, the solvent changes viscosity more slowly with temperature than water alone.

2.) Sedimentation Constants

We may write the sedimentation coefficient, from Eq. (2.91), as

$$S = \frac{M}{f} (1 - \bar{\rho}v) . \quad (4.17)$$

We normalize S to standard conditions by correcting our measured value to the viscosity and density of water at 20°C. Hence, using the viscosity dependence of f given in Eq. (4.15), we may write

$$S_{20,w} = S(\eta, \rho) \frac{(1 - \bar{\rho}\eta_{20,w})}{(1 - \bar{\rho}\eta)} \frac{\eta}{\eta_{20,w}} , \quad (4.18)$$

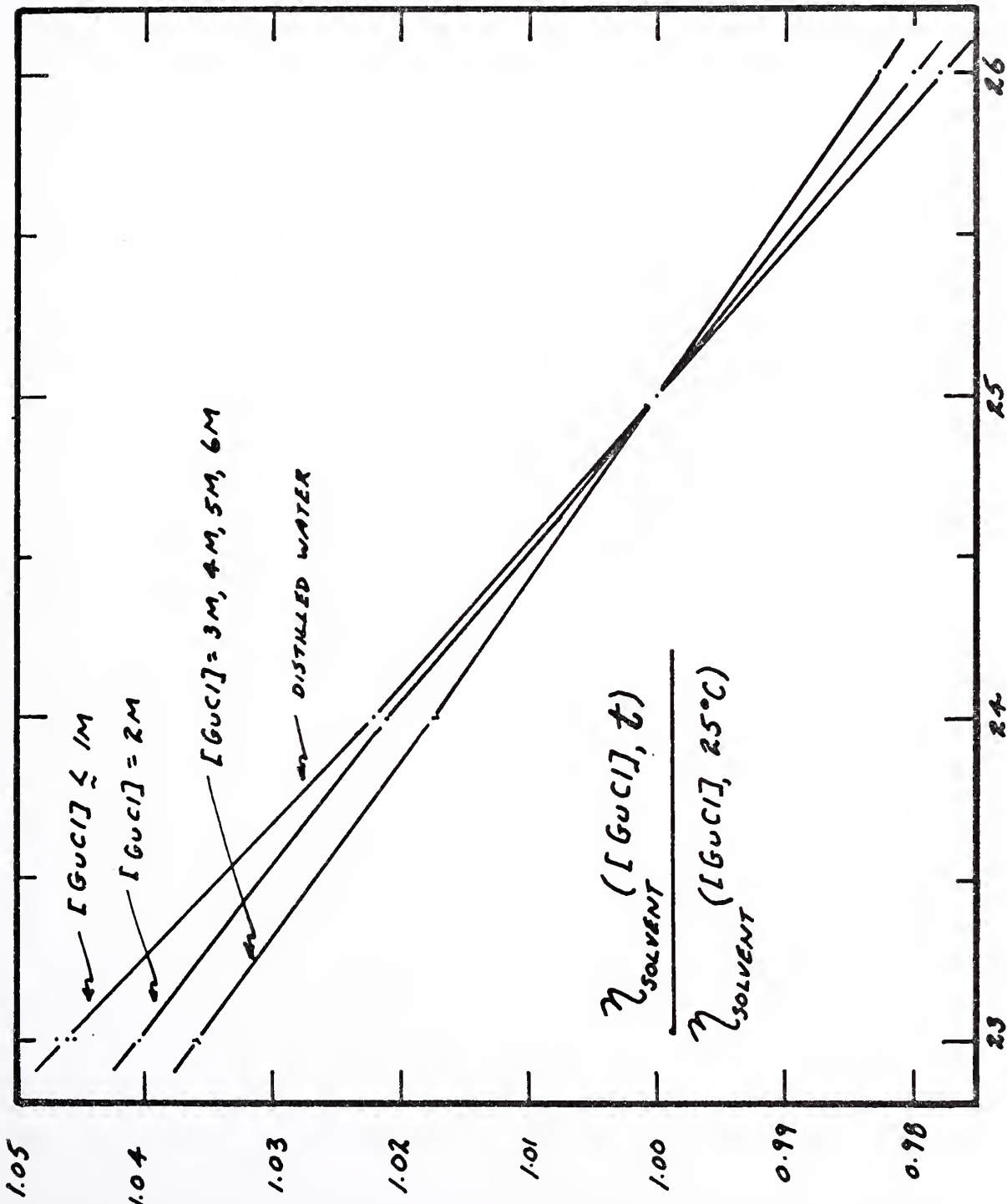


Fig. 4.3 Temperature Dependence of the Viscosity of Buffered Guanidine Hydrochloride Solutions

where S is the measured sedimentation constant, $\rho_{20,w}$ is the density of water at 20°C, and ρ is the density of the solvent in which the experiment is performed.

The solvent densities were determined by assuming that the constituent densities of the solvent salt solutions were additive and the densities of these solutions are tabulated in the International Critical Tables.⁽³⁾ This density correction is very small, never exceeding 1%. The viscosity correction was the same as already described in section IV.C.1.

References for Chapter IV

1. This best fit least squares Lorentzian fitting program was written by Joe Lunacek.
2. Kielley, W., and Harrington, W. F., Biochim. Biophys. Acta, 41, 401 (1960).
3. "International Critical Tables", E. W. Washburn, Editor-in-Chief, McGraw-Hill Book Co., Inc., New York, 1929.
4. "Handbook of Chemistry and Physics", C. D. Hodgman, Editor-in-Chief, Chemical Rubber Publishing Co., Cleveland, O., 1946, p. 1743.
5. French, M. J., Angus, J. C., and Walton, A. G., Science, 163, 345 (1969).
6. Tanford, C., "Physical Chemistry of Macromolecules", John Wiley and Sons, Inc., New York, 1961, p. 356.
7. ref, 6, p. 332.
8. Kawahara, K., and Tanford, C., J. Biol. Chem., 241, 3228 (1966).

CHAPTER V

Results and Discussion

"She's an artist: she don't look back."

Bob Dylan

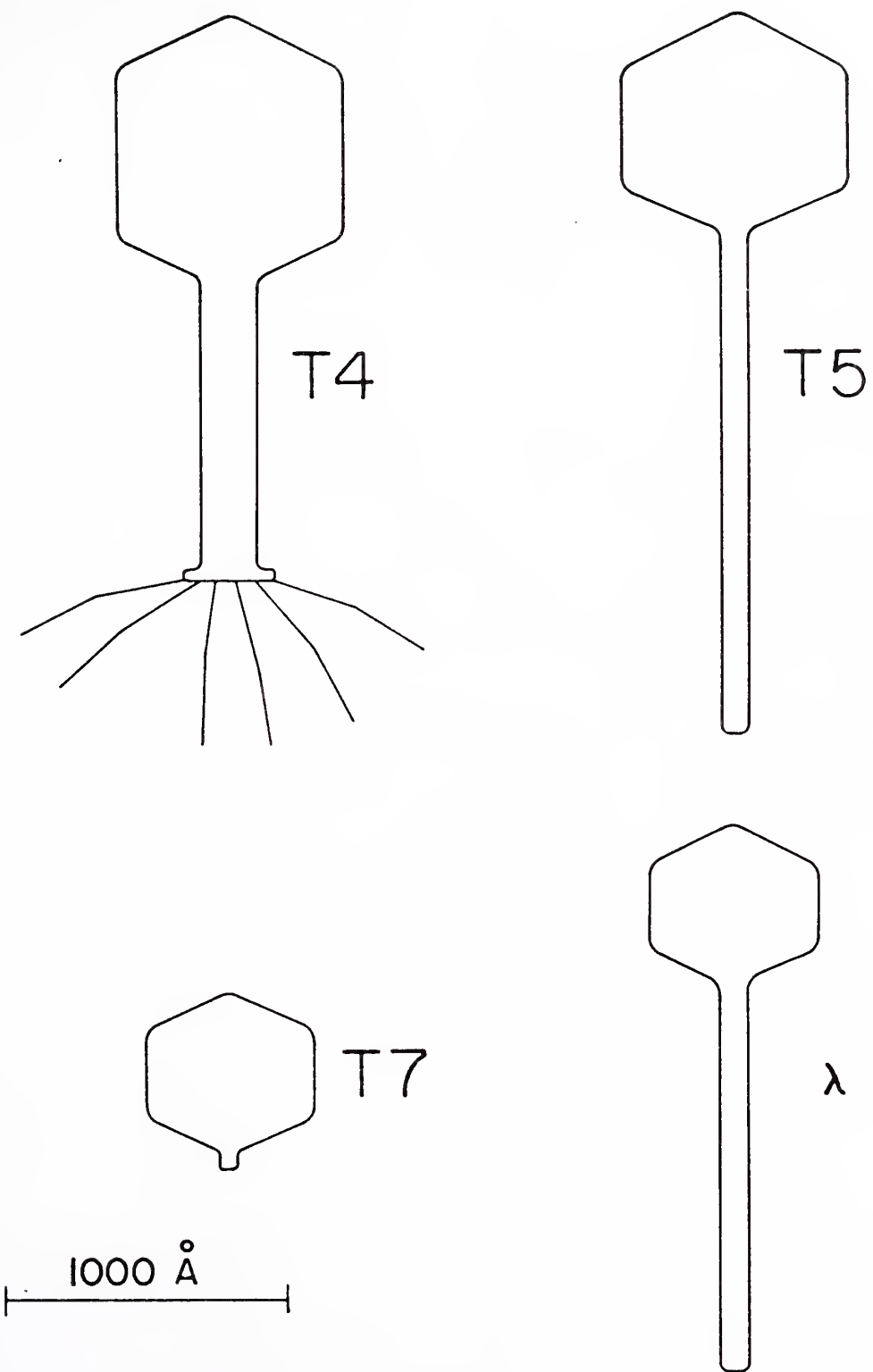
A. Introduction

We present in this chapter the experimental results obtained on bacteriophage molecular weights, phage DNA molecular weights, the chemical denaturation of lysozyme, the determination of the diffusion constant of guanidine hydrochloride, and the determination of the rotational diffusion constant of tobacco mosaic virus. We include a discussion of these results and comparison with the pertinent literature.

B. Experimental Results1. Bacteriophage Molecular Weights

When we derived the spectrum of light scattered by concentration fluctuations, we tacitly assumed that the molecules diffused isotropically. The outlines of the four phages we studied in this thesis (Fig. 5.1) indicate that they are generally quite asymmetric, and thus the assumption of isotropic diffusion may be invalid. We thus studied in detail the spectral shape and angular dependence of the light scattered by the very asymmetric T4 bacteriophage, in order to verify the predictions of a Lorentzian spectral profile and a K^2 dependence of the width of the scattered light (section II.D).

In Fig. 5.2 we display the "self-beat" spectrum of the light scattered by a 30 $\mu\text{g}/\text{cc}$ solution of T4 phage. The open circles are a least squares Lorentzian fit of width $2\Gamma_D/2\pi = 55.2 \text{ Hz}$, a remarkably narrow profile. The trace was obtained with a predetection band-



Outlines of several Bacteriophages

Fig. 5.1

width (ν_1) of 3 Hz, which is such a small value that an integration time of 60 seconds and a total experimental run time of six hours were required to obtain the signal-to-noise visible in the figure. The data are clearly accurately Lorentzian.

In Fig. 5.3, we show the self-beat spectrum for the same sample now studied at $\theta = 160^\circ$, a factor of about 11 larger in K^2 . Once again, the curve is seen to be accurately Lorentzian, with a width of $2\Gamma_D/2\pi = 665$ Hz. The spectrum of the photocurrent is thus shown to be Lorentzian over the entire range of K^2 readily available in a light-scattering experiment.

We studied the self-beat spectrum of the light scattered by T4 phage at seven other angles between 33.9° and 160° . In all cases, the spectrum was found to be Lorentzian and, by plotting $\Gamma_D/2\pi$ vs K^2 in Fig. 5.4, we see that the spectral width varies precisely as K^2 , as predicted by Eq. (2.85). Our simple theory is thus shown to be valid, even for the very asymmetric phage T4, and hence the other phages were studied only at the single scattering angle of 90° .

From the slope of the line given in Fig. 5.4, we have

$D_{20,w} = (0.295 \pm 0.003) \times 10^{-7} \text{ cm}^2/\text{sec}$ for T4 phage. This includes an approximately 1/2% residual error present in all our results due to a temperature drift of about 0.2°C over the course of a run and wave analyzer frequency calibration non-linearities.

To determine whether there was any measurable concentration dependence of the phage diffusion constants, we studied T5 and T7 bacteriophages as a function of concentration. All data were obtained at $\theta = 90^\circ$. As seen in Fig. 5.5, the phage diffusion constant was independent of concentration for all values of C studied. From the

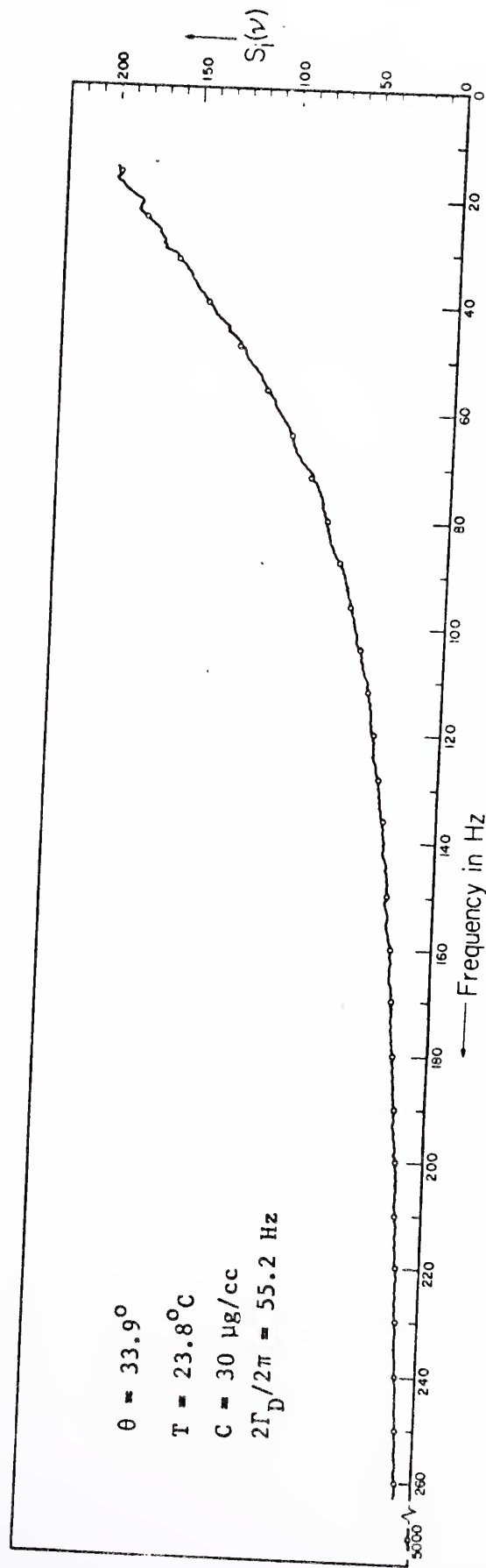


Fig. 5.2 Self-Beat Spectrum of the Light
Scattered at $\theta = 33.9^\circ$ by
 T_4 Bacteriophage

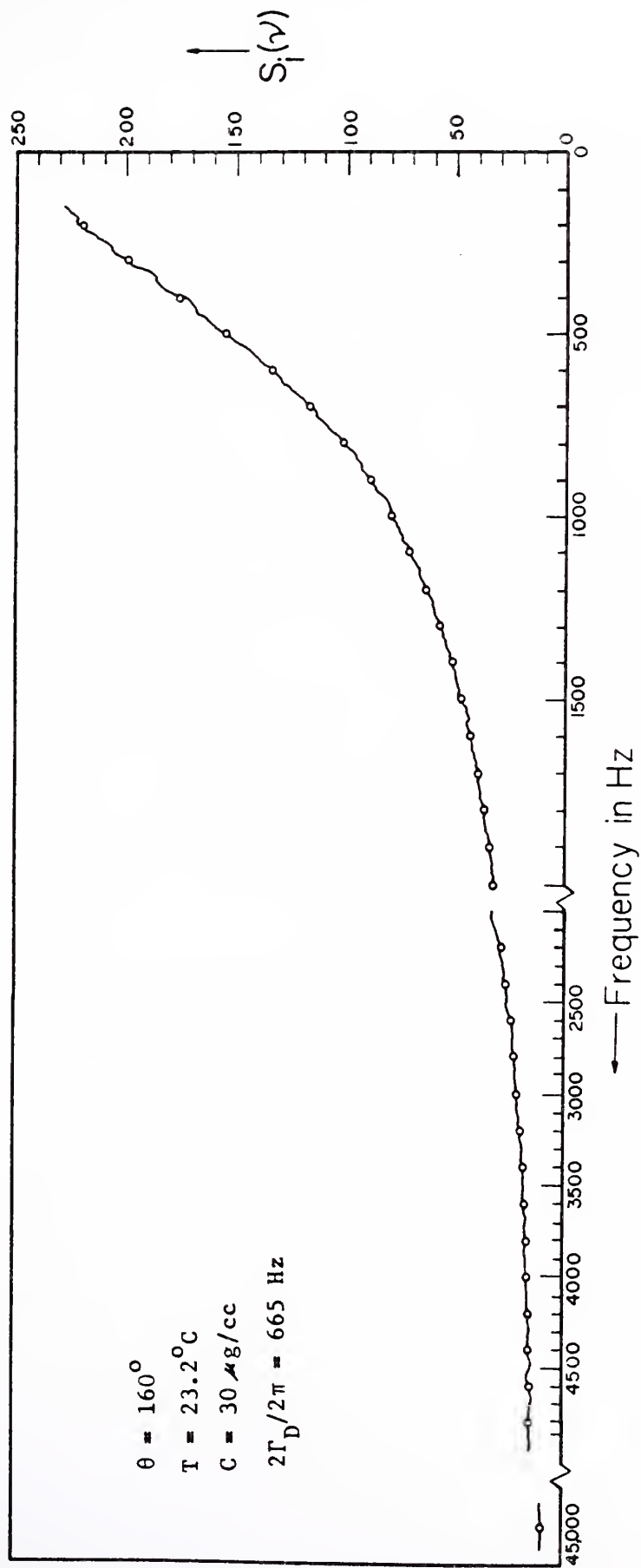


Fig. 5.3 Self-Beat Spectrum of the Light
Scattered at $\theta = 160^\circ$ by
 T_4 Bacteriophage

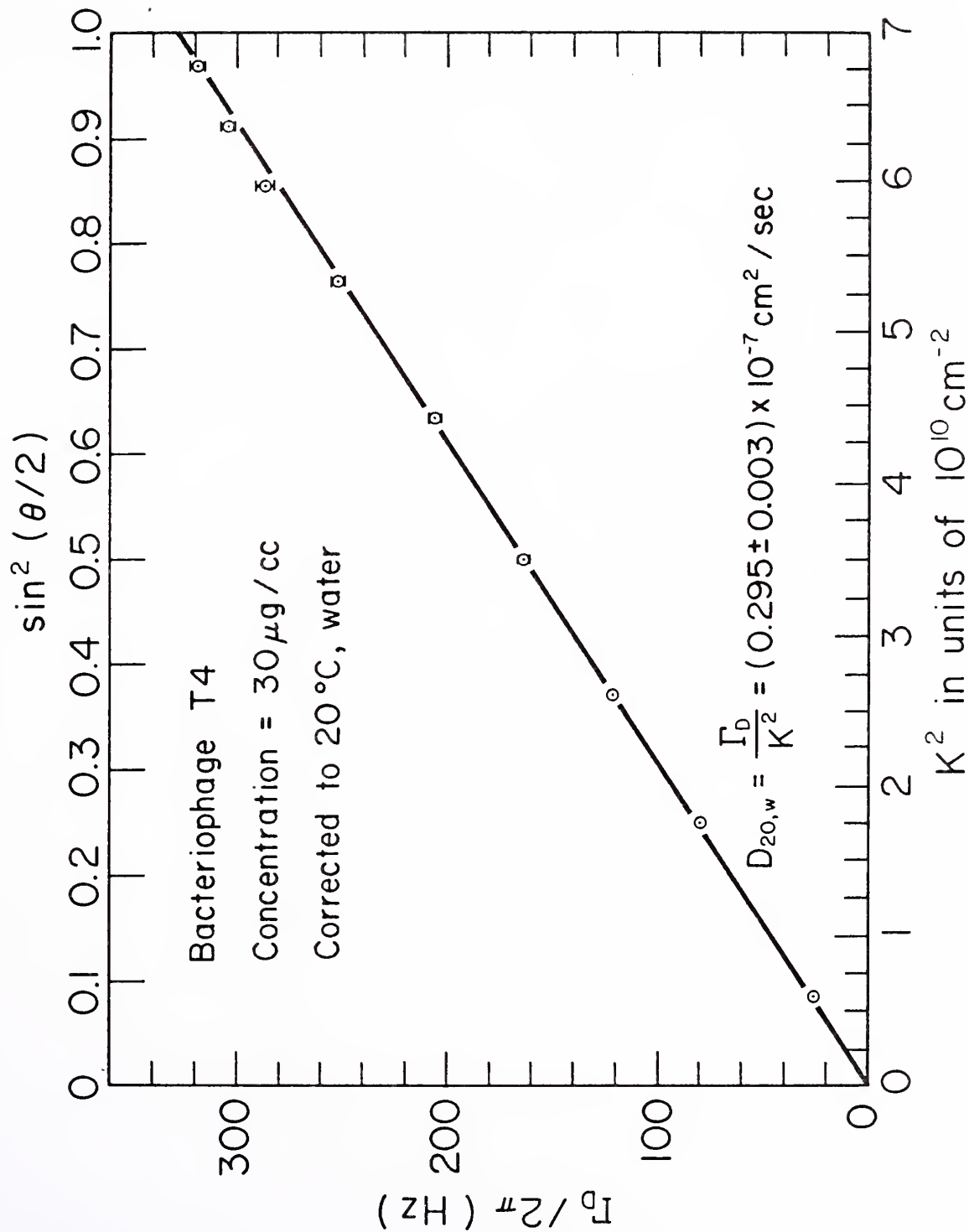


Fig. 5.4 $(\Gamma_D/2\pi)$ versus K^2 for T4
Bacteriophage

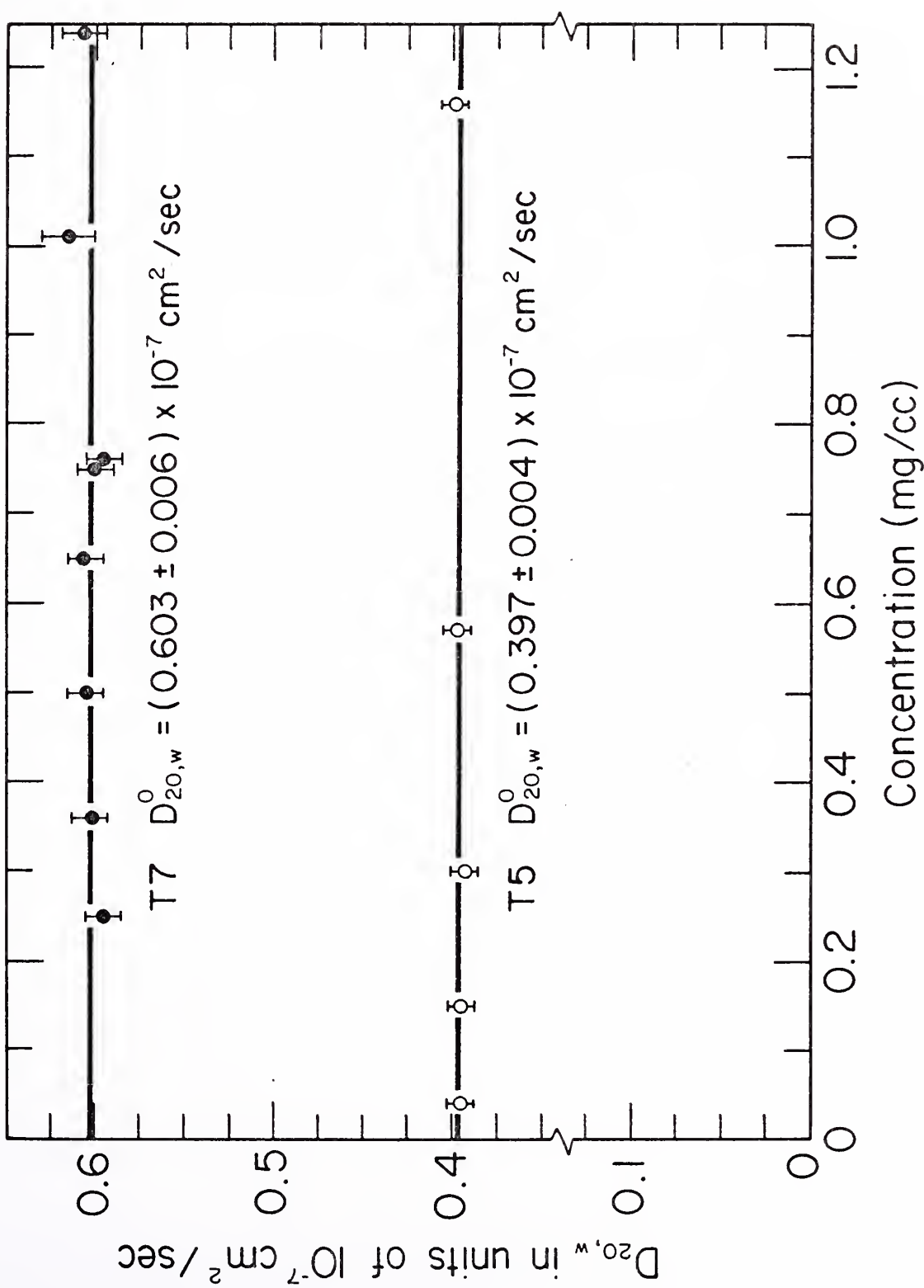


Fig. 5.5 Concentration Dependence of the Diffusion Constants of the Bacteriophages T5 and T7

data presented in Fig. 5.5, we have

$$D_{20,w}^0 = (0.397 \pm 0.005) \times 10^{-7} \text{cm}^2/\text{sec} \text{ for T5 and}$$

$$D_{20,w}^0 = (0.603 \pm 0.006) \times 10^{-7} \text{cm}^2/\text{sec} \text{ for T7. The superscript}$$

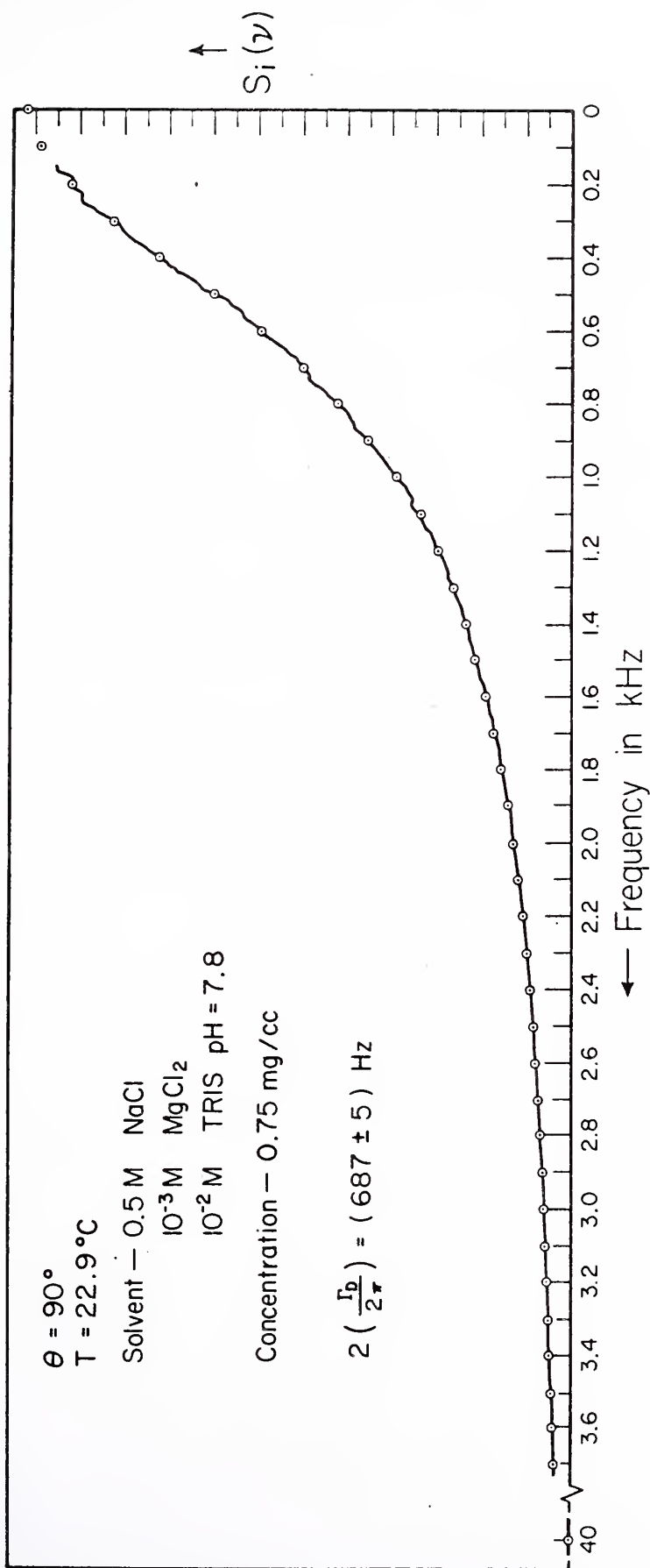
"0" here indicates that the quoted value has been extrapolated to zero concentration. These data indicate that phage diffusion coefficients determined for $C \lesssim 1 \text{ mg/cc}$ are essentially the zero concentration values and the extrapolation to zero concentration is unnecessary. This is generally not the case for the sedimentation constant, S .

The self-beat spectrum of the light scattered at 90° by a 0.75 mg/cc solution of T7 phage is shown in Fig. 5.6. Once again, the spectrum is seen to be quite accurately Lorentzian.

Since we have shown the diffusion constant to be independent of concentration for dilute phage solutions, we studied λ phage at a single concentration of $200 \mu\text{g/cc}$ at 90° scattering angle, and found $D_{20,w}$ for this phage to be $(0.497 \pm 0.005) \times 10^{-7} \text{cm}^2/\text{sec}$.

We now turn to the presentation of the sedimentation constant data for these four phages. Since S usually shows a dependence on concentration, we took all our data for values of $C < 100 \mu\text{g/cc}$ and extrapolated these values to zero concentration to obtain $S_{20,w}^0$. As we see from Fig. 5.7, there was essentially no dependence on C for the low values of concentration used, and we obtained $S_{20,w}^0$ (in units of 10^{-13}sec) for T4, T5, T7 and λ phage respectively as: (890 ± 15) , (615 ± 10) , (453 ± 8) and (360 ± 10) .

We may now use the Svedberg equation (Eq. 2.94) to determine the phage molecular weights if we know \bar{v} , the partial specific volume,



"Self-beat" spectrum of the light scattered by Bacteriophage T7

Fig. 5.6

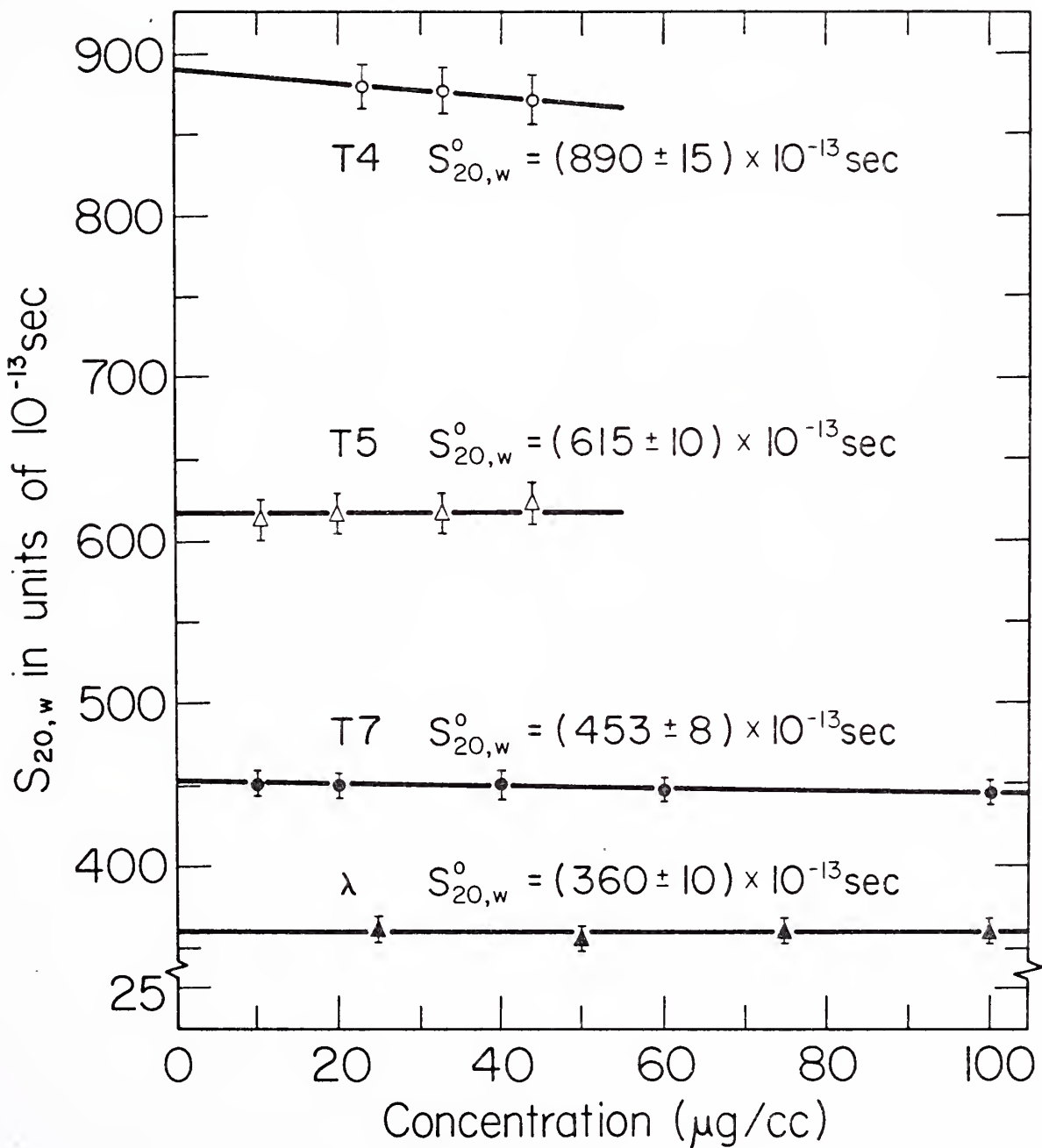


Fig. 5.7 Concentration Dependence of the Sedimentation Constants of Bacteriophages T4, T5, T7, and λ

for each phage. These have been determined for T4, T5 and T7 in a very careful series of experiments by Bancroft and Freifelder.⁽¹⁾ In principle, one determines \bar{v} by simply measuring the volume of solvent displaced by a given mass of dry phage. However, drying the phage usually leads to its decomposition, so that the measured value for \bar{v} is often erroneous. This accounts for the notable lack of data on bacteriophage partial specific volumes. Bancroft and Freifelder⁽¹⁾ have avoided this problem by determining the mass of phage in a given volume of solution by a chemical analysis. They have therefore been able to determine \bar{v} for T4, T5 and T7 phage with a very high reliability, giving values of $(0.617 \pm 0.007) \text{cc/g}$, $(0.658 \pm 0.006) \text{ cc/g}$, and $(0.639 \pm 0.006) \text{cc/g}$ respectively.*

Bancroft and Freifelder did not, however, determine \bar{v} for λ phage. An indirectly determined value of $\bar{v}_\lambda = 0.61$ has been given by Dyson and van Holde.⁽²⁾ Since this value was obtained by making the assumption that protein and DNA \bar{v} 's are additive (which we will show not to be generally true), to determine the phage \bar{v} , we cannot give the same credence to this value as to those provided by Bancroft and Freifelder. However, we shall give direct, self-consistent evidence that $\bar{v}_\lambda = 0.61$ is indeed quite accurate.

We first consider the phage and phage-DNA molecular weights implied by these values of \bar{v} .

The above values of S, D, and \bar{v} are all summarized in Table 5.1 below:

* These values were determined at 26°C, but \bar{v} shows negligible temperature dependence down to the range of 23°C - 25°C, at which our experiments were performed: Hunter, M.J., J. Phys. Chem. 70, 3285 (1966).

Table 5.1

$S_{20,w}^0$, $D_{20,w}$, and \bar{v} for Phages T4, T5, T7 and λ

Phage	$D_{20,w}^*$ in units of $10^{-7} \text{ cm}^2/\text{sec}$	$S_{20,w}^0$ in units of 10^{-13} sec.	\bar{v} cc/g
T4	0.295 ± 0.003	890 ± 15	0.617 ± 0.007
T5	0.397 ± 0.004	615 ± 10	0.658 ± 0.006
T7	0.603 ± 0.006	453 ± 8	0.639 ± 0.006
λ	0.497 ± 0.005	360 ± 10	0.61^{**}

* Values for T5 and T7 are extrapolated to zero concentration

** See text

Using the values given in Table 5.1, we obtain the phage molecular weights via Eq. (2.94). These values for M are listed in Table 5.2, along with the percentage DNA, hence the DNA molecular weight for each phage. The percent by weight of DNA in T4, T5 and T7 was determined chemically by Bancroft and Freifelder.⁽¹⁾ We determined the percentage DNA in λ by the following method. If we assume $\bar{v}_\lambda = 0.61$, then $M_\lambda = 45.8 \times 10^6$ as shown in Table 5.2. Dyson and van Holde⁽²⁾ determined \bar{v} for the λ phage protein component as 0.725 cc/g in a direct pycnometric measurement. They were thus able to obtain the molecular weight of the λ protein as 21×10^6 in a conventional measurement by the sedimentation-equilibrium technique.⁽³⁾ Thus, since M_λ is 45.8×10^6 under the assumption that $\bar{v}_\lambda = 0.61$, we

see that $M_{\lambda \text{DNA}}$ is 24.8×10^6 , since the DNA and protein constitute 100% of the phage.

Table 5.2

Molecular Weights and % DNA of T4, T5, T7 and λ Bacteriophages

Phage	M_{Phage} (Millions)	% DNA	M_{DNA} (Millions)
T4	192.5 ± 6.6	54.9 ± 0.5	105.7 ± 3.8
T5	109.2 ± 4.0	61.7 ± 1.7	67.3 ± 3.1
T7	50.4 ± 1.8	51.2 ± 0.5	25.8 ± 1.0
λ	45.2 ± 2.0	*	$24.2 \pm 1.0^*$

* See text for discussion

We may employ the results of Table 5.2 to substantiate our use of $\bar{v}_{\lambda} = 0.61$ as given by Dyson and van Holde.⁽²⁾ We see that the molecular weights of the DNA's in T4, T5 and λ phage stand in the ratio of $(105.7 \pm 3.8)/(67.3 \pm 3.1)/24.8$, where we have not yet assigned confidence limits to $M_{\lambda \text{DNA}}$. We may thus write

$$\frac{M_{T4 \text{DNA}}}{M_{T5 \text{DNA}}} : \frac{M_{T5 \text{DNA}}}{M_{\lambda \text{DNA}}} = (4.36 \pm 0.15) : (2.78 \pm 0.12) : 1 .$$

(5.1)

Burgi and Hershey⁽⁴⁾ determined the ratio $\frac{M_{T2 \text{DNA}}^*}{M_{T5 \text{DNA}}} : \frac{M_{T5 \text{DNA}}}{M_{\lambda \text{DNA}}}$ by the method of zone centrifugation, which permits the measurement of relative molecular weights. They obtained:

* T2 phage is morphologically very similar to T4 and is thought to be of about the same molecular weight (\pm a couple of %).

$$\frac{M_{T2}}{DNA} : \frac{M_{T5}}{DNA} : \frac{M_{\lambda}}{DNA} = 4.2/2.7/1. \quad (5.2)$$

The agreement between Eqs. (5.1) and (5.2) is remarkable and indicates that the Dyson-van Holde⁽²⁾ value of $\bar{v}_{\lambda} = 0.61 \text{ cc/g}$ is indeed correct. We thus conclude that the accuracy of \bar{v} and % DNA for λ phage is about the same as that for the three phages determined by Bancroft and Freifelder, namely better than $\sim 1.5\%$. We thus believe that

$$\frac{M_{\lambda}}{} = (45.2 \pm 2) \times 10^6 \quad (5.3)$$

$$\frac{M_{\lambda}}{DNA} = (24.2 \pm 1) \times 10^6. \quad (5.4)$$

We may now comment on the additivity of partial specific volumes. If the partial specific volumes of the phage protein and phage DNA are denoted \bar{v}_p and \bar{v}_{DNA} respectively, the

$$\bar{v}_{phage} = \frac{\frac{M_p}{M_{phage}} \bar{v}_p + \frac{M_{DNA}}{M_{phage}} \bar{v}_{DNA}}{} \quad (5.5)$$

if \bar{v}_p and \bar{v}_{DNA} do not change when the protein is combined with the DNA in the intact phage. That this latter requirement is not always met is clear from our results in Table 5.2. For example, \bar{v}_{DNA} is usually found to be around 0.55 cc/g, and \bar{v}_p about .72 cc/g.⁽⁴⁾ Hence, using Eq. (5.5) and our results in Table 5.2, we obtain the values given in Table 5.3 below:

Table 5.3

Comparison of Derived Phage Partial Specific Volumes
(Assuming \bar{v} Additivity)
and Actual Partial Specific Volumes

Phage	Derived \bar{v} (cc/g)	Actual \bar{v} (cc/g)
T4	0.625 \pm 0.009	0.617 \pm 0.007
T5	0.616 \pm 0.009	0.658 \pm 0.006
T7	0.634 \pm 0.009	0.639 \pm 0.006
λ	0.63 \pm 0.01	0.61 \pm 0.01*

* See text

It is interesting to note from Table 5.3 that all of the derived and actual \bar{v} values agree (within their confidence limits) except for T5. A possible explanation for this one exception is that a different amount of solvent is excluded from the interior of the intact phage than from the interior of the protein coat after the DNA has been liberated. In any event, we must conclude that Eq. (5.5) does not have general applicability, contrary to its frequent use in the experimental literature.

Because of the difficulty of measuring D for viruses by classical techniques, little experimental literature exists in the sedimentation-diffusion method for determining phage molecular weights. It is noteworthy, however, that our value of $(S_{20,w}^0/D_{20,w})$ for T4 is $(301 \pm 7) \times 10^{-7}$ (sec/cm)². Cummings and Kozloff,⁽⁵⁾ in a classical

determination, found this ratio to be $(300 \pm 12) \times 10^{-5}$ (sec/cm)² in the case of the morphologically very similar T2 bacteriophage. This agreement is quite good indeed.

Another independent means we have to determine the accuracy and validity of our diffusion constant determination occurs in the case of T7 phage. Under the electron microscope, this phage appears as a regular icosahedron* with face-to-face distance of about (630 ± 15) Å.⁽⁵⁾ The diffusion constant of a regular icosahedron is 0.94 times D for a sphere of diameter (630 ± 15) Å. We may use the Stokes-Einstein relation, Eq. (2.88), to calculate $D_{20,w}$ for such a sphere and obtain $D_{20,w} = (0.678 \pm 0.016) \times 10^{-7}$ cm²/sec. Hence, the expected value of $D_{20,w}$ for the icosahedron is 0.94 times as large, or

$$D_{20,w} = (0.638 \pm 0.015) \times 10^{-7} \text{ cm}^2/\text{sec.} \quad (5.6)$$

[calculated for icosahedron]

This value is to be compared with our measured value for T7 phage of

$$D_{20,w} = (0.603 \pm 0.006) \times 10^{-7} \text{ cm}^2/\text{sec.} \quad (5.7)$$

[value for T7 phage from Table 5.1]

This agreement is good, particularly considering the fact that we have neglected the phage tail structure. This result indicates that, at least for T7 phage, the solvent suspended particle has the hydrodynamic properties we would anticipate from its appearance in the

* We neglect the very short tail visible in Fig. 5.1



electron microscope, that is, that no appreciable distortion of the phage occurs upon drying.

Finally, it is appropriate to consider the significance of our values for the phage-DNA molecular weights, the primary goal of this study. The values for M_{DNA} given in Table 5.2 are systematically about 20% lower than those usually quoted. A careful reading of the literature reveals that very few primary phage-DNA molecular weight determinations have actually been made. Instead, due to the difficulty of making such absolute measurements, there has been a tendency to obtain relative molecular weights, usually defining T2 DNA as the standard⁽⁷⁾ with $M_{T2DNA} = 130 \times 10^6$. It is startling to observe that if the "standard" is abandoned, the apparent disagreement with the literature in large measure vanishes.

Very recently, Schmid and Hearst⁽⁸⁾ have applied the method of density gradient sedimentation equilibrium to the determination of the molecular weights of the DNA in T4, T5 and T7. They included in their work an analysis of corrections required due to thermodynamic non-ideality of the system, and found these corrections to be non-negligible. Using this analysis, they determined that the values of M_{DNA} for T4, T5 and T7 are 104×10^6 , 65.7×10^6 , and 23.2×10^6 respectively. The agreement with our results for T4 DNA and T5 DNA is seen to be within about 2%, a convincing result. Unfortunately, they find T7 DNA to be about 10% smaller than our value. Nevertheless, it would appear that there is now strong evidence that T4 (and T2) DNA molecular weights referenced in the literature are substantially too large, as well as, therefore, those DNA molecular weights which are determined relative to these standards. The

present results, combined with those of Schmid and Hearst,⁽⁸⁾ indicate about a 20% reduction in such values is required.

2. The Denaturation of Lysozyme

Using the detailed data reduction procedure described in section V.B.2, we have analyzed the spectrum of the light scattered by a 1% lysozyme solution for 30 values of the denaturant (GuCl) concentration between 0 M and 6 M GuCl. We would expect a single Lorentzian fit to describe accurately the self-beat spectrum of the light scattered by lysozyme in the absence of GuCl. In Fig. 5.8 we show the self-beat spectrum in this case. The open circles represent a least squares best fit with $2\Gamma_D/2\pi = 6,872$ Hz. We see that a single Lorentzian indeed describes the experimental data accurately. We see that the predetection signal-to-noise ratio is about 1/1, compared with the value of 6/1 predicted by Eq. (3.31).

As the concentration of GuCl was increased, the light scattered by the denaturant became significant, and the spectrum was fit according to Eq. (4.11). In Fig. 5.9 we display the self-beat spectrum of the photocurrent when $[GuCl] = 4.37$ M. It is clear from the figure that a two-parameter fit (i.e., a single Lorentzian) indicated by open square is inadequate to describe the experimental data. The open circles indicate a three-parameter fit, which includes the contribution of the GuCl via Eq. (4.11). It is thus seen that Eq. (4.11) accurately describes the spectrum of the photocurrent.

We analyzed our data for 30 values of $[GuCl]$ according to Eq. (4.11). We typically took three successive spectra at each GuCl concentration and the error bars on our determinations of $D_{20,w}$ for

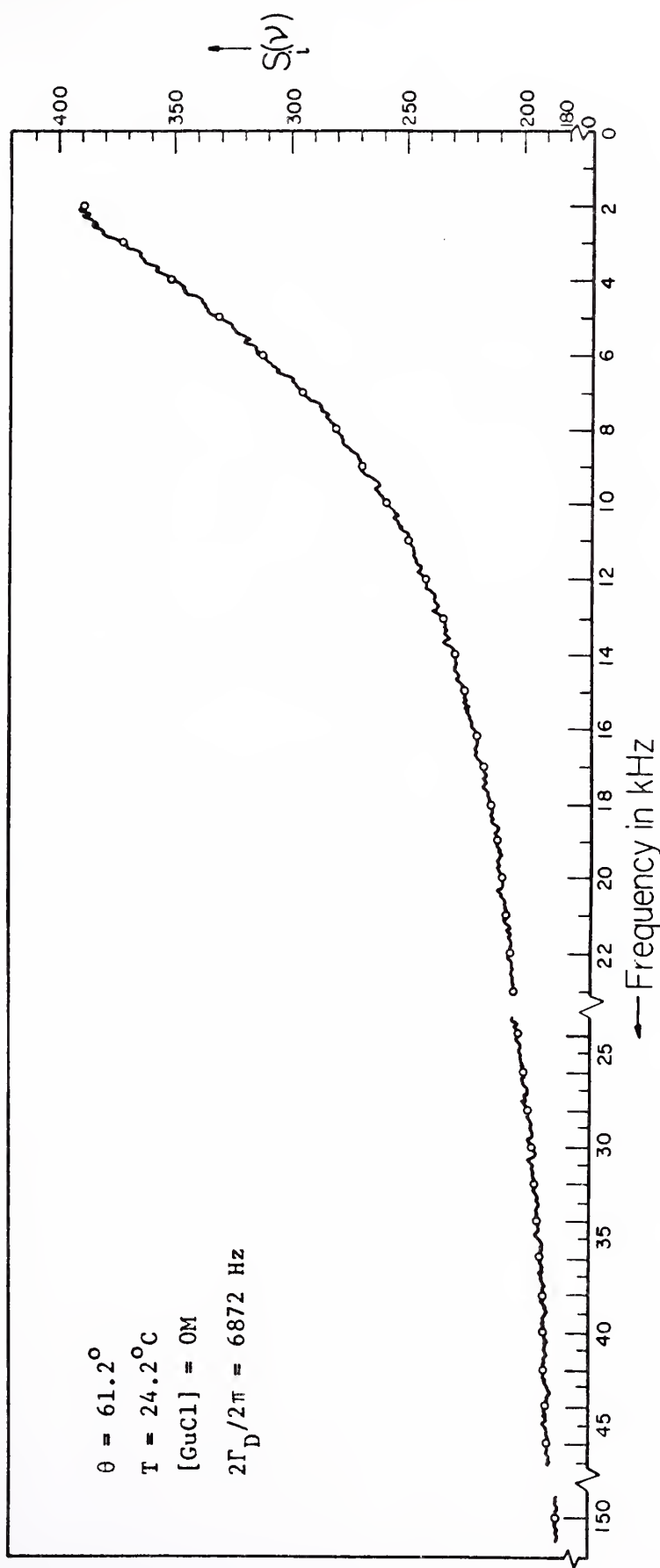


Fig. 5.8 Self-Beat Spectrum of the Light Scattered by a 1% Lysozyme Solution

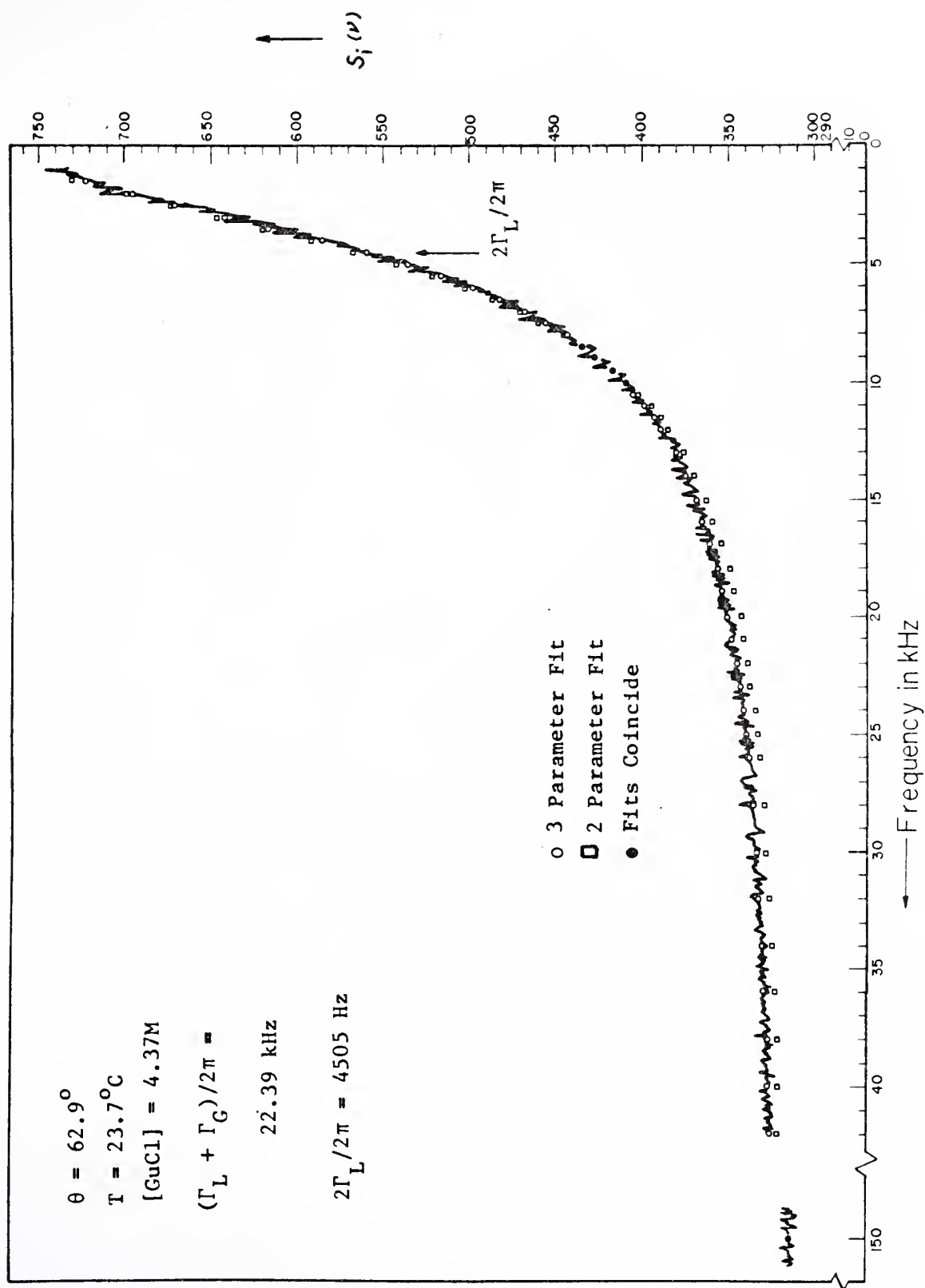


Fig. 5.9 Self-Beat Spectrum of the Light Scattered by a 1% Lysozyme-4.37M GuCl Solution

lysozyme and GuCl are the observed fluctuations in these three values. The results are summarized in Table 5.4 and in Fig. 5.10 we display $D_{20,w}$ for lysozyme versus the concentration of GuCl. The five points in the figure without error limits correspond to single determinations, for which the rms deviation of the best fit from Eq. (4.11) was about 1/2%, a value typical of all the lysozyme data. That is, the experimental data were fit very accurately by Eq. (4.11), but, as the error bars on the points in Fig. 5.10 indicate, the trace-to-trace reproducibility at a given GuCl concentration was less good, being typically a couple percent. It was found in all experiments in this thesis that the experimental reproducibility was generally poorer than the consistently highly accurate fits might lead one to expect.

From Fig. 5.10 we see that the native form of lysozyme has a value of $D_{20,w}$ of $(10.6 \pm 0.1) \times 10^{-7} \text{ cm}^2/\text{sec}$. This is in agreement with the value reported by Calvin⁽⁹⁾ who obtained $D_{20,w} = (10.4 \pm 0.1) \times 10^{-7} \text{ cm}^2/\text{sec}$. However, this latter value was obtained at pH = 6.8, where aggregation may occur (see section III.C.3), so the agreement may be fortuitous. Calvin⁽⁹⁾ also reported $S_{20,w}$ for lysozyme to be $(1.87 \pm 0.02) \times 10^{-13} \text{ sec}$. If we combine our value of $D_{20,w}$, and use the recent determination of the partial specific volume of lysozyme by Sophianopoulos, Rhodes, Holcomb and van Holde⁽¹⁰⁾ of $\bar{v} = (0.703 \pm 0.004) \text{ cc/g}$ we obtain from Eq. (2.94) that the molecular weight of lysozyme is $14,500 \pm 300$. This value is in excellent agreement with $M_{\text{Lys}} = 14,600$ as determined from the complete X-ray diffraction map of the molecule.⁽¹¹⁾ This

TABLE 5.4

Effect of Chemical Denaturation on the Diffusion Constant
of Lysozyme

[GuCl] Molar	$D_{20,w}$ (units of $10^{-7} \text{cm}^2/\text{sec}$)
0.00	10.75 ± 0.10
0.22	10.72 ± 0.10
0.51	10.50 ± 0.15
0.80	10.57 ± 0.10
1.13	10.48 ± 0.10
1.49	10.41 ± 0.10
1.80	10.42 ± 0.09
1.96	10.68 ± 0.10
2.08	10.41 ± 0.08
2.20	10.42 ± 0.16
2.27	10.39 ± 0.18
2.35	10.29 ± 0.05
2.40	9.98 ± 0.05
2.48	9.85 ± 0.11
2.55	10.14 ± 0.10
2.66	9.82 ± 0.10
2.81	9.97 ± 0.28
2.88	10.22 ± 0.10
2.97	9.79 ± 0.17
3.20	9.62 ± 0.21
3.52	9.40 ± 0.33
3.76	9.03 ± 0.20
4.03	8.57 ± 0.25
4.37	7.97 ± 0.10
4.56	7.77 ± 0.22
4.78	7.65 ± 0.25
4.98	7.26 ± 0.28
5.29	7.34 ± 0.32
5.46	7.27 ± 0.12
5.90	7.50 ± 0.16

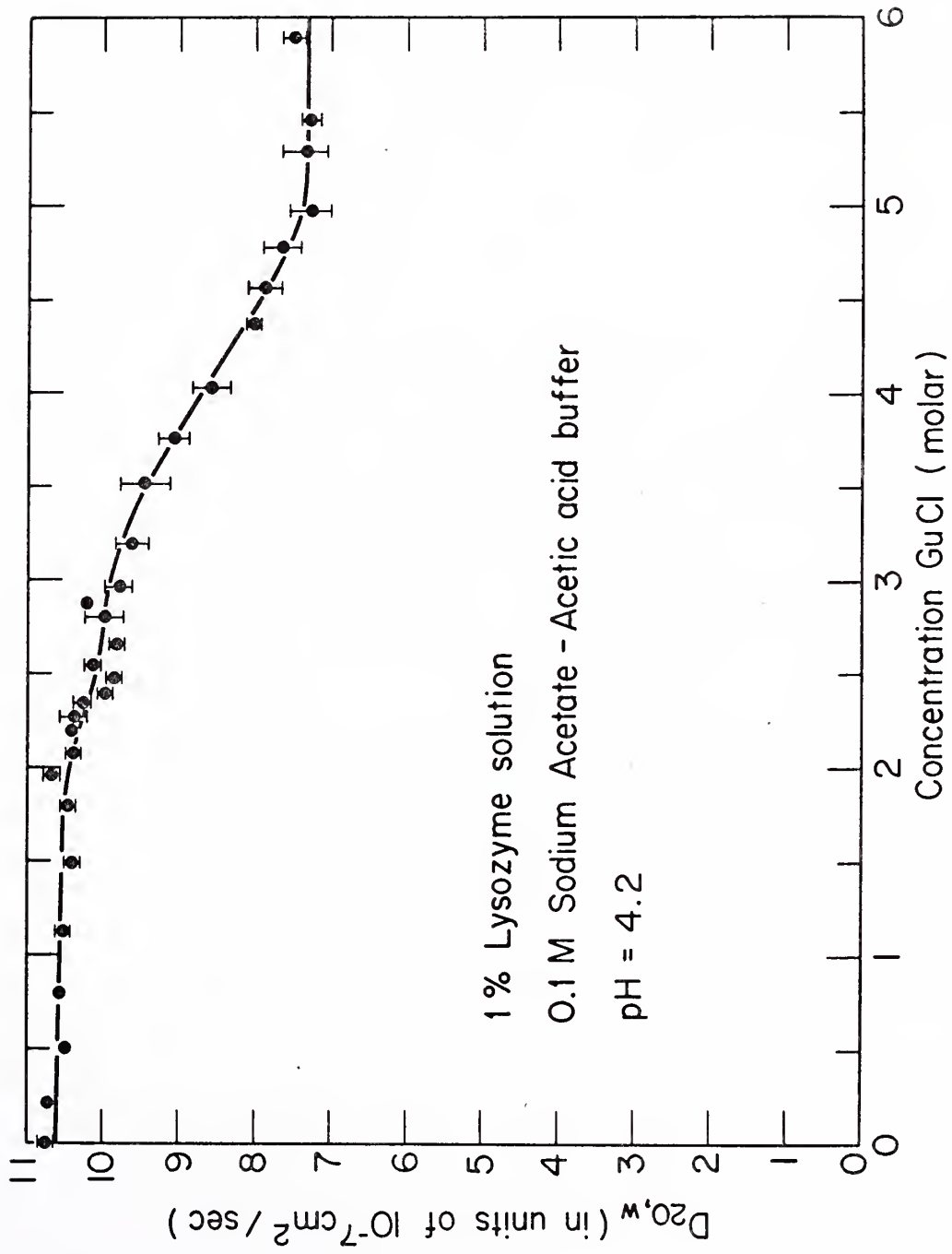


Fig. 5.10 Effect of chemical denaturation on the diffusion constant of Lysozyme

agreement allows us to conclude that our method for the determination of D for lysozyme is indeed valid.

As we discussed in section IV.B.2, the change in D upon denaturation of lysozyme as shown in Fig. 5.10 is not large enough to determine whether or not more than one species was present at any concentration of GuCl. If we use the NMR results of Glickson, McDonald, and Phillips⁽¹²⁾ that only the native and denatured species are present, or a mixture of these, for any value of [GuCl], we can conclude from Fig. 5.10 the percentage of each present at a given value of the GuCl concentration. Our results in section IV.B.2 indicate that for a mixture of two molecules of the same molecular weight, but of diffusion constants differing by a factor of about 1.5 or less, the self-beat spectrum of the photocurrent gives the mass percent weight average of the two different diffusion constants. We see, then, that Fig. 5.10 indicates a smooth transfer between completely native and completely denatured molecules, with equal numbers of each existing at the value of [GuCl] for which $D_{20,w} = \frac{10.6 + 7.3}{2} \times 10^{-7} \text{ cm}^2/\text{sec} = 9.0 \times 10^{-7} \text{ cm}^2/\text{sec}$.

From Fig. 5.10, this is seen to occur at [GuCl] = 3.8 M. By 5 M GuCl the value of $D_{20,w}$ has plateaued and the protein is thus considered to be completely in the denatured form.

From Eq. (2.88) we can define an effective radius, r_{eff} , to be proportional to the reciprocal of the diffusion constant. If we then define an effective volume, V_{eff} , which is proportional to r_{eff}^3 we see that the ratio of the effective volume of the native lysozyme to that of the denatured lysozyme is given by

$$\frac{V_{\text{eff}}^{\text{native}}}{V_{\text{eff}}^{\text{denatured}}} = \left(\frac{D_{20,w}^{\text{denatured}}}{D_{20,w}^{\text{native}}} \right)^3 \quad (5.8)$$

From Fig. 5.10 we see that

$$D_{20,w}^{\text{native}} = (10.6 \pm 0.1) \times 10^{-7} \text{ cm}^2/\text{sec}, \text{ and}$$

$$D_{20,w}^{\text{denatured}} = (7.3 \pm 0.1) \times 10^{-7} \text{ cm}^2/\text{sec. Hence, Eq. (5.8)}$$

indicates that

$$\frac{V_{\text{eff}}^{\text{native}}}{V_{\text{eff}}^{\text{denatured}}} = 0.32. \quad (5.9)$$

That is, the native molecule has only about 1/3 the effective volume of the denatured form.

We observe that the "effective volume" referred to here is simply the volume of the sphere hydrodynamically equivalent to the macromolecule under study. This hydrodynamic volume may also be determined by the measurement of the molecule's intrinsic viscosity, $[\eta]$, to which is proportional.⁽¹³⁾ Hamaguchi and Kurono⁽¹⁴⁾ found that

$$\frac{[\eta]_{\text{Lys}}^{\text{native}}}{[\eta]_{\text{Lys}}^{\text{denatured}}} = \frac{0.033 \text{ dl/g}}{0.087 \text{ dl/g}} \quad (5.10)$$

The agreement between Eqs. (5.9) and (5.10), while not perfect, does indicate that the two different techniques show about the same change in the hydrodynamic volume of lysozyme upon denaturation.

The shape of Fig. 5.10 is very similar to that observed for the

change in optical rotation by lysozyme upon denaturation. (14,15)

There is, however, a slight hint of structure in our data for $D_{20,w}$ between 2 and 3 M GuCl concentration, which does not appear in the optical rotation data. By taking many spectra in this region, we hoped to determine whether or not structure was present. However, our reproducibility of about 2% was inadequate to determine clearly whether this structure was apparent or real.

We have obtained, in addition, the diffusion constant of GuCl itself by using the three-parameter fit to Eq. (4.11). Our data are summarized in Fig. (5.11) where we plot $D_{20,w}$ of GuCl for all the values of [GuCl] were studied. The error limits refer to the spread in values for the three spectra observed at each value of [GuCl]. The points without error limits were determined in those experiments in which only a single experimental spectrum was taken. Although the data presented in Fig. 5.11 show substantial scatter, it is remarkable that they are even this reproducible, considering the rather small experimental "handle" that the GuCl ($M = 95.6$) provides in the interpretation of the spectrum. The average value, $D_{20,w} = 79 \times 10^{-7} \text{ cm}^2/\text{sec}$, compares favorably with $D_{20,w}$ for urea (see section IV.B.2) which is $128 \times 10^{-7} \text{ cm}^2/\text{sec}$.

3. The Rotational Diffusion Constant of Tobacco Mosaic Virus

We have observed the spectrum of light scattered by isotropy fluctuations in a 0.01% solution of tobacco mosaic virus. The scattering was studied at $\theta = 1.61^\circ$ and at $\theta = 3.07^\circ$, using the experimental setup shown in Fig. 3.5.

In Fig. 5.12 we see the self-beat spectrum obtained at a

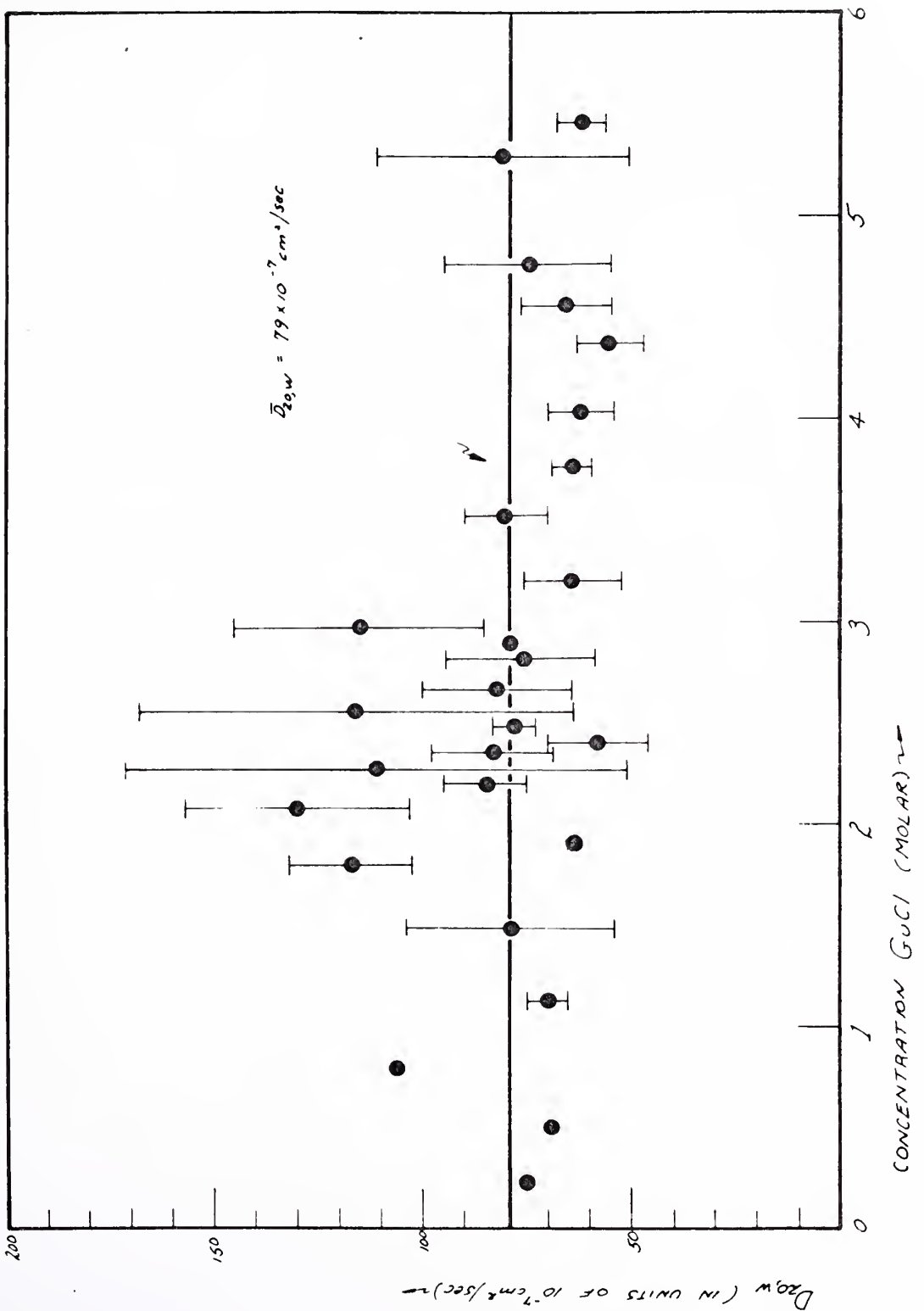


Fig. 5.11 $D_{20,w}$ versus Concentration for
Guanidine Hydrochloride

scattering angle of 1.61° . The open circles refer to a Lorentzian spectrum of width $2\Gamma_R/2\pi = 595$ Hz. This value of Γ_R then yields from Eq. (2.87b) that

$$(D_R)_{20,w} = 284/\text{sec. } (\theta = 1.61^\circ). \quad (5.11)$$

At $\theta = 3.07^\circ$ we obtain

$$(D_R)_{20,w} = 269/\text{sec } (\theta = 3.07^\circ). \quad (5.12)$$

It is clear from Fig. 5.12 that the single Lorentzian fit does not properly describe the experimental spectrum in the region below about 400 Hz. The spectrum below 400 Hz was not included in the fitting program. However, we can account reasonably well for this discrepancy by an analysis of Fig. 3.8 which indicates the distribution of lengths of TMV in our sample. For the very small angles we studied, the scattering form factor for TMV is unity (see section III.C.3). Hence, we can determine the relative intensity contributions of the different lengths present in our sample from their respective products of number density $\times M^2$ (see Eq. 2.27b). We thus conclude that the species of RMV with lengths greater than 3000 \AA contribute about 10% to the total scattered light, which is consistent with the area between the single Lorentzian fit and the experimental fit. These longer molecules would, of course, make their contribution at the observed lower frequencies, since $D_R \propto \frac{1}{L^3}$ [Eq. (2.89)].

The molecules of length less than $\sim 3000 \text{ \AA}$ also contribute about 10% of the total scattered light, but the width of the spectrum of

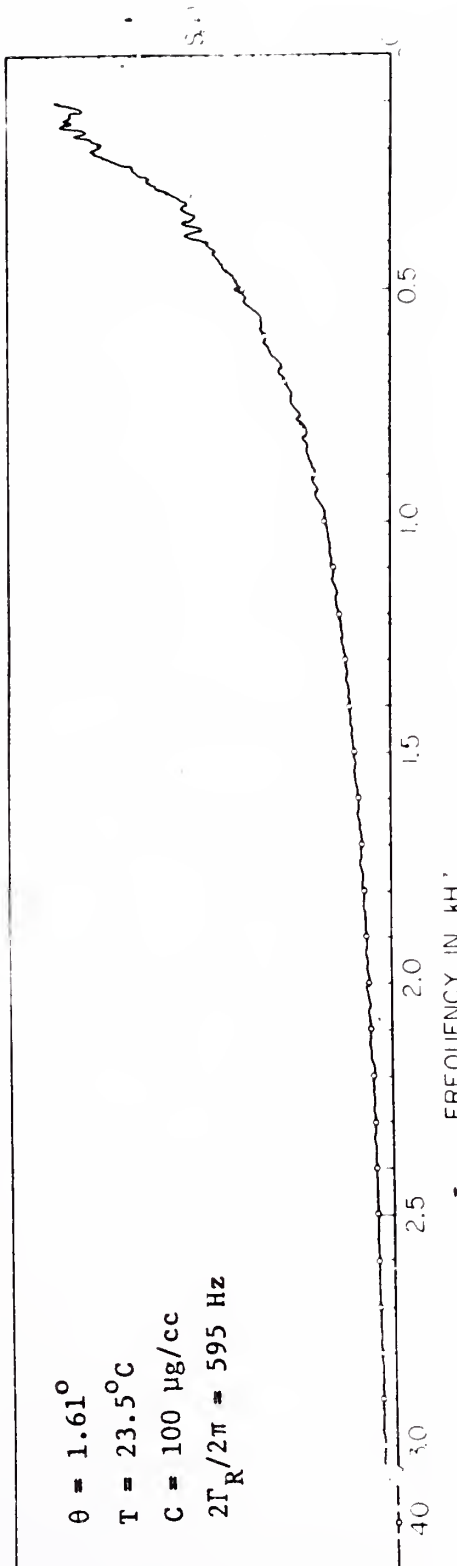


Fig. 5.12 Self-Beat Spectrum of the Anisotropy Scattering at $\theta = 1.61^\circ$ from Tobacco Mosaic Virus

this light will be reasonably wide, due to the $(1/L)^3$ dependence of D_R . Hence, it will not make a conspicuous contribution to the observed spectrum.

We cannot conclude that our measured value for D_R is completely accurate due to the polydispersity problem discussed above. However, it is reasonable that the average value of Eqs. (5.11) and (5.12) is a good approximation, namely:

$$(D_R)_{20,w} = (276 \pm 10)/\text{sec.} \quad (5.13)$$

We will now proceed to compare this value with that expected from hydrodynamic arguments. It has been shown experimentally by torque tank studies on macroscopic cylinders^(16,17) that an ellipsoid of revolution of the same length and diameter as a cylinder is a poor hydrodynamic equivalent for the cylinder. Burgers⁽¹⁸⁾ attempted to determine the rotational diffusion constant for a cylinder, and obtained

$$D_R = \frac{KT(\ln \frac{2a}{b} - 0.8)}{\left(\frac{8}{3}\right)\pi \eta a^3}, \quad (5.14)$$

where $2a$ = length of cylinder

$2b$ = diameter of cylinder

where replacing 0.8 by 0.5 in this expression converts it to the result for an ellipsoid of revolution. Burgers obtained this expression by making approximations which did not include all terms to first-order in (b/a) . Broesma⁽¹⁷⁾ showed that Burger's approximations were inadequate, because the effects of the abrupt ends of the cylinder were underestimated in this approach. He calculated

D_R to an accuracy of all terms of first-order in (b/a) and obtained

$$D_R = \frac{kT(\ln \frac{2a}{b} - \gamma)}{\left(\frac{8}{3}\right) \pi n a^3} \quad (5.15)$$

where γ is a function of (a/b) . Broersma⁽¹⁷⁾ has tabulated γ for various values of a/b and has shown that γ is independent of a/b for $10 < a/b < 25$ and is equal to 1.62 over that range. We may thus calculate $(D_R)_{20,w}$ for TMV using our distribution peak value of 3000 Å [Fig. 3.8] and the X-ray diffraction⁽¹⁹⁾ value for the virus diameter of 180Å. We then obtain

$$D_R = 269/\text{sec.} \quad (5.16)$$

The agreement between this and our value of $(276 \pm 10)/\text{sec.}$, from Eq. (5.13) is excellent, although perhaps somewhat fortuitous due to the length distribution present in our sample. The agreement does indicate, however, that a proper hydrodynamic description of the rotational diffusion constant of a cylinder is valid over the range of sizes from centimeters^(16,17) down to even a few thousand Å. Finally, we can conclude that the assumption of uncoupled translational and rotational motion which was employed in the derivation of Eq. (2.67) is met at least reasonably well.

In a heterodyne beat experiment, Wada, Suda, Tsuda, and Soda⁽²⁰⁾ measured the somewhat larger value of $D_R = 350/\text{sec.}$ The authors do not indicate whether or not this value is corrected to standard conditions. Cummins, Carlson, Herbert, and Woods⁽²¹⁾ were able to determine $(D_R)_{20,w} = (320 \pm 18)/\text{sec}$ by analyzing the concentration

fluctuation scattering from TMV and properly accounting for the modulation of this scattered light due to the rotation of the molecule.

C. Concluding Remarks

Because the field of light mixing spectroscopy is a new one, we have devoted a considerable portion of this thesis to the pertinent theory as applied to scattering from macromolecules. In order to calculate the signal-to-noise ratio obtainable in light-mixing experiments, and hence the feasibility of such experiments, we have presented a determination of the expected intensity of the light scattered by fluctuations in concentration and optical isotropy in a solution of macromolecules.

The operation of the "self-beating" spectrometer has been described in detail, along with such practical considerations as sample and cell cleaning, and cell filling techniques.

Finally, we have presented experimental results which demonstrate the utility and wide range of application of self-beating spectroscopy in the study of macromolecules: the determination of the molecular weights of T4, T5, T7 and λ bacteriophages as well as the molecular weights of the DNA contained in these phages; the observation of the chemical denaturation of lysozyme; the determination of the diffusion constant of guanidine hydrochloride; the determination of the rotational diffusion constant of tobacco mosaic virus.

References for Chapter V

1. Bancroft, F. C., and Freifelder, D., to be published.
2. Dyson, R. D., and van Holde, K. E., Virology, 33, 559 (1967).
3. Tanford, C., "Physical Chemistry of Macromolecules", John Wiley and Sons, Inc., New York, 1961, pp. 259-272.
4. Freifelder, D., private communication.
5. These conclusions were reached by us upon examination of electron micrograph pictures of T7 kindly shown to us by Dr. Peter Davison.
6. Markham, R., in Maramorosch, K., and Koprowski, H. (eds.), "Methods in Virology", Vol. 2, Academic Press, New York, 1967, p. 276.
7. Rubenstein, I., Thomas, C. A., Jr., and Hershey, A. D., Proc. Nat. Acad. Sci., 47, 1113 (1961).
8. Schmid, C. W., and Hearst, J. E., J. Mol. Biol., 44, 143 (1969).
9. Colvin, J. R., Can. J. Chem., 30, 831 (1952).
10. Sophianopoulos, A. J., Rhodes, C. K., Holcomb, D. N., and van Holde, K. E., J. Biol. Chem., 237, 1107 (1962).
11. Phillips, D. C., Proc. Nat. Acad. Sci., 57, 484 (1967).
12. Glickson, J. D., McDonald, C. C., and Phillips, W. D., Contribution No. 1553, Central Research Department, E.I. du Pont Co., Wilmington, Delaware.
13. ref. 7, p. 391.
14. Hamaguchi, K., and Kurono, A., J. Biochem., 54, 111 (1963).
15. Tanford, C., Pain, R. H., and Otchin, N. S., J. Mol. Biol., 15, 489 (1966).
16. Haltner, A. J., and Zimm, B. H., Nature, 184, 265 (1959).
17. Broersma, S., J. Chem. Phys., 32, 1626 (1960).
18. Burgers, J. M., in "Second Report on Viscosity and Plasticity", North Holland Publishing Co., Amsterdam, 1938, pp. 113 - 184.
19. Settow, R. B., and Pollard, E. C., "Molecular Biophysics", Addison-Wesley Publishing Co., Inc., Reading, Mass., 1962, p. 151.

20. Wada, A., Suda, N., Tsuda, T., and Soda, K., J. Chem. Phys., 50, 31 (1969).
21. Cummins, H. Z., Carlson, F. D., Herbert, T. J., and Woods, G., Biophys. J., 9, 518 (1969).

APPENDIX

The Effect of Polydispersity on the Spectrum
of the Light Scattered by Macromolecules

We discussed in section IV.B.2 the self-beat spectrum of the light scattered by a mixture of macromolecules. We proceed here to show that even the heterodyne-beat spectrum of such a mixture cannot be readily distinguished from a single Lorentzian spectrum.

If we have a mixture of equal numbers of molecules of the same molecule weight but of diffusion constants D_1 and D_2 respectively, then the spectrum of the scattered light is given by

$$S(v) \propto \frac{(\Gamma_1/2\pi)}{(\Gamma_1/2\pi)^2 + (v - v_o)^2} + \frac{(\Gamma_2/2\pi)}{(\Gamma_2/2\pi)^2 + (v - v_o)^2}, \quad (A.1)$$

where

$$\begin{aligned}\Gamma_1 &= D_1 K^2 \\ \Gamma_2 &= D_2 K^2.\end{aligned}$$

The signal portion of the heterodyne-beat spectrum (section IV.B.2) is then given as

$$\langle S(v) \rangle \propto \frac{(\Gamma_1/2\pi)}{(\Gamma_1/2\pi)^2 + v^2} + \frac{(\Gamma_2/2\pi)}{(\Gamma_2/2\pi)^2 + v^2}. \quad (A.2)$$

We have generated Eq. (A.2) for various value of D_2/D_1 ranging from one to four. In Fig. A.1 the width of the best single Lorentzian fit divided by the average value of the separate heterodyne widths (Γ_1 and Γ_2) is shown as a function of (D_2/D_1) . We also display the rms deviation of this single Lorentzian fit as a percentage of its amplitude at zero frequency (see section IV.B.2). Even for $\frac{D_2}{D_1} = 2$, this error is less

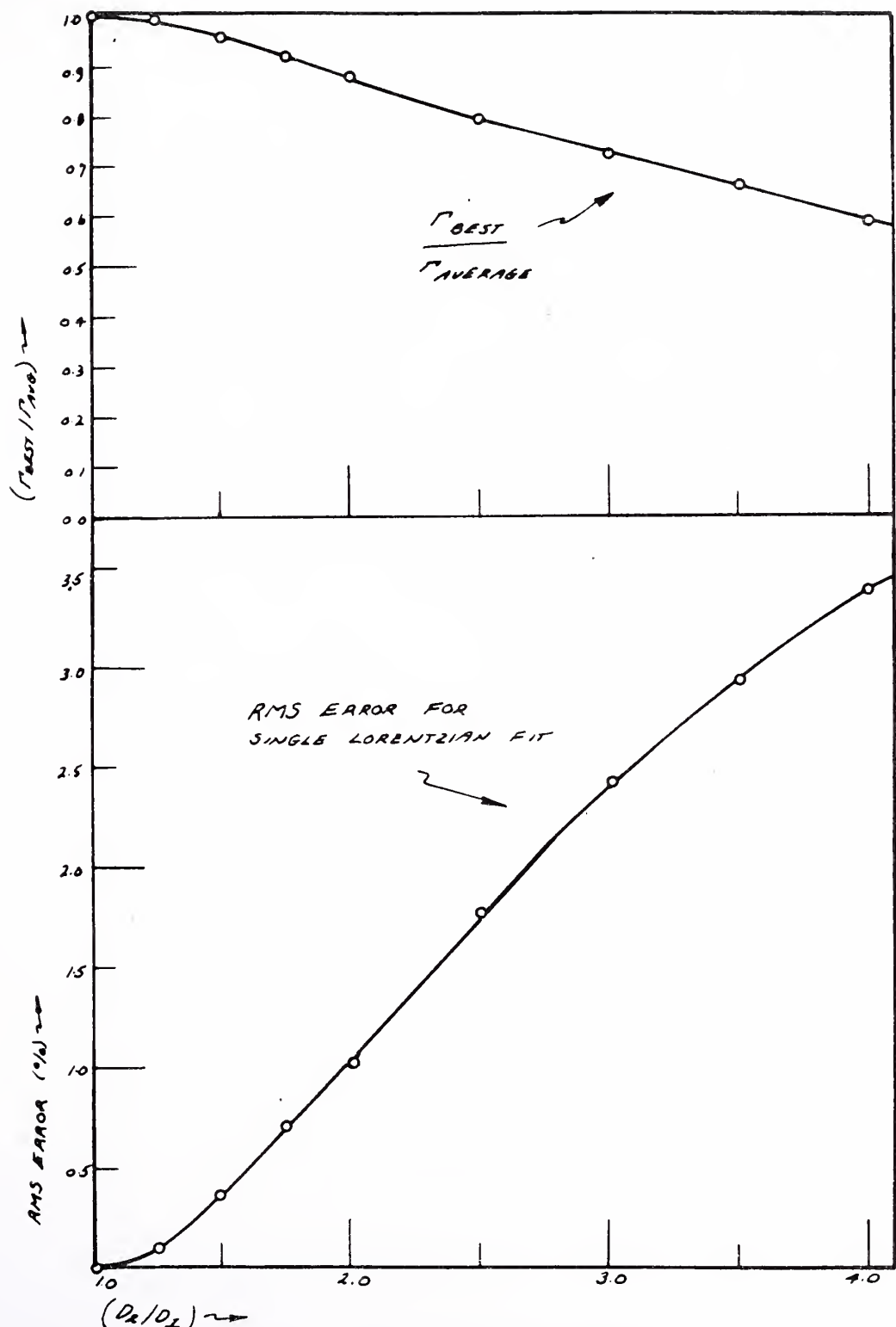


Fig. A.1 Width and RMS Deviation of Best Single Lorentzian Fit to the Heterodyne-Beat Spectrum of the Light Scattered by Various Two-Component Mixtures

than 1%, once again indicating our inability to distinguish the actual photocurrent spectrum from a single Lorentzian.

In light of the above results, and those discussed in section IV.B.2, we investigated the possibility of discerning polydispersity in various mixtures by heterodyne mixing. We first consider a uniform mixture (equal numbers of each type) of molecules with effective radii ranging from R_{\min} to R_{\max} , all of which have the same molecular weight. We define

$$\Delta = \frac{R_{\max} - R_{\min}}{R_o} , \quad (A.3)$$

where R_o is the average radius. Then, since $\Gamma \propto 1/R$, we have

$$\begin{aligned} \langle S(v) \rangle &\propto \int_{R_{\min}}^{R_{\max}} \frac{1/R}{(1/R)^2 + v^2} dR \\ &\propto \frac{1}{2} \frac{1}{v^2} \ln \left\{ 1 + \frac{v^2}{\Gamma_{\min}^2} \right\}_{\Gamma_{\min}}^{\Gamma_{\max}} , \end{aligned} \quad (A.4)$$

$$\text{where } \Gamma_{\max} \propto \frac{1}{R_{\max}}$$

$$\Gamma_{\min} \propto \frac{1}{R_{\min}} .$$

We have tabulated Eq. (A.4) for values of $\Delta = \frac{R_{\max} - R_{\min}}{R_o}$ running from 0 (monodispersity) to 2 (completely polydisperse). Fig. A.2 displays the best single Lorentzian fit to these generated data as a function of Δ . We see that even for $\Delta = 2$, the rms deviation as a per cent of the spectrum at zero frequency is only

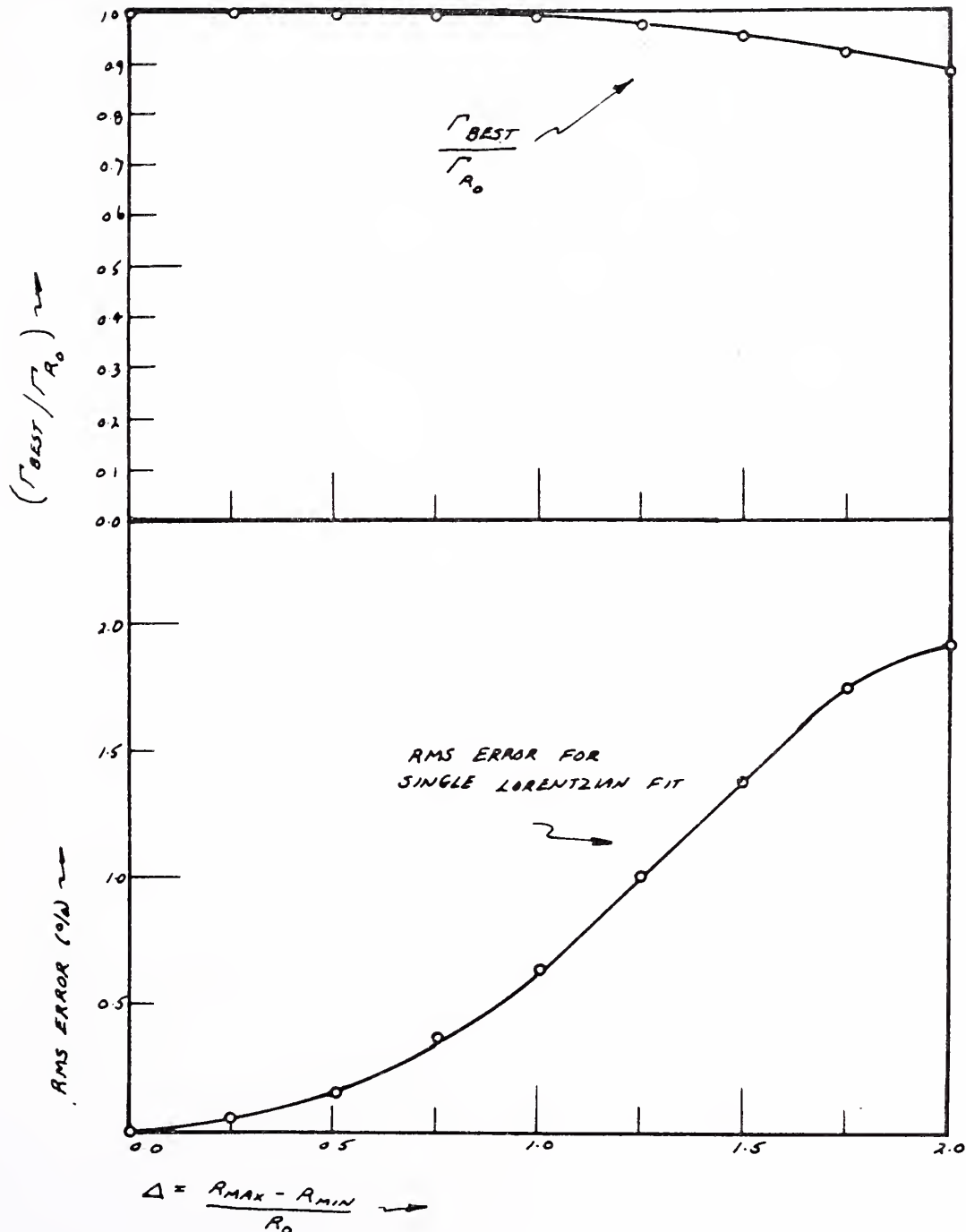


Fig. A.2 Width and RMS Deviation of Best Single Lorentzian Fit to the Heterodyne-Beat Spectrum of the Light Scattered by Various Uniform Uniform Distributions of Molecules Differing Only in Diffusion Constant

2%. In addition, we see that the spectral width of the best fit is very nearly that expected for the light which is scattered by molecules of the mean radius, R_o .

We now consider a uniform mixture of spheres ranging in molecular weight from M_{\min} to M_{\max} . Since the intensity of the light scattered is proportional to the square of the molecular weight, and the spectral linewidth proportional to the radius of the sphere and hence to $(1/M)^{1/3}$, we see that

$$\langle S(v) \rangle \propto \int_{M_{\min}}^{M_{\max}} \frac{M^2 \Gamma}{\Gamma^2 + v^2} dM$$

$$\propto -3 \int_{X_{\min}}^{X_{\max}} \frac{x^{-9}}{x^2 + v^2} dx$$

where $x = M^{-1/3}$.

We then have

$$\begin{aligned} \langle S(v) \rangle &\propto 3 \left[\frac{1}{8v^2 x^8} - \frac{1}{6v^4 x^6} + \frac{1}{4v^6 x^4} \right. \\ &\quad \left. - \frac{1}{2v^8 x^2} + \frac{1}{2v^{10}} \left\{ 1 + \frac{v^2}{x^2} \right\} \right]_{X_{\min}}^{X_{\max}} . \end{aligned} \quad (A.5)$$

Eq. A.5 has been evaluated for

$$\Delta = \frac{M_{\max} - M_{\min}}{M_o} ,$$

where M_o is the average molecular weight, and Δ runs from 0 (monodisperse system) to 2 (complete polydispersity). The results of fitting this generated data with a single Lorentzian spectrum are shown in Fig. A.3. It is clear that even for the most polydisperse case ($\Delta = 2$) it is impossible to distinguish the heterodyne spectrum of the photocurrent from a single Lorentzian. The best fit has a width slightly less than that expected for light scattered by spheres of molecular weight

$$M_o = \frac{M_{\max} + M_{\min}}{2}$$

We finally consider the case for rods. If the rods are more than a few times longer than their diameter, the translational diffusion constant is very nearly proportional to the reciprocal of their length, $L^{(1)}$. Hence, for such rods, $\Gamma \propto (1/L)$, while their molecular weights of course are proportional to their lengths.

We thus have

$$\begin{aligned} \langle \mathbf{S}(v) \rangle &\propto \int_{M_{\min}}^{M_{\max}} \frac{M^2 \Gamma}{\Gamma^2 + v^2} dM \\ &\propto - \int_{X_{\min}}^{X_{\max}} \frac{1}{X^3 (X^2 + v^2)} dX \\ &\propto \left[\frac{\frac{1}{2v^2 X^2}}{2v^4} - \frac{\frac{1}{2v^4}}{X} \ln \left\{ 1 + \frac{v^2}{X^2} \right\} \right]_{X_{\min}}^{X_{\max}} \end{aligned} \quad (A.6)$$

where $X = 1/M$.

We have evaluated eq. A.6 for $\Delta = \frac{M_{\max} - M_{\min}}{M_o}$ running between 0 and 2, and display the results of a single Lorentzian fit to this data in Fig. A.4. Once again we must conclude we are unable to

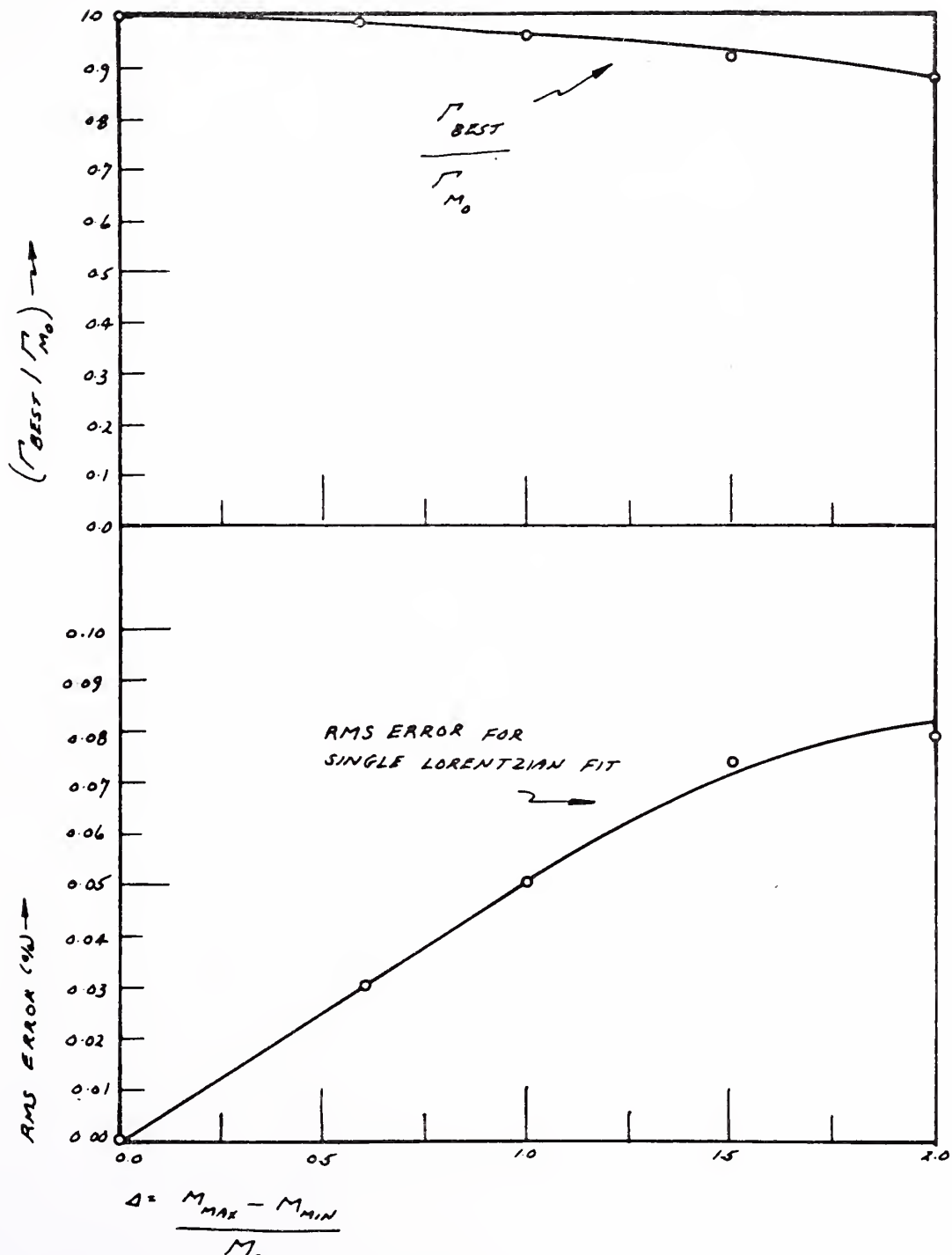


Fig. A.3 Width and RMS Deviation of Best Single Lorentzian Fit to the Heterodyne-Beat Spectrum of the Light Scattered by Various Uniform Distributions of Spheres

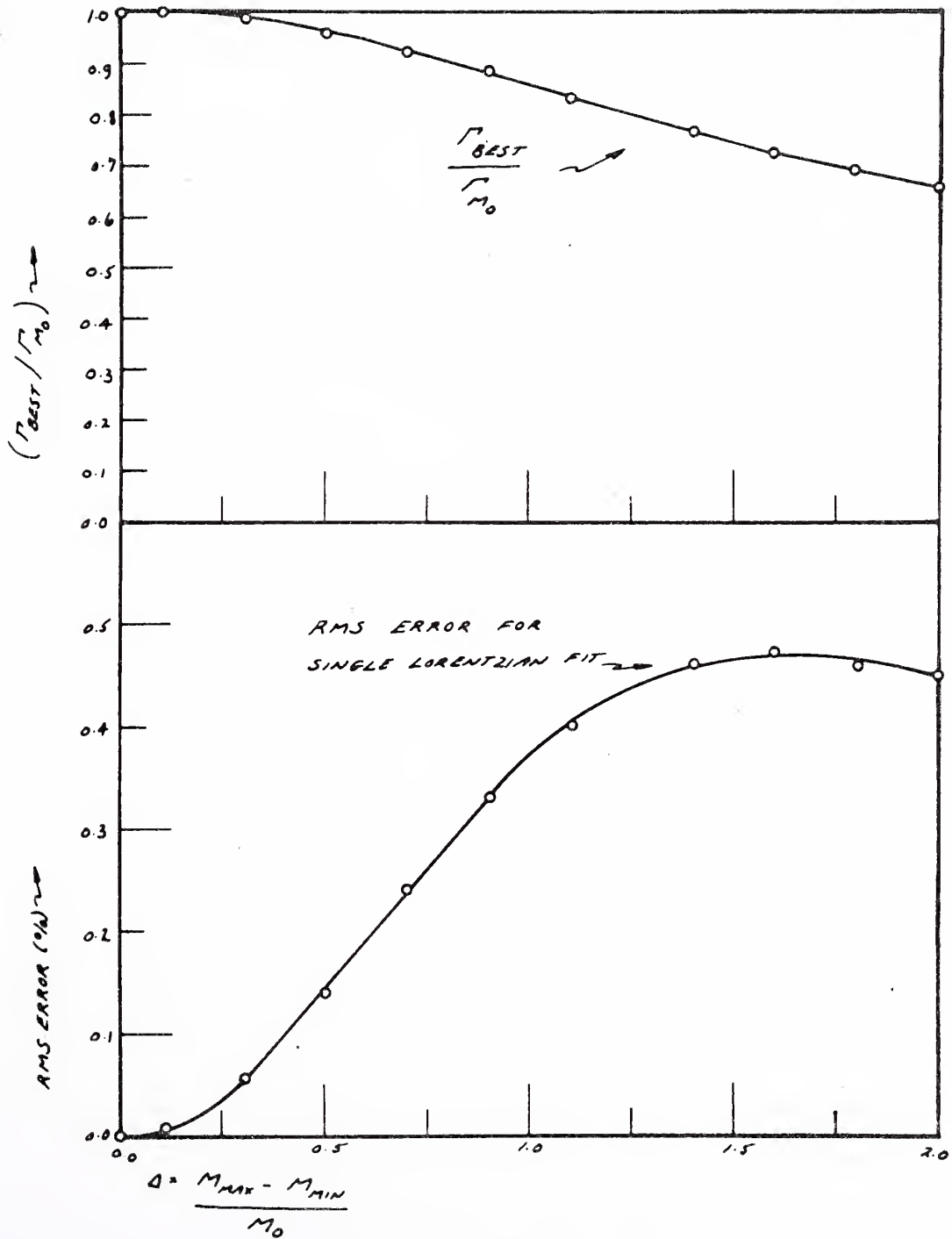


Fig. A.4 Width and RMS Deviation of Best Single Lorentzian Fit to the Heterodyne-Beat Spectrum of the Light Scattered by Various Uniform Distributions of Rods

to distinguish (from spectral analysis) the mixture from a single species. We note, however, that the width of the best fitting single Lorentzian is pulled considerably below the width of the light scattered by molecules of the mean molecular weight, $M_o = \frac{M_{\max} - M_{\min}}{2}$.

We conclude from these representative examples that it is generally impossible to detect a reasonably uniform polydispersity in a solution of macromolecules by the technique of light-mixing spectroscopy.

Reference for Appendix

1. Tanford, C., "Physical Chemistry of Macromolecules", John Wiley and Sons, Inc., New York, 1961, p. 326.

BIOGRAPHICAL NOTE

Born November 5, 1943, in Buffalo, New York, Stuart Brian Dubin attended primary and secondary school in Cincinnati, Ohio, and graduated from Yale College in June, 1965.

ACKNOWLEDGMENTS

I am grateful to Professor George Benedek for the opportunity to participate in this study in his research group, and for the research assistantship which provided the financial support that made this thesis possible.

All of the members of this group have contributed to whatever merit is in this work. Discussions among us, often at 4:00 o'clock in the morning, helped clarify many an obscure point. Joe Lunacek was a continual source of advice and discussion, and to him I offer special and sincere thanks.

It is a pleasure to acknowledge the suggestion of Professor David Freifelder that we undertake the bacteriophage molecular weight experiment and the many informative discussions with him and Dr. Carter Bancroft during this study. Professor George Feher suggested the study of the chemical denaturation of lysozyme.

The manuscript was cheerfully and expertly typed by Mrs. Evelyn Holmes on very short notice, and her cooperation is greatly appreciated.

Finally, I owe a special debt to Professor Albert Hill, who made some of the black appear at least gray, for providing me with a graduate assistantship during the actual writing of this thesis.

YALE MEDICAL LIBRARY

Manuscript Theses

Unpublished theses submitted for the Master's and Doctor's degrees and deposited in the Yale Medical Library are to be used only with due regard to the rights of the authors. Bibliographical references may be noted, but passages must not be copied without permission of the authors, and without proper credit being given in subsequent written or published work.

This thesis by _____ has been
used by the following persons, whose signatures attest their acceptance of the
above restrictions.

NAME AND ADDRESS

medical libr. Doc. De I 12/18/06 DATE

